

**Novel Piperidinium/pyrrolidinium-functionalized Styrene-b-ethylene-b-butylene-b-styrene Copolymer Based Anion Exchange Membrane with Flexible Spacers for Water Electrolysis**

Von der Fakultät Energie-, Verfahrens- und Biotechnik der Universität Stuttgart zur Erlangung der Würde eines Doktors der Ingenieurwissenschaft (Dr.-Ing.) genehmigte  
Abhandlung

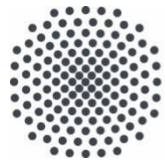
Vorgelegt von  
**Ziqi Xu**  
aus Dalian, China

Hauptberichter: Prof. Dr. rer. nat. Andreas Friedrich  
Mitberichter: Prof. Dr.-Ing. Elias Klemm  
Vorsitzender: Prof. Dr.-Ing. Jörg Starflinger  
Tag der mündlichen Prüfung: 12.03.2024

Universität Stuttgart  
Institut für Gebäudeenergetik, Thermotechnik und Energiespeicherung

2024





**Universität Stuttgart**



**DLR** Deutsches Zentrum  
für Luft- und Raumfahrt





# Table of content

Table of content .....	3
Acknowledgement .....	4
Erklärung .....	5
Declaration .....	5
Abstract .....	6
Zusammenfassung .....	8
List of Publications .....	10
Abbreviation.....	11
Symbol definition and unit.....	12
1 Introduction .....	13
1.1 Challenges and Motivations .....	13
1.2 State of the Art and Motivation .....	15
1.3 Thesis Outlines .....	15
2 Fundamentals.....	17
2.1 AEM Principle and Polymer Systems.....	17
2.2 Chemical Stability of AEM.....	18
2.3 Hydroxide conductivity of AEMs .....	22
2.4 Principle of the AEM electrolysis.....	23
3 Materials and Characterization Techniques .....	29
3.1 Chemicals .....	29
3.2 Characterization Techniques .....	30
4. Discussion.....	34
4.1 Conductivities of Piperidinium/Pyrrrolidinium Functionalized Membranes Based on SEBS .....	34
4.2 AEM Water Electrolysis Measurements .....	36
5. Conclusion .....	37
6. General Outlook.....	39
7. References.....	41
Article I .....	49
Article II .....	60
Article III.....	76

# Acknowledgement

First and foremost, I would like to thank my Doktorvater Prof. K. Andreas Friedrich. I want to express my heartfelt gratitude to him for giving me the opportunity to pursue my PhD research at the German Aerospace Center (DLR). I really appreciate his kind support during last five years with scientific discussions, suggestions, and guidance to enlighten my way to the field of hydrogen. Especially during the hard time of pandemic, he gave me significant encouragement, great help and enough time to get over the shadow of pandemic. I would also like to thank China Scholarship Council to fund my PhD for first four years.

I want to thank my supervisor in DLR Dr. Aldo Saul Gago and in ICVT Dr. Vladimir Atanasov for their relentless effort to guide me through the years.

I wish to express my gratitude to my DLR colleagues, especially Dr. Tobias Morawietz, Dr. Li Wang, Vincent Wilke, Jagoda Justyna Chmielarz, Sofia Delgado in scientific aspect and Jörg Bürkle for his technical support.

I also want to show my thanks to my colleagues in ICVT, especially Dr. Hyeongrea Cho, Dr. Johannes Bender, Julian Seiler, Inna Kharitonava, Galina Schumski and Saeed Sadeghi. In ICVT I had a feeling of home and no matter where I go in my later life, there will always be one place for ICVT in the bottom of my heart.

Now, I will express my heartfelt gratitude to my parents, who are the biggest supporters on whatever I do. They told me how to respect others, be humble and keep motivated whenever possible.

Last but not the least, my heartfelt thanks go to my friends in Stuttgart. no matter I am happy, frustrated or worried, they are always there willing to listen to me. They are the light for me in my whole PhD period.

# Erklärung

Hiermit versichere ich, dass ich die vorliegende Arbeit mit dem Titel"

**Novel Piperidinium/pyrrolidinium-functionalized Styrene-b-ethylene-b-butylene-b-styrene Copolymer Based Anion Exchange Membrane with Flexible Spacers for Water Electrolysis"**

Selbstständig verfasst und keine anderen als die angegebenen Quellen und Hilfsmittel benutzt habe, dass alle Stellen der Arbeit, die wörtlich oder sinngemäß aus anderen Quellen übernommen wurden, als solche kenntlich gemacht sind.

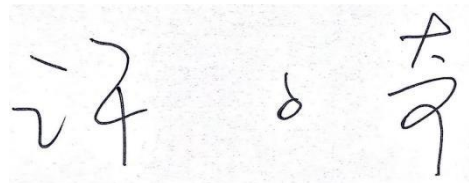
Ich versichere außerdem, dass die vorliegende Dissertation nur in diesem und keinem anderen Promotionsverfahren eingereicht wurde und dass diesem Promotionsverfahren keine endgültig gescheiterten Promotionsverfahren vorausgegangen sind.

# Declaration

I herewith duly declare that I have authored the dissertation

**" Novel Piperidinium/pyrrolidinium-functionalized Styrene-b-ethylene-b-butylene-b-styrene Copolymer Based Anion Exchange Membrane with Flexible Spacers for Water Electrolysis"**

independently and only with use of specified aids. I have mentioned all sources used and cited correctly according to scientific rules.



Stuttgart, 09.29.2023

---

Ziqi Xu

## Abstract

Anion exchange membranes (AEMs) are crucial components for alkaline electrochemical energy technology, including AEM water electrolysis and AEM fuel cells. They are seen as promising alternatives to proton exchange membrane-based systems due to the potential for using noble metal-free electrocatalysts. However, the chemical stability and conductivity of the membrane remain the primary challenges of the electrolyzer system.

The fundamental goal of this dissertation is to design and develop high-conductive and chemically stable AEMs that can be used for AEM electrolysis. In the first part of the dissertation, an AEM with a styrene-*b*-ethylene-*b*-butylene-*b*-styrene copolymer (SEBS) as a backbone and piperidinium functionalized flexible ethylene oxide spacer structure as side-chains (SEBS-P2O6) is highlighted. This membrane achieved  $20.8 \text{ mS cm}^{-1}$  hydroxide ion conductivity at room temperature, which is higher compared to previously obtained piperidinium-functionalized SEBS with  $10.09 \text{ mS cm}^{-1}$ . The SEBS-P2O6 was tested in a single cell AEM electrolysis cell with platinum group metal (PGM) catalyst (Pt/C and Ir black), achieving current densities of  $275 \text{ mA cm}^{-2}$  and  $680 \text{ mA cm}^{-2}$  at  $60^\circ\text{C}$  and 2 V cell potential in ultra-pure water (UPW) and 0.1 M KOH, respectively. Remarkably, in UPW, the degradation rate was only  $140 \mu\text{A h}^{-1} \text{ cm}^{-2}$  for more than 300 hours, the lowest reported up to now. In the second part of the dissertation, a pre-functionalized end-structure was designed to increase the ion exchange capacity (IEC) of the membrane. Moreover, all the benzyltrimethylammonium groups were replaced by piperidinium/pyrrolidinium to improve the chemical stability of the membrane. Functionalization of the polymer was done during the solvent evaporation process instead of the post-treatment process to minimize the loss of mechanical properties for the membrane. Finally, the membrane (SEBS-Py2O6) achieved  $27.8 \text{ mS cm}^{-1}$  hydroxide ion conductivity at room temperature, which is higher compared to previously obtained piperidinium-functionalized SEBS reaching up to  $10.09 \text{ mS cm}^{-1}$ . The SEBS-Py2O6 combined with PGM-free electrodes (OER catalyst  $\text{NiFeO}_x$  and HER catalyst  $\text{MoC}_x$ ) in an AEM water electrolysis (AEMWE) cell achieved  $520 \text{ mA cm}^{-2}$  at 2 V in 0.1 M KOH and  $171 \text{ mA cm}^{-2}$  in ultra-pure water (UPW). This high performance indicates that SEBS-Py2O6 membranes are suitable for application in water electrolysis.

In the third part of the dissertation, a membrane electrode assembly (MEA) free of noble metals was investigated and exhibited remarkable high performance ( $>0.7 \text{ A cm}^{-2}$  at 2 V,  $60^\circ\text{C}$ , UPW) while running continuously for more than 80 hours in pure water with the lowest reported degradation rate for pure water conditions ( $<5 \text{ mV h cm}^{-2}$ ). Our prepared MEA was composed of a pyrrolidinium-functionalized styrene-*b*-ethylene-*b*-butylene-*b*-styrene copolymer AEM, and it outperformed the state-of-the-art AEMWE composed to commercial  $\text{IrO}_2|\text{Sustainion membrane}| \text{Pt/C}$ . Additionally, the activation conditions of the innovative pyrrolidinium multi-cation comb-shaped polymer structure-based membrane in an alkaline solution (1 M KOH for 72 hours) and the concentration of the same formulation-based ionomer (20% Ionomer/Catalyst) in the MEA were discovered to be key factors in ensuring long-term stability in continuous, pH-neutral operation without any corrosive electrolyte in circulation. These findings suggest that devices that employ PGM-free and earth-abundant materials and function in pure water might replace high-cost proton exchange membrane electrolyzers.





## Zusammenfassung

Anionenaustauschmembranen (AEM) sind zentrale Komponenten für die alkalische elektrochemische Energietechnik, wie sie in der AEM-Wasserelektrolyse und der AEM-Brennstoffzelle eingesetzt werden. Sie gelten als vielversprechende Alternative zu Systemen auf Basis von Protonenaustauschmembranen, da sie die Möglichkeit bieten, edelmetallfreie Elektrokatalysatoren zu verwenden. Allerdings stellen die chemische Stabilität und die Leitfähigkeit der Membran nach wie vor die größten Herausforderungen für das Elektrolyseursystem dar.

Das grundlegende Ziel dieser Dissertation ist es, hochleitfähige und chemisch stabile AEMs zu entwerfen und zu entwickeln, die für die AEM-Elektrolyse verwendet werden können. Zunächst wird eine AEM mit einem Styrol-B-Ethylen-B-Butylen-B-Styrol-Copolymer (SEBS) als Grundgerüst und einer flexiblen Ethylenoxid-Spacer-Struktur mit Piperidinium-Funktion als Seitenkette (SEBS-P2O6) vorgestellt. Diese Membran erreichte eine Hydroxidionenleitfähigkeit von 20,8 mS/cm bei Raumtemperatur, was höher ist als die zuvor erzielte Leitfähigkeit von mit Piperidinium funktionalisierten SEBS-Membranen mit 10,09 mS/cm. Das SEBS-P2O6 wurde in einer einzelligen AEM-Elektrolysezelle mit Platingruppenmetall (PGM)-Katalysator getestet und erreichte Stromdichten von 275 mA/cm<sup>2</sup> und 680 mA/cm<sup>2</sup> bei 60°C und 2 V Zellpotential in ultrareinem Wasser (UPW) bzw. 0,1 M KOH. Bemerkenswerterweise betrug die Verlustrate in UPW nur 140 µA h/cm<sup>2</sup>, was die bisher niedrigste Rate in der Literatur ist.

Im zweiten Teil der Dissertation wurde eine vorfunktionalisierte Endstruktur entworfen, um die IEC der Membran zu erhöhen. Außerdem wurden alle Benzyltrimethylammonium-Gruppen durch Piperidinium/Pyrrolidinium ersetzt, um die chemische Stabilität der Membran zu verbessern. Schließlich wurde die Funktionalisierung des Polymers während der Lösungsmittelverdampfung und nicht erst nach der Behandlung vorgenommen, um den Verlust der mechanischen Eigenschaften der Membran zu minimieren. Die resultierende Membran (SEBS-Py2O6) erreichte eine Hydroxidionenleitfähigkeit von 27,8 mS/cm bei Raumtemperatur, was höher ist als die zuvor erzielte Leitfähigkeit von mit Piperidinium funktionalisierten SEBS-Membranen mit bis zu 10,09 mS/cm. Das SEBS-Py2O6 in Kombination mit PGM-freien Elektroden in einer AEM-Wasserelektrolysezelle (AEMWE) erreichte eine Stromdichte von 520 mA/cm<sup>2</sup> bei 2 V in 0,1 M KOH und 171 mA/cm<sup>2</sup> in ultrareinem Wasser (UPW).

In Teil drei der Dissertation wurde eine edelmetallfreie Membranelektrodenanordnung (MEA) untersucht, die eine bemerkenswert hohe Leistung (> 0,7 A cm<sup>-2</sup> bei 2 V, 60 °C, pH=7) in reinem Wasser aufweist und mehr als 80 Stunden lang in reinem Wasser betrieben werden kann, während sie die niedrigste für ähnliche Bedingungen gemeldete Verlustrate (<5 mV h cm<sup>-2</sup>) aufweist. Die von uns hergestellte MEA besteht aus einem Pyrrolidinium-funktionalisierten Styrol-b-Ethylen-b-Butylen-b-Styrol-Copolymer AEM und übertrifft den Stand der Technik der AEMWE, die aus einer kommerziellen IrO<sub>2</sub>|Sustainion-Membran|Pt/C besteht. Die Aktivierungsbedingungen der innovativen Pyrrolidinium-Multikation-Membran mit kammförmiger Polymerstruktur in alkalischer Lösung (1 M KOH für 72 h) und die Konzentration des Ionomers, der auf derselben Formulierung basiert (20 % Ionomer/Katalysator), erwiesen sich ebenfalls als Schlüsselfaktoren für die

Gewährleistung der Langzeitstabilität im kontinuierlichen, pH-neutralen Betrieb ohne korrosiven Elektrolyten im Umlauf. Diese hohe Leistungsfähigkeit zeigt, dass SEBS-Py2O6-Membranen für die Wasserelektrolyse geeignet sind und dass kostenintensive Protonenaustauschmembran-Elektrolyseure unter Umständen durch Hydroxid leitende Membranen ersetzt werden könnten, die auch mit reinem Wasser funktionieren, aber ohne Edelmetalle und kritische Materialien auskommen.

## List of Publications

This is a cumulative thesis, which is based on three scientific articles listed as follows:

**Article I : Novel Piperidinium-functionalized Crosslinked Anion Exchange Membrane with Flexible Spacers for Water Electrolysis**

*Ziqi Xu, Vincent Wilke, Jagoda Justyna Chmielarz, Tobias Morawietz, Vladimir Atanasov, Aldo Saul Gago\*, Kaspar Andreas Friedrich\**

*Journal of Membrane Science 670 (2023) 121302; <https://doi.org/10.1016/j.memsci.2022.121302>*

**Contribution: Conceptualization, Methodology, membrane synthesis, membrane characterization and manuscript writing.**

**Article II : Novel Pyrrolidinium-Functionalized Styrene-b-ethylene-b-butylene-b-styrene Copolymer Based Anion Exchange Membrane with Flexible Spacers for Water Electrolysis**

*Ziqi Xu\* †, Sofia Delgado†, Vladimir Atanasov, Tobias Morawietz, Aldo Saul Gago\* and Kaspar Andreas Friedrich*

*Membranes 2023, 13(3), 328; <https://doi.org/10.3390/membranes13030328>*

**Contribution: Conceptualization, methodology, membrane synthesis, membrane characterization, and manuscript writing**

**Article III: Highly Efficient and Durable Anion Exchange Membrane Water Electrolyzers with Non-Precious Metal Catalysts in Pure Water: key components and fabrication strategies**

*S. Delgado†, Z. Xu†, A. Gago, K. A. Friedrich, A. Mendes\**

Submitted

S. Delgado and Z. Xu are both first authors.

**Contribution: Conceptualization, membrane synthesis, membrane characterization and manuscript reviewing**

## Abbreviation

AEM	Anion exchange membrane
SEBS	Styrene-b-ethylene-b-butylene-b-styrene copolymer
PGM	Platinum group metal
UPW	Ultra-pure water
AEMWE	Anion exchange membrane water electrolysis
GISS	Goddard Institute for space studies
SPE	Solid polymer electrolyte
PEM	Proton exchange membrane
MEA	Membrane electrode assembly
CCM	Catalyst coated membrane
CCS	Catalyst coated substrate
PPO	Poly (phenylene oxides)
BTAA	Benzyltrialkylammoniums
IEC	Ion-exchange capacity
DABCO	1,4-diazabicyclo [2,2,2] octane
QA	Quaternary ammonium
HER	Hydrogen evolution reaction
OER	Oxygen evolution reaction
NMR	Nuclear magnetic resonance
FT-IR	Fourier-transform infrared spectroscopy
TMS	Tetramethylsilane
AFM	Atomic force spectroscopy
SPM	Scanning probe microscopy
WU	Water uptake
SR	Swelling ratio
CR%	Conductivity retention rate
BPP	Bipolar plates
PTL	Porous transport layer
PSL	Porous sintered layer
EIS	Electrochemical impedance spectrum

## Symbol definition and unit

Description	Symbols	Unit
Conductivity	$\sigma$	$\text{mS cm}^{-1}$
Ion mobility	$\mu$	$\text{m}^2 \text{S}^{-1} \text{V}^{-1}$
Ion activity	$\alpha$	-
Acid dissociation constant	pKa	-
Ion exchange Capacity	IEC	$\text{mmol g}^{-1}$
Electrical potential	E	V
Faraday's constant	F	$\text{C mol}^{-1}$
Current density	J	$\text{A cm}^{-2}$
Temperature	T	$^{\circ}\text{C}$
Frequency	F	MHz
Wavenumber	N	$\text{cm}^{-1}$
Chemical shift	$\delta$	Ppm
Resistivity	$R_{\text{sp}}$	$\Omega \text{ cm}$
Thickness of membrane	D	Cm
Ohmic resistance	R	$\Omega$
Electrode area	A	$\text{cm}^2$
Weight of wet membrane	$m_{\text{wet}}$	G
Weight of dry membrane	$m_{\text{dry}}$	G
Concentration of the solvent	C	$\text{mol L}^{-1}$
Time	T	h, s
Scan rate	S	$\text{mv s}^{-1}$
Current	I	A

# 1 Introduction

## 1.1 Challenges and Motivations

Fossil fuels have played a significant role in human development due to their ability to rapidly produce heat when combust under controlled conditions in internal combustion engines. Until the mid-21<sup>st</sup> century, they remained an integral part of the power supply system. However, with the growth of society and population, greenhouse gas emissions from burning fossil fuels have sharply increased in recent years. This is believed to be one of the main causes of global warming, which presents unprecedented challenges in human history.

According to the NASA Goddard Institute for Space Studies (GISS) [1], the world average temperature has significantly increased since 1970, as shown in Figure 1.1.1 [2] below, which depicts temperature changes since 1880. Global warming can lead to the loss of sea ice, melting glaciers and ice sheets, rising sea levels, and more intense heat waves. Scientists predict that if this trend continues until 2050, 15-37% of species on our planet will face extinction [3]. Therefore, reducing emissions is imperative, and alternative energy sources must be developed to slow down global warming.

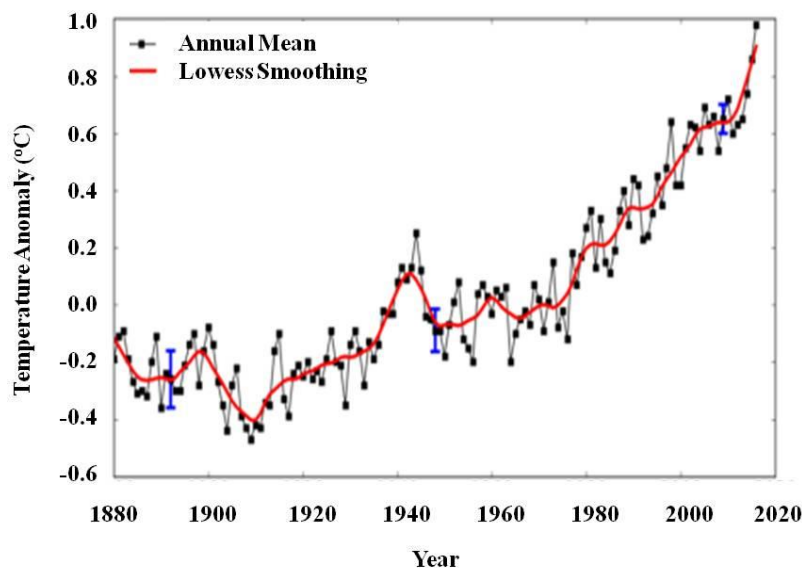


Fig. 1.1.1 The change of global mean temperature from 1880 to 2020 [2]

One of the most environmentally friendly ways to mitigate the risks of global warming is to replace fossil fuels in the energy supply system with sustainable energy sources such as wind, solar, wind and hydro-energy. To store the sustainable energy, Hydrogen can offer many advantages as an alternative energy carrier, including its high energy content ( $118 \text{ MJ kg}^{-1}$  at 298 K), which is much higher than that of most fuels (e.g., gasoline at  $44 \text{ MJ kg}^{-1}$  at 298 K), and the fact that it only produces water when it burns in the air or consumed in a fuel cell, which making it very clean [4, 5].

Today, hydrogen fuel can be produced through several methods such as natural gas reforming, electrolysis, solar-driven processes, and biological processes (Figure 1.1.2). According to the Hydrogen Energy Earth shot goal of the U.S. Department of Energy, the cost of clean hydrogen will be reduced by 80% to \$1 per kilogram in one decade (hydrogen 1-1-1 goal) [6]. To achieve this goal, water electrolysis is believed to be a leading carbon-free option to produce green hydrogen. This process needs electricity to split water into hydrogen and oxygen which is performed with electricity in an electrolyzer- a reactor for conversion of water into its constituents. The polymer electrolyte membrane electrolyzer is one of many types of electrolyzers that could produce green hydrogen with almost no production of green-house gases that could harm the environment. Furthermore, the absence of a corrosive liquid electrolyte in the polymer electrolyte membrane electrolyzer offers many benefits, including the absence of leaking, volumetric stability, ease of handling, and a reduction in the size and weight of the electrolyzer [7-9].

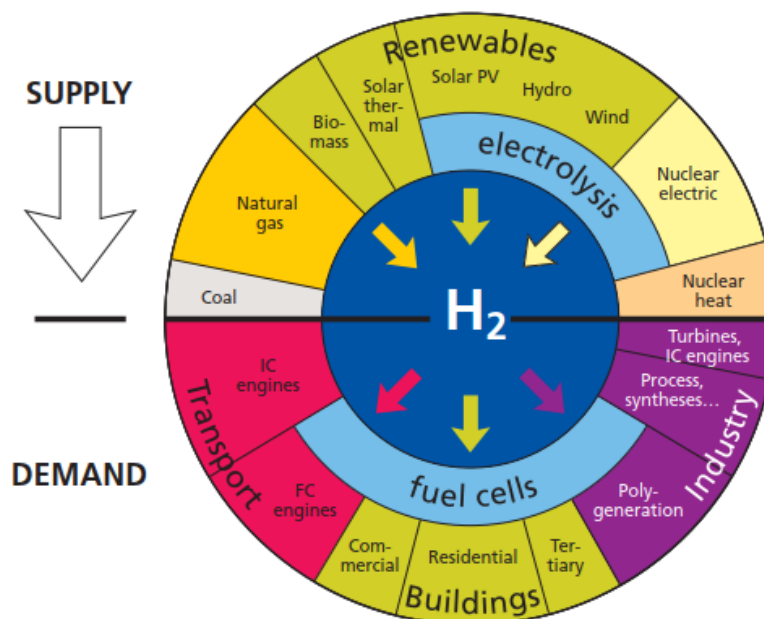


Fig. 1.1.2: Hydrogen: primary energy sources, energy converters and applications. Reproduced from [10]

The polymer electrolyte membrane is typically used in water electrolysis cells with a polymer electrolyte membrane, which conducts hydrogen ions, separates gas productions and electrically insulates the electrodes from each other. There are two mature and low temperature water electrolysis technologies for producing hydrogen: alkaline electrolysis (AE) and proton exchange membrane (PEM) electrolysis. In PEM water electrolysis, which is currently commercially available, protons are transferred through the PEM in a highly acidic environment. Therefore, PEM electrolyzers require platinum group metals (PGM) as catalysts and expensive titanium bipolar plates to survive the highly corrosive acidic environment. On the other hand, anion exchange membrane water electrolysis (AEMWE) has become a promising alternative because cost effective materials such as non-PGM catalysts and steel bipolar plates can be used sufficient for effective hydrogen production in the AEM electrolyzer [11, 12]. which also enables high performance and good gas quality. In summary, hydrogen is expected to play a major role in addressing the energy system and environmental crises of the 21st century, and AEMWE shows great potential to be a



low-cost and sustainable method for producing hydrogen.

## 1.2 State of the Art and Motivation

The AEMWE comprises a membrane electrode assembly (MEA), which includes an assembled stack of AEM, a cathode for hydrogen evolution reaction (HER), an anode for oxygen evolution reaction (OER), and bipolar plates. The MEA is considered to be the key component of AEM water electrolysis. Figure 1.2.1 illustrates the structure of the MEA and the contact status of the catalyst and ionomer. The membrane acts as the electrolyte separator between the anode and cathode while conducting ions. However, to date, there are still no reliable AEMs with the desired conductivity and stability, which presents a major challenge in developing high-performance AEMWE.

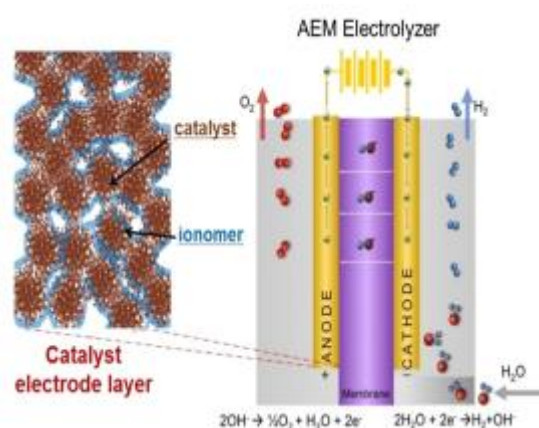


Fig 1.2.1 MEA and catalyst electrode layer for AEMWE. Copied from[13]

Therefore, it is important to develop AEMs that are chemically stable and highly ionic conductive. The motivation of my research is to design, produce and test such AEMs, which can be used as sustainable and functional MEAs, leading to high-performance AEMWE. Additionally, this research investigates the chemical structure of the ionomer and MEA fabrication methods to further improve MEA performance. Moreover, the MEA designed in this work employs PGM-free catalysts in the electrodes to eliminate the need for precious platinum and iridium, and the electrolyzers are tested in pure water, which is an extremely challenging condition without any additional electrolyte.

## 1.3 Thesis Outlines

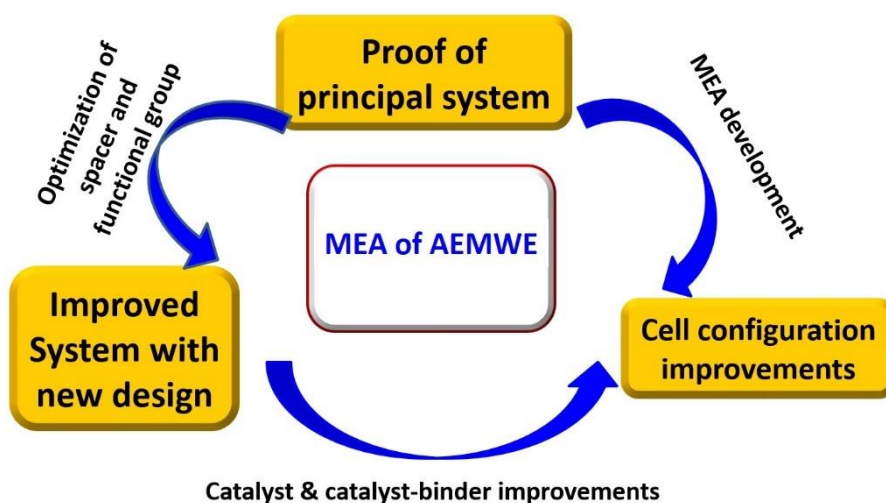
This thesis focuses on designing, synthesizing, characterizing, and testing different membrane structures to obtain highly conductive and chemically stable AEMs for AEMWE application. Throughout the thesis, a multi-block copolymer styrene-*b*-ethylene-*b*-butylene-*b*-styrene copolymer (SEBS) is used as a backbone due to its excellent stability and mechanical integrity (Scheme 1.3.1).

In the first part of the work, piperidinium is chosen as the main functional group for its resistance towards nucleophilic substitution and  $\beta$ -elimination (Hofmann elimination). Different structures of the side chain are investigated, including the number of cations per chain, carbon chain length

between two piperidinium groups, and the length of the spacer. After the membrane is prepared, AEM electrolyzers are assembled and tested in both KOH and water.

In the second part of the work, to further improve membrane conductivity, more hydrophilic ethylene glycol-based side chains are achieved by using prefunctionalized-ends of the spacer. Only chemically stable 6-membered and 5-membered cycloaliphatic quaternary ammoniums (piperidinium and pyrrolidinium) are applied to create a stable membrane. Finally, a PGM-free catalyst is designed and assembled with the AEM in a new design MEA, and cell performance is tested and evaluated.

In the last part of the thesis, based on the experience from both system, the most suitable materials for cell configuration are investigated to further improve the electrolyzer's performance. Improved methods of MEA fabrication, such as catalyst coated membrane (CCM) and catalyst coated substrate (CCS), are investigated, and cell stability tests are performed.



Scheme 1.3.1: Outline of the thesis in a nutshell

## 2 Fundamentals

### 2.1 AEM Principle and Polymer Systems

AEMs are polymer electrolytes that conduct anions, such as  $\text{OH}^-$  and  $\text{Cl}^-$ , while simultaneously blocking gases, such as hydrogen, oxygen and electrons [14]. They are widely used in fuel cells, electrolyzers, redox flow batteries, reverse electro dialysis cells, and bioelectrochemical systems, including microbial fuel cells.

Typically, AEMs contain positively charged functional groups that are covalently attached to the polymer backbone. These functional groups can be located on a side or directly incorporated in the backbone chain. Commonly, backbones can be divided into several categories: (i) based on polystyrene (Fig 2.1.1(a)) and poly(vinylbenzyl chloride) [15-17] (such as SEBS), (ii) with heteroatoms such as polysulfones [18-20] (Fig 2.1.1(b)) (such as phthalazinone, fluorenyl, etc.), poly(phenylene oxides) (PPO) [21-23] (Fig 2.1.1(c)), poly(ether ketones) [20, 24, 25] (Fig 2.1.1(d)), (iii) backbones based on polyphenylene such as poly(arylene piperidinium) [26] (Fig 2.1.1(e)), polyfluorene [27] (Fig 2.1.1(f)), etc.

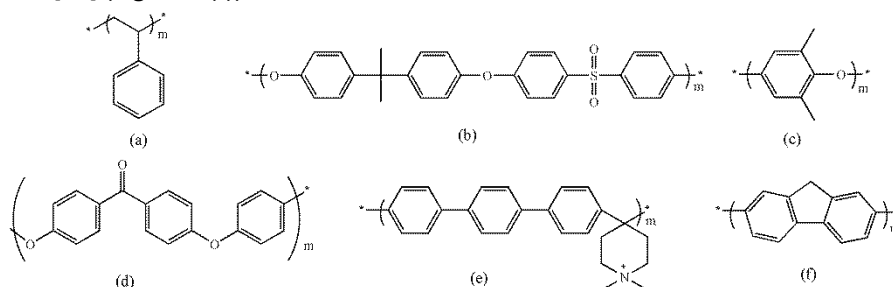


Fig 2.1.1 Common encountered backbones in AEM (a polystyrene, b polysulfones, c polyphenylene oxide, d poly(ether ketones), e poly(arylene piperidinium), f polyfluorene) [14]

The positively charged functional groups that are commonly studied on AEMs are:

(a) quaternary ammonium groups including benzyltrialkylammoniums (BTAA)[28] (Fig 2.1.2(a)) which is most common one in this field, alkyl-bound (benzene-ring-free) quaternary ammoniums (QAs)[29, 30] (Fig 2.1.2(b)), and QAs based on cyclic ammonium systems such as piperidinium[31, 32] (Fig 2.1.2(c)) and 1,4-diazabicyclo [2.2.2] octane (DABCO)[21, 33] (Fig 2.1.2(d)).

(b) Heterocyclic systems such as imidazolium[17, 34, 35] (Fig 2.1.2(e)), benzimidazoliums[36], PBI based systems[37, 38], pyridinium types[39, 40] (Fig 2.1.2(f)) (which is normally not stable in high PH)

(c) Guanidinium systems[41-43] (Fig 2.1.2(g))

(d) P-based systems types[44, 45] (Fig 2.1.2(h)) and P-N systems[46]

(e) Sulfonium types[47], Metal-based systems[48]

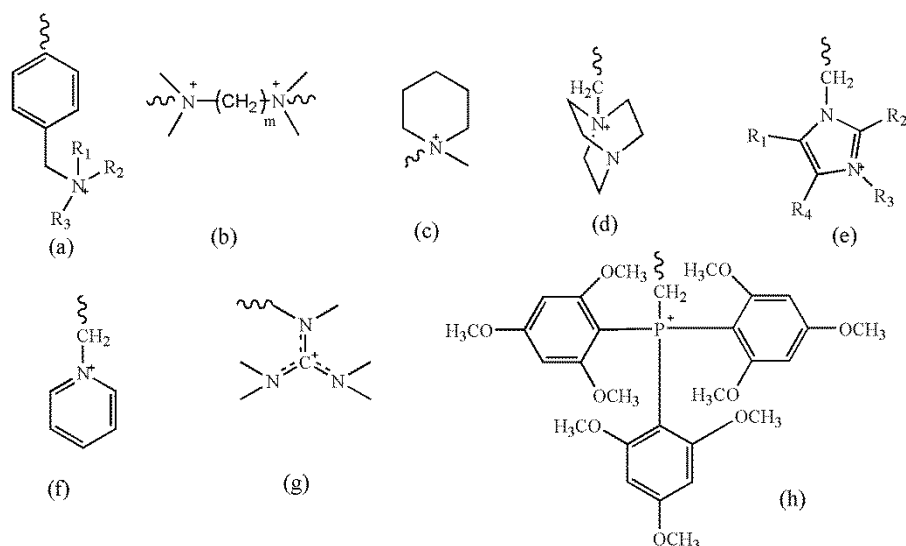


Fig 2.1.2 Common encountered functional groups in AEM (a BTAA, b alkyl-bound (benzene-ring-free) QAs, c piperidinium, d DABCO based QA, e imidazolium, f pyridinium types, g Guanidinium systems, h P-based systems types) [14]

Ion-exchange capacity (IEC) is one of the most crucial properties for AEMs and ionomers, as it represents the number of functional groups (in molar equivalents, eq.) per unit mass of polymer. Typically,  $\text{Cl}^-$  based titrations or  $\text{OH}^-$  based titrations are used to determine the IEC [49].

## 2.2 Chemical Stability of AEM

One of the most significant challenges faced by AEMs in electrochemical devices such as fuel cells and electrolysis is their stability, especially in high pH environments in the presence of strong nucleophilic hydroxide ions. Although radical degradation can occur in these applications when  $\text{OH}^\cdot$  radicals are produced and attack the membrane (which is the major degradation mechanism for PEM), hydroxide attack is believed to be the primary reason for AEM degradation [50, 51]. Radical stability is considered to be more critical for ionomers in AEM electrolysis, and suffers more than alkaline stability.

Specifically, to ensure the alkaline stability of the membrane, the alkaline stabilities of both backbones and functional groups need to be studied. As there are various types of functional groups, quaternary ammonium-based AEMs are explained as an example in this part. Common degradation and membrane reactions are listed as methods to prevent degradations are shown in Figure 2.2.1.

Many degradation mechanisms can occur in the ammonium when strong nucleophilic  $\text{OH}^-$  is present. One of the most critical reactions that take place is Hofmann elimination [52, 53] (Fig 2.2.1(a)). Hofmann elimination is a  $\beta$ -CH elimination reaction of an ammonium to form an alkene, which follows the E2 elimination mechanism. The scheme of the E2 mechanism is shown in Fig 2.2.1(b) in detail. E2 is a one-step elimination with a single transition state and two leaving groups ( $\beta$ -hydrogen and an ammonium) need to be antiperiplanar to the result in the formation of a  $\pi$  bond. Therefore, to avoid Hofmann elimination and improve the chemical stability of AEMs, several designs on the chemical structure of the membrane are preferred:

(1) elimination of  $\beta$ -hydrogens in the structure (as in the case of BTAA shown in Fig 2.1.2(a)), and

(2) preventing  $\beta$ -hydrogen from rotating to the antiperiplanar position of ammonium, which can be achieved by introducing a rigid ring system (as in the case of DABCO shown in Fig 2.1.2(d)) or incorporating bulky groups to create steric hindrance at the  $\beta$ -hydrogen position

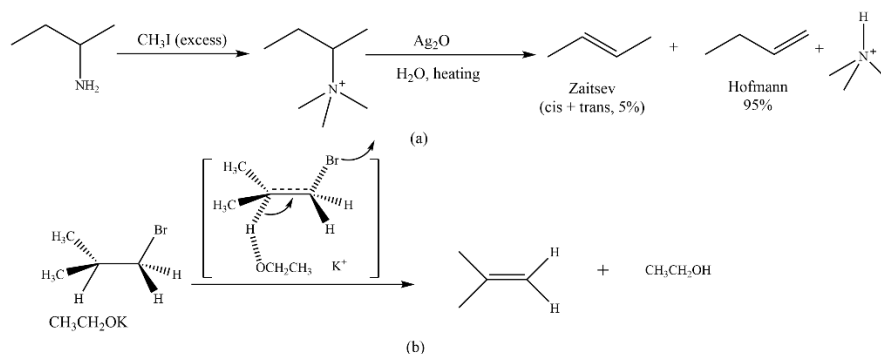


Fig 2.2.1 (a) Reaction steps of Hofmann elimination (b) E2 mechanism of elimination

Another important degradation reaction that can occur in the membrane is nucleophilic substitution. For example, in the case of BTAA, hydroxide ions can attack the  $\alpha$ -carbon to which the quaternary ammonium is attached [52], as shown in Fig 2.2.2. This is a typical  $\text{S}_{\text{N}}2$  mechanism substitution reaction, where the breaking of the C-N bond and the formation of the new bond (C-O) are both rate-determining steps. To improve the stability of the membranes against nucleophilic substitution, it is typically preferred to increase the steric hindrance of the  $\alpha$ -carbon, which slows down the  $\text{S}_{\text{N}}2$  substitution.

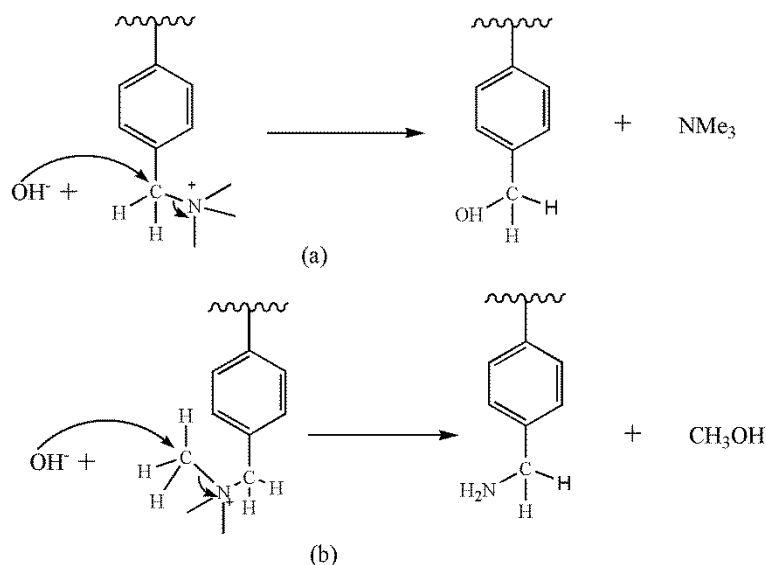


Fig 2.2.2 (a) (b) Nucleophilic substitution of BTAA with hydroxide (Me is short for methyl group)

In addition to Hofmann elimination and nucleophilic substitution, some other reactions can also occur in certain polymers. For example, in the case of BTAA, Sommelet-Hauser and Stevens rearrangements can also take place, as shown in Fig 2.2.3 [54]. However, in most cases, Hofmann elimination and nucleophilic substitution are considered as major reactions that occur during degradation. Therefore, the polymer's structure is designed to minimize these two reactions to

ensure chemical stability of the AEM functional group. Despite having functional groups like alkyl-bound (benzene-ring-free) QAs (Fig 2.1.2 (b)), which should be easily attacked by hydroxide, they surprisingly exhibit high stability. One hypothesis is that the high electron density around the  $\beta$ -hydrogens in longer alkyl chains inhibits the Hofmann elimination reaction [55-57].

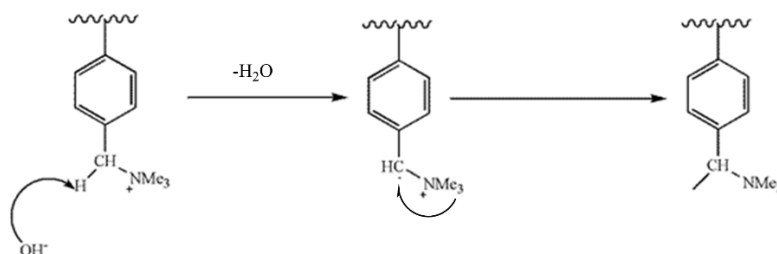


Fig 2.2.3 Sommelet-Hauser and Stevens rearrangements on BTAA[54] (Me is short for methyl group)

Imidazolium systems are another important functional group that is widely reported in the literature. When ionized, all atoms form resonance structure and the stabilization offered due to the delocalization of electrons in all atoms (resonance stabilization). Resonance stabilization is once thought to be an effective strategy for improving the chemical stability of these functional groups. However, due to their planar structure, they require more steric resistance to achieve greater chemical stability. For example, positions R2, R4, and R5 as is shown in Fig 2.2.4, (which are all hydrogen atoms) are unstable, and replacing them with alkyl or phenyl groups can improve stability. Substitution at the R3 position can also affect alkaline stability, as shown in further investigations. Geoffrey W. Coates reported that substituting R4 and R5 with methyl groups, R2 with 2,6-dimethylphenyl substitution, and alkyl substitution at the R3 position is the most suitable choice, considering both alkaline stability and conductivity [58].

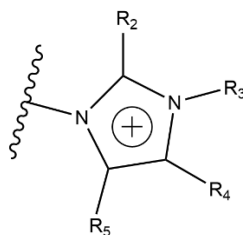


Fig 2.2.4 Substitutes of imidazolium [58]

The chemical stability of backbones is also critical, as hydroxide attacks not only the functional groups but also the backbone. Perfluorinated backbones, such as Nafion, are widely used in PEMs but can rapidly degrade in alkaline environments (Fig 2.2.5). Additionally, some polymers, such as PBI and polysulfone, are stable in alkaline solutions, but when functional groups are attached to them, complex hydrophilic and hydrophobic interactions occur, leading to degradation and reduced stability [59, 60] (Fig 2.2.6). PPO is also a common backbone for AEM, but degradation still occurs when the membrane is exposed to alkaline solution for a long time [61]. Typically, for the most commonly used functional group, trimethylammonium, the order of backbone stability is polystyrene > PPO > polysulfone [62]. Overall, when heteroatoms are present in the backbone, they are much easier to be attacked by hydroxide. Therefore, C and H backbones have become the

best choice for a backbone selection with improved stability.

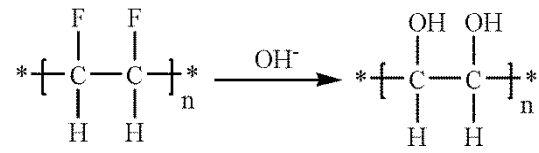


Fig 2.2.5 degradation of C-F based backbone in alkaline solution

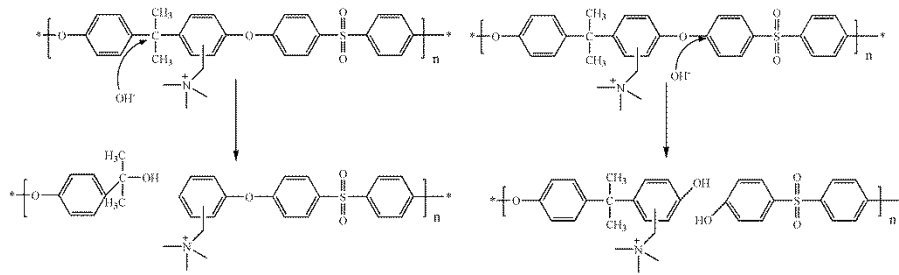


Fig 2.2.6 Degradation reactions of polysulfone backbone in alkaline solution[62]

## 2.3 Hydroxide conductivity of AEMs

Hydroxide conductivity is another key characteristic of AEM that indicates the mobility of hydroxide ions within the membrane. As shown in Equation 2.1, ion conductivity ( $\sigma$ ) is always determined by the ion mobility ( $\mu$ ) and ion activity ( $a$ ). In comparison to PEM, AEM always has lower conductivity due to two main reasons:

$$\sigma \propto F \mu a \quad (\text{Equation 2.1})$$

(1) The hydroxide ion has a relatively lower mobility than the proton [63]. For example, the ion mobility of the proton is  $36.23 \times 10^{-8} \text{ m}^2 \text{ s}^{-1} \text{ V}^{-1}$  (Table 2.3.1), which is 1.75 times higher than that of the hydroxide ion.

(2) The ionization of the hydroxide and ammonium groups in AEMs is lower than that of the sulfonic acid groups (R-SO<sub>3</sub>H) in PEMs.

Specifically, AEMs in the OH<sup>-</sup> form can be slowly converted to the HCO<sub>3</sub><sup>-</sup> and CO<sub>3</sub><sup>2-</sup> forms when exposed to air, and these forms have much lower ion mobility. Therefore, it is important to remove CO<sub>2</sub> from AEM systems to avoid a decline in membrane conductivity. However, this restriction has also hindered the development of AEMs.

Table 2.3.1 Ion mobilities ( $m$ ) at infinite dilution in H<sub>2</sub>O at 298.15 K[64]

Ion	Mobility ( $\mu$ )/10 <sup>-8</sup> m <sup>2</sup> s <sup>-1</sup> V <sup>-1</sup>
H <sup>+</sup>	36.23
OH <sup>-</sup>	20.64
CO <sub>3</sub> <sup>2-</sup>	7.46
HCO <sub>3</sub> <sup>-</sup>	4.61

The ionization process of the ammonium base is shown in Equation 2.2. A larger pK<sub>a</sub> value (Equation 2.3, Equation 2.4) indicates a higher level of dissociation for the ammonium base, which enables it to have higher OH<sup>-</sup> activity with a similar IEC. However, quaternary ammonium functional groups have very high pK<sub>a</sub> values, which is believed to have a pK<sub>a</sub> value greater than 13 [65].



$$K_b = \frac{a(\text{OH}^-) a(\text{RN}^+\text{HMe}_2)}{a(\text{RNMe}_2) a(\text{H}_2\text{O})} \quad (\text{Equation 2.3})$$

$a(\text{OH}^-)$ ,  $a(\text{RN}^+\text{HMe}_2)$ ,  $a(\text{RNMe}_2)$ ,  $a(\text{H}_2\text{O})$  is the ion activity of OH<sup>-</sup>, RN<sup>+</sup>HMe<sub>2</sub>, RNMe<sub>2</sub>, H<sub>2</sub>O, respectively.

$$\text{p}K_a = 14 - \text{p}K_b \quad (\text{Equation 2.4})$$

To improve the conductivity of AEMs, the ion activity in membranes needs to be enhanced. Increasing the IEC of AEMs is one approach to achieve this goal. However, a too high IEC can lead to greater water uptake and membrane swelling, which can affect the mechanical properties and dimensional stability of the AEMs. Membranes with poor mechanical properties tend to become



brittle, while AEMs with low dimensional stability often face issues during MEA fabrication. Several strategies have been explored to enhance the conductivity of AEMs without increasing the IEC too much. These strategies include phase separation, covalent crosslinking [66, 67], and increasing the number of positive charges on the side chain [48, 68]. Building a phase separation structure is an effective approach that has been proposed in recent works and has become the preferred option for developing AEMs with a low swelling ratio, low IEC, but high conductivity. While the ion mobility of hydroxide is lower than that of proton, it is still higher than that of other ions, such as carbonate and chloride. Therefore, if hydroxide transport can be improved, AEMs can still achieve sufficient ion conductivity for practical applications. The conduction of ions, such as OH<sup>-</sup>, relies on the presence of water, so the structure of hydrophilic domains in polymer electrolytes is a decisive factor for ion transport. Thus, building an ion transport highway by phase separation is a practical way to organize the structure of hydrophilic domains. For example, Nafion™ is believed to have such high conductivity due to its phase separation structure [69]. Nafion has a highly hydrophobic fluorocarbon backbone and hydrophilic flexible side chains containing the sulfonic acid functional group, which leads to hydrophobic/hydrophilic phase separation. The hydrophilic ion clusters/channels interact with each other, forming an ion transport highway. Although Nafion has a relatively low IEC (<1 mmol g<sup>-1</sup>), its conductivity is very high (more than 0.1 S cm<sup>-1</sup>, at 80°C in 100% RH).

Since the OH<sup>-</sup> transport mechanism is similar to that of proton [70], many researchers have adopted the phase separation structure to improve the conductivity of AEMs. Zhuang et al. reported three main strategies and methodologies for constructing an ionic highway, known as p-APE (APE stands for alkaline polymer electrolyte), t-APE, and a-APE, and subsequently developed aQAPS-S8 at 80°C, which conductivity exceeded that of Nafion 112 [71]. Michael A. Hickner et al. reported a multi-cation side chain AEM with triple-cation side chains and 5 or 6 methylene groups between cations, where phase separation was observed and the membrane exhibited high conductivity and excellent stability (93% retention) and ionic conductivity (90% retention) [72]. Xu et al. have reported AEMs with ethylene oxide spacer side chains, which has facilitated self-assembly of the ionic side chains to form continuous conducting channels, resulting in a significant boost in conductivity (65 mS cm<sup>-1</sup> at 60°C in OH<sup>-</sup> form) [73]. Finally, for AEMs with SEBS backbone, which exhibit lower conductivity than AEMs with other backbones, Bae et al. have used acid-catalyzed Friedel–Crafts alkylation for the side chains. These have resulted in a microphase-separated morphology on the 35 nm length scale of the hydrophilic domain. This microphase-separated morphology with functional groups away from the backbone not only improved the conductivity of the AEMs (41 mS cm<sup>-1</sup> at 60°C) but also exhibited excellent chemical stability (almost no loss in 1M KOH at 80°C for 800 hours) [74].

## 2.4 Principle of the AEM electrolysis

### 2.4.1 Traditional alkaline electrolysis

Traditional alkaline electrolysis is a commercially mature technology that is widely used and can reach MW scale [75-77]. It typically involves two electrodes immersed in a 20-30% KOH solution and a thin diaphragm that separates the production gases. The diaphragm allows OH<sup>-</sup> and water to pass through, but the technology faces three main challenges.

Firstly, the electrolyte is highly corrosive. Secondly, due to the low conductivity of the diaphragm,

the current density is typically lower compared to PEM electrolysis, and it is difficult to improve. Thirdly, the diaphragm cannot fully prevent the crossover of gases from one side to the other, leading to a decrease in cell performance due to the entry of hydrogen into the anode and the formation of water on the anode side. This issue is particularly prominent at low loads (<40%), where the production rate of O<sub>2</sub> is reduced, resulting in a dangerous concentration of H<sub>2</sub> crossover (lower explosion limit >4 mol% H<sub>2</sub>) when hydrogen diffuses to the oxygen evolution side. This makes traditional alkaline electrolysis difficult to coordinate with wasted green electricity, such as that produced by wind, solar, and hydropower which cannot always consistently produce energy at all hours of the day (intermittency of renewables).

#### 2.4.2 Proton exchange membrane (PEM) electrolysis

PEM electrolysis is a more recent and promising technology that has been applied in certain industrial fields. In PEM electrolysis, the catalysts used are typically IrO<sub>2</sub> and Pt/C, and there is a perfluorosulfonic PEM electrolyte between the electrodes instead of a liquid electrolyte. The cells and chemistries of PEM electrolysis are shown in Figure 2.4.1. Currently, PEM electrolysis can reach 2A cm<sup>-2</sup> at 50-80°C at about 2.1 V. Comparing PEM electrolysis to traditional alkaline electrolysis, PEM electrolysis has three main advantages:

- (1) The kinetics of the hydrogen evolution reaction (HER) in PEM electrolysis are faster than in alkaline electrolysis due to the low pH of the electrolyte and the high active metal surface of Pt electrodes.
- (2) Because there is no corrosive electrolyte, PEM electrolysis is believed to be much safer than traditional alkaline electrolysis and doesn't require corrosion protected Balance of Plant (BoP) components.
- (3) There is the possibility of having the cathode working in high pressure while the anode can still be operated at atmospheric pressure.

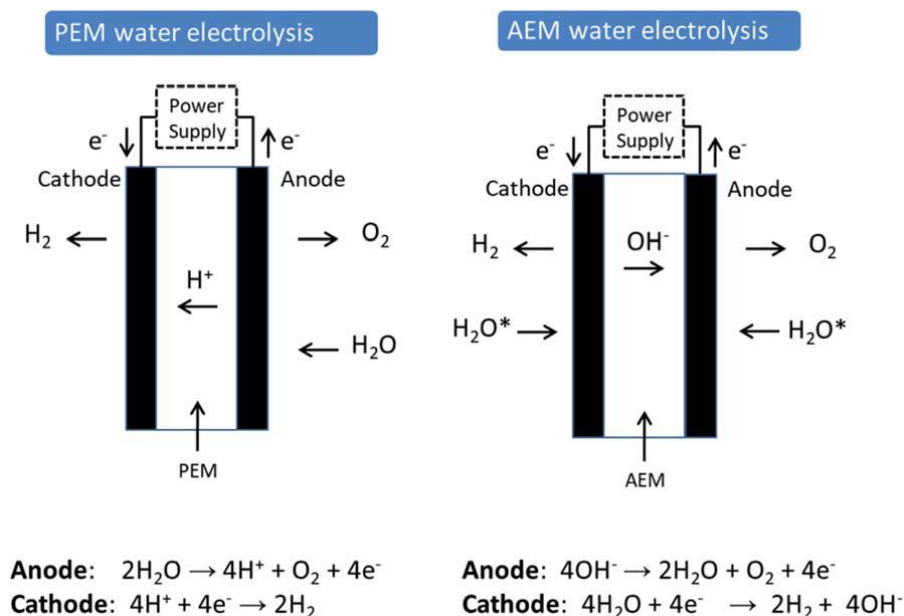


Fig 2.4.1 Comparison of water electrolysis cells and their electrochemical reactions using either a PEM or an AEM (H<sub>2</sub>O\* means it is water or alkaline solution) [11].

Despite its promising potential, the development of PEM electrolysis still faces significant

challenges. One major challenge is the highly corrosive acidic operating environment, which places stringent requirements on all cell materials. These materials must not only withstand the low pH environment, but also operate at high voltages (up to 2V) and high current densities. For example, the catalyst used in PEM electrolysis, such as Pt, Ru, and Ir, is limited to platinum group metals (PGMs) only. Additionally, current collectors and separator plates must be made of expensive titanium to prevent corrosion. However, iridium is a rare and expensive metal, which limits its availability and hinders the widespread adoption of PEM electrolysis. To overcome this challenge, alternatives to iridium must be developed to enable the further development and commercialization of PEM electrolysis.

#### 2.4.3 AEM electrolysis

AEM electrolysis is a promising technology because it can work at low electricity loads and use PGM-free catalysts. In the earlier stages of research, most efforts focused on developing HER and OER catalysts. Thus, due to the DOE AEM electrolysis projects in the USA and FCH-JU projects in the EU, the development of AEM electrolysis has been boosted, and single cell and stack operation have been conducted in both alkaline solution and pure water.

Compared with PEM electrolyzers, AEM contain a polymer backbone with positively charged functional groups. The biggest challenges faced by AEM electrolysis are:

- (1) Developing AEMs that are highly conductive and stable in alkaline environments.
- (2) Developing ionomers with high conductivity that can also resist radical attacks.
- (3) Developing PGM-free HER and OER catalysts with high performance and durability.

AEMs and ionomers are fundamental components in all parts of the electrolyzer for AEM electrolysis. As mentioned earlier, highly conductive and chemically stable AEMs are essential to achieve high-performance AEM electrolyzers. However, in the past few years, this has been a major limitation, and extensive research has been carried out to develop new anion exchange membranes with higher chemical stability in alkaline environments for use in electrochemical applications. The following section describes recent research on AEMs for AEM electrolysis.

Before 2010, the most widely used commercial AEM was A-201 Tokuyama. I. Dincer et al. have reported that AEM electrolysis with commercially available AEM A-201, ionomer AS-4, Pt black as the cathode catalyst, and IrO<sub>2</sub> as the anode catalyst achieving a current density of 0.399 A cm<sup>-2</sup> at 50°C in deionized water [78].

Table 2.1 State of the art literature reports of AEM electrolysis cell conditions and performance

Anode	Membrane	Cathode	Ionomer	Water feed	Cell Voltage (V)	Current density (A cm <sup>-2</sup> )	Cell Temperature (°C)	Ref
IrO <sub>2</sub>	A-201 Tokuyama	Pt black	AS-4	DI water	1.8	0.399	50	[78]
CuCoO <sub>3</sub>	A-201 Tokuyama	NiCeO <sub>2</sub> -La <sub>2</sub> O <sub>3</sub> /C	PTFE	1% K <sub>2</sub> CO <sub>3</sub> /KHCO <sub>3</sub>	1.9	0.47	50	[79]
Pb <sub>2</sub> Ru <sub>2</sub> O <sub>6.5</sub>	Chloromethylated PSF	Pt black	PSF-TMA <sup>+</sup> Cl <sup>-</sup>	Ultrapure water	1.8	0.4	50	[80]
Ni-Fe	xQAPS	Ni-Mo	xQAPS	Ultrapure water	1.85	0.4	70	[81]
CuCoO <sub>x</sub>	A-201 Tokuyama	Pt/C	AS-4	K <sub>2</sub> CO <sub>3</sub> 10%	1.95	1	50	[82]
IrO <sub>2</sub>	FAA-3-50	Pt/C	FAA-3-Br	1M KOH	1.9	1.5	70	[83]
NiFeO <sub>x</sub> :Fe	FAA-3	Pt black	FAA-3	Pure water	2.25	0.8	50	[84]
Ni	A-201 Tokuyama	Ni	-	1M KOH	1.9	0.15	50	[85]
CuCoO <sub>3</sub>	LDPE-g-VBC	Ni/CeO <sub>2</sub> -La <sub>2</sub> O <sub>3</sub> /C	PTFE	1% K <sub>2</sub> CO <sub>3</sub> /KHCO <sub>3</sub>	2.1	0.46	50	[86]
Cu <sub>0.7</sub> Co <sub>2.3</sub> O <sub>4</sub>	QPDTB	Nano Ni	Poly (DMAEMA-co-TFEMA-co-BM)	DI water	1.9	0.1	50	[87]
CuCoO <sub>3</sub>	Mg-Al layered double hydroxide	Ni/CeO <sub>2</sub> -La <sub>2</sub> O <sub>3</sub> /C	PTFE	1% K <sub>2</sub> CO <sub>3</sub> /KHCO <sub>3</sub>	2.2	0.28	70	[88]
Ce <sub>0.2</sub> MnFe <sub>1.8</sub> O <sub>4</sub>	FAA-3-PK-130	Pt on Ti	-	DI water	1.8	0.3	-	[89]
Pd/TNTAweb	A-201 Tokuyama	Pt/C	PTFE	2M NaOH	2	2	80	[90]
CuCoO <sub>x</sub> (on Ni foam)	A-201 Tokuyama, FAA-3, FAA-3-PP-75	Ni/CeO <sub>2</sub> -La <sub>2</sub> O <sub>3</sub> /C on carbon paper	I2	1% K <sub>2</sub> CO <sub>3</sub>	1.95	0.5	60	[91]
NiCo <sub>2</sub> O <sub>4</sub>	Polyethylene based radiation grafted	Pt	SEBS	0.1M KOH	1.65	0.1	60	[92]
Cu <sub>x</sub> Co <sub>3-x</sub> O <sub>4</sub>	PTFE based	Pt/C	q-ammonium polymethacrylate	DI water	1.6	0.1	22	[93]

NiFeO <sub>4</sub>	Sustanion 37-50	NiFeCo	Nafion	1M KOH	1.9	1	60	[94]
NiAl	HTM-PMBI	NiAlMo	-	1M KOH	2.1	2	60	[95]
IrO <sub>2</sub>	HTMA-DAPP	PtRu/C	TMA-53	DI water	2	1.6	85	[96]
NiCo <sub>2</sub> O <sub>4</sub>	PSEBS-CM-DABCO	NiFeO <sub>4</sub>	PSEBS-CM	10wt% KOH	2	0.13	40	[97]
IrO <sub>2</sub>	SEBS-Pi	Pt/C	CMSEBS	5.6wt% KOH	2	0.4	50	[88]
IrO <sub>2</sub>	SEBS-P2O6	Pt/C	SEBS-TMA	0.1M KOH	2	0.680	60	I
IrO <sub>2</sub>	SEBS-P2O6	Pt/C	SEBS-TMA	Ultrapure water	2	0.275	60	I
OXYGEN-N	SEBS-Py2O6	H2GEN-M	SEBS-TMA	0.1M KOH	2	0.520	60	II, III
OXYGEN-N	SEBS-Py2O6	H2GEN-M	SEBS-TMA	Ultrapure water	2	0.171	60	II, III

Zhuang et al. have reported the use of a new type of AEM, ionomer, and non-precious metal catalysts for a MEA, which has enabled the electrolyzer to work only with pure water. The MEA has been constructed by placing a self-crosslinking quaternary ammonium polysulfone (xQAPS) membrane between a Ni-Fe anode and a Ni-Mo cathode, both impregnated with xQAPS ionomer. The cell exhibited a performance of about 1.8-1.85 V at 70°C under a current density of 0.4 A cm<sup>-2</sup>. This initial prototype of AEM water electrolysis demonstrated better performance compared to the well-developed alkaline water electrolyzer at that time [81].

Yu Seung Kim et al. have reported the development of an ammonium-enriched anion exchange ionomer, which significantly improved the performance of an AEM electrolyzer, approaching that of state-of-the-art proton exchange membrane electrolyzers. Through rotating-disk electrode experiments, they discovered that a high pH (>13) in the electrode binder is a critical factor for enhancing the activity of the hydrogen- and oxygen-evolution reactions in AEM electrolyzers. Based on this finding, they prepared and tested several quaternized polystyrene electrode binders in an AEM electrolyzer. Using the binder with the highest ionic concentration and a NiFe oxygen evolution catalyst, they have demonstrated a performance of 2.7 A cm<sup>-2</sup> at 1.8 V without using a corrosive alkaline solution. However, the limited durability of the AEM electrolyzer remains a challenge that needs to be addressed in the future [96].

Martin Paidar et al. reported a novel alkaline polymer electrolyte membrane based on SEBS functionalized by 1,4-diazabicyclo [2.2.2] octane (DABCO) for use as an electrode compartment separator and catalytic layer binder in the AEMWE. The aim has been reducing the concentration of KOH in the liquid electrolyte and to construct an efficient zero gap-type cell. This material has been chosen due to the promising properties of both individual components resulting from their molecular structure. The polymer electrolyte has been tested in a laboratory alkaline water electrolyzer using 10 wt.% KOH as a circulating medium, showing promising current density of 150 mA cm<sup>-2</sup> at 40°C. In a 150-hour experiment, the SEBS functionalized by DABCO has showed very good stability and high potential for optimization for this process, without any signs of chemical

degradation [97].

Mohamed Mamlouk has reported a SEBS-based soluble anion exchange ionomer with high OH<sup>-</sup> conductivity comparable to the proton conductivity of Nafion. The TMA-functionalized SEBS-based ionomer has been used with NiCo<sub>2</sub>O<sub>4</sub> PGM-free catalysts for water electrolysis. The ionomer has shown an ion exchange capacity of 1.9 mmol g<sup>-1</sup> and an ionic conductivity of 0.14 S cm<sup>-1</sup> at 50°C. The cell performance was improved to 1.65 V at 100 mA cm<sup>-2</sup> at 60°C in 0.1 M KOH with CCS MEA and 10 mg cm<sup>-2</sup> NiCo<sub>2</sub>O<sub>4</sub> catalyst loading. However, the cell showed limited performance when operating with deionized water compared to PEM and alkaline electrolyzers [92].

Yan et al. have reported a novel piperidinium-functionalized SEBS (SEBS-Pi) alkali membrane to improve the low efficiency and durability of AEMWE. The membrane not only displayed high conductivity (> 10 mS cm<sup>-1</sup> at 30°C), but also possessed excellent thermal stability and mechanical properties. A good performance of water electrolysis has been achieved (400 mA cm<sup>-2</sup> at 2 V, 50°C). During a long-term electrochemical stability test carried out with a current density of 400 mA cm<sup>-2</sup> at 50 °C for 105 h, the voltage has remained almost constant (around 2.08 V), indicating good cell durability [88].

## 3 Materials and Characterization Techniques

### 3.1 Chemicals

Materials used in this thesis work are mentioned in the following table

Material	Specification	Supplier	Used in Article
SEBS	30%wt styrene	TSRC cooperation	I , II , III
Tin (IV) Chloride	1M in dichloromethane	Merck	I , II , III
Chloroform	≥ 99%	Merck	I , II , III
1,3,5-Trioxane	For synthesis	Merck	I , II , III
Chlorotrimethylsilane	≥ 98%	Merck	I , II , III
Acetone	≥ 99.5%	Merck	I , II , III
Ethanol	≥ 99%	Merck	I , II , III
p-Xylene	≥ 99%	Merck	I
Piperidine	For synthesis	Merck	I , II
Pyrrrolidine	99%	Merck	II , III
N, N, N', N'-Tetramethyl-1,6-hexandiamine	99%	TCI	I
N, N, N', N'-Tetramethyl-1,4-butandiamine	98%	TCI	I
N, N, N', N'-Tetramethyl-1,3-propandiamine	≥ 99%	TCI	I
1,6-dibromohexane	96%	TCI	I , II , III
Anhydrous pottassium carbonate	≥ 99%	Merck	I , II , III
Dichloromethane	≥ 99%	TCI	I , II , III
Trimethylamine	≥ 43%-49% in water	Merck	I , II , III
Acetonitrile	≥ 99.5%	TCI	I , II , III
Dimethyl sulfoxide-d <sub>6</sub>	≥ 99.9% atom D	Merck	I , II , III
CDCl <sub>3</sub>	≥ 99.8% atom D	Merck	I , II , III
Sodium chloride	≥ 99%	Merck	I , II , III
Potassium hydroxide	≥ 85%	Merck	I , II , III

---

Hydrochloric acid	ACS reagents, 37%	Merck	I , II
Ultrapure water	HPLC grade	Alfa Aesar	I , II , III
Pt/C	40% wt Pt	Merck	I
Ir black	-	Merck	I
Tetrahydrofuran	≥ 99.5%	Merck	I , II , III

## 3.2 Characterization Techniques

### 3.2.1 Nuclear magnetic resonance (NMR) spectroscopy

NMR spectroscopy is a technique used to observe local magnetic fields around atomic nuclei. This spectroscopy is based on the measurement of the absorption of electromagnetic radiation in the radio frequency region, typically ranging from 4 to 900 MHz. The absorption of radio waves in the presence of a magnetic field is accompanied by a specific type of nuclear transition, which is why this spectroscopy is referred to as Nuclear Magnetic Resonance Spectroscopy.

In this dissertation, NMR was utilized to analyze the chemical structure of the membrane. The Bruker Avance III HD 400 NanoBay NMR spectrometer was employed to measure the  $^1\text{H}$  and  $^{13}\text{C}$  NMR spectra of the polymer at room temperature, using either DMSO- $d_6$  or  $\text{CDCl}_3$  as solvents, with tetramethylsilane (TMS) serving as the internal reference.

### 3.2.2 Fourier-transform infrared spectroscopy (FT-IR)

FT-IR is a technique utilized to obtain the infrared absorption or emission from a solid, liquid, or gas. An FT-IR spectrometer simultaneously collects high-resolution spectral data across a broad spectral range. This provides a significant advantage over dispersive spectrometers, which measure intensity within a narrow range of wavelengths at a time.

In this dissertation, specific changes in chemical bonds within the membrane were detected using FT-IR. A Nicolet iS5 spectrometer (ThermoFisher Scientific, Karlsruhe, Germany) equipped with a diamond attenuated total reflectance (ATR) module was employed to record FT-IR spectra of the membranes. The spectra were obtained with 64 scans in the wavenumber range of 4000 to 400  $\text{cm}^{-1}$ .

### 3.2.3 Atomic force microscope (AFM)

AFM is a type of scanning probe microscopy (SPM) that demonstrates resolution on the order of fractions of a nanometer, surpassing the optical diffraction limit by more than 1000 times. It gathers information by physically "feeling" or "touching" the surface with a mechanical probe. Precise scanning is achieved through the use of piezoelectric elements that enable accurate and precise movements based on electronic commands. Despite its name, the Atomic Force Microscope does not utilize the nuclear force.

In this dissertation, phase separation in various membranes was investigated using AFM. The Icon XR system (Bruker Karlsruhe, Germany) was employed to conduct atomic force microscopy in



PeakForce Tapping Mode, allowing for the measurement of nanomechanical properties of the membranes. At each measurement point, the AFM mode records and analyzes force-distance curves. Height, adhesion, stiffness, and deformation were measured simultaneously. Bruker Scanasyt-Air tips ( $k = 0.4 \text{ N m}^{-1}$ ) with a tip radius of 2 nm were utilized. The membranes were affixed to 15 mm AFM steel discs using adhesive carbon tape (Plano) and measured under ambient conditions. The image size for all membranes was  $1 \mu\text{m}^2$ , measured at 0.977 Hz with 512 x 512 pixels.

### 3.2.4 Membrane conductivity

Ion conductivity refers to the mobility of the ions within membranes and is considered as one of the most crucial properties of the membrane. In this dissertation, the through-plane conductivity of the membrane was measured using a Teflon contact cell and the four-electrode method. The electrodes were composed of gold (Au), and an IM6 device from Zahner elektrik (Zahner-elektrik GmbH, Kronach, Germany) was utilized to perform electrochemical impedance spectroscopy, measuring the membrane resistances in a 1 M NaCl solution or 1 M KOH at room temperature. By analyzing the intersection of the impedance curve with the x-axis, the resistance was determined in the frequency range of 200 kHz to 8 MHz. As our setup did not include  $\text{CO}_2$  removal, the  $\text{OH}^-$  conductivity was immediately measured after converting the membrane to its  $\text{OH}^-$  form. Four samples were collected for each membrane. The conductivity was calculated using Equation (1) as shown below.

$$\sigma = \frac{1}{R_{sp}} = \frac{d}{R \times A} \quad (1)$$

where  $\sigma$  is the conductivity ( $\text{S cm}^{-1}$ ),  $R_{sp}$  is the resistivity ( $\Omega \text{ cm}$ ),  $d$  is the thickness of membrane (cm),  $R$  is the ohmic resistance ( $\Omega$ ), and  $A$  is the electrode area ( $\text{cm}^2$ )

### 3.2.5 Water uptake and swelling ratio

Water uptake and swelling ratio refer to the changes in weight and dimensions when dry membranes fully absorb water. The swelling ratio can serve as an indicator of the dimensional stability of the membranes and is closely related to the process of fabricating the membrane-electrode assembly (MEA).

In this dissertation, the weight and dimensional differences of the membranes were measured after immersing them in deionized water at room temperature for 48 hours and subsequently drying them in a vacuum oven at  $60^\circ\text{C}$  for 24 hours. These measurements were used to calculate the water uptake (WU) and swelling ratio (SR) in the  $\text{Cl}^-$  form. The water uptake is calculated using Equation 2 as follows:

$$\text{WU}\% = \left[ \frac{(m_{\text{wet}} - m_{\text{dry}})}{m_{\text{dry}}} \right] \times 100 \quad (2)$$

where  $m_{\text{wet}}$  and  $m_{\text{dry}}$  are the weight of wet and dry membranes in  $\text{Cl}^-$  forms in grams, respectively.

The SD was calculated by the equation 3 as follows:

$$SD\% = \frac{(l_{wet} - l_{dry})}{l_{dry}} \times 100 \quad (3)$$

where  $l_{wet}$  and  $l_{dry}$  are the geometric length of the wet and dry membranes in  $Cl^-$  forms, respectively.

### 3.2.6 Ion Exchange Capacity (IEC)

The ion exchange capacity (IEC) was determined using a back-titration method. The membrane sample was immersed in a 1M NaOH solution, washed with deionized (DI) water, and then soaked in a sodium chloride solution at room temperature for 1 day. Afterward, the membranes were removed from the solution. A standard hydrochloric acid solution (3 mL, 0.1 M) was added, and the mixture was stirred at room temperature for 1 day. The resulting solution was titrated with a standard 0.1 M sodium hydroxide solution. The membrane was thoroughly washed with DI water and dried overnight at 90°C. The dry weight of the membrane was then determined using a balance. The IEC was calculated using equation (4).

$$IEC = \frac{C_{HCl} \times V_{HCl} - C_{NaOH} \times V_{NaOH}}{m_{dry}} \quad (4)$$

where IEC is the ion exchange capacity ( $Cl^-$  form,  $mmol\ g^{-1}$ ),  $C_{HCl}$  is the concentration of the hydrochloric acid solution ( $mmol\ mL^{-1}$ ),  $V_{HCl}$  is the volume of the hydrochloric acid solution used (mL),  $C_{NaOH}$  is the concentration of the sodium hydroxide solution ( $mmol\ mL^{-1}$ ),  $V_{NaOH}$  is the added volume of the sodium hydroxide solution (mL), and  $m_{dry}$  is the dry weight of the membrane (g).

### 3.2.7 Chemical stability of the membranes

The chemical stability was evaluated by immersing several pieces of membrane in a 1 M KOH solution at 90°C for 30 days. Prior to immersion, the membrane pieces were extensively washed with water for one day. They were then placed in an oven at 90°C within the alkaline solution. Every 5 days during the test, a small piece of membrane was cut for conductivity testing, and fresh KOH solution was replaced. Subsequently, the membranes were thoroughly rinsed with deionized water before being tested for  $OH^-$  conductivity. The conductivity retention rate (CR%) of the membrane was calculated using the following equation.

$$CR\% = \frac{\sigma_1}{\sigma} \times 100 \quad (5)$$

where  $\sigma$  is the conductivity of the membrane before treatment in KOH,  $\sigma_1$  is the conductivity after treatment in KOH.

### 3.2.8 Fabrication of Membrane Electrode Assemblies (MEAs) for AEMWEs

Catalyst-coated substrates (CCS) were prepared by manually spraying H<sub>2</sub>GEN-M and OXYGN-N catalysts (bought from CENMat) onto carbon paper substrates. Chloromethylated SEBS (cmSEBS) was used as the ionomer precursor and dissolved in tetrahydrofuran.

The catalyst suspensions were then prepared using isopropanol and ultra-pure water as solvents, maintaining an ionomer to catalyst ratio of 3:7. CCSs with an active area of 4 cm<sup>2</sup> and certain catalyst loading (anode with OXYGEN-N and cathode with H2GEN-M catalyst) were fabricated. These CCSs were immersed in a 500 mL trimethylamine solution overnight to convert the cmSEBS binder to ammonium SEBS. Subsequently, the CCSs were thoroughly washed with ultra-pure water and submerged in a 1 M KOH solution at room temperature for 15 hours to convert the chloride anion to the hydroxide anion. Finally, the membranes were rinsed with water before assembly.

A similar procedure was followed to prepare CCSs for testing in ultra-pure water (UPW). In this case, the previously in situ activated CCS in 0.1 M KOH was flushed with UPW for half an hour until the outlet of the anion exchange membrane water electrolyzer (AEMWE) reached a neutral pH.

### 3.2.9 AEMWE Cell Test

The anion exchange membrane water electrolyzer (AEMWE) cell was constructed using titanium bipolar plates (BPPs) and porous transport layers (PTL) consisting of a Ti porous sintered layer (PSL) on a Ti mesh (PSL/mesh-PTL) (GKN Sinter Metals), as well as carbon paper for both the cathode and anode (carbon paper on anode for comparison). Different cell assemblies were achieved by tightly packing the catalyst-coated substrates (CCSs) together with the SEBS-Py206/SEBS-P2O6 membrane. The membrane was immersed in a 1 M KOH solution for 15 hours and then thoroughly rinsed with deionized water. The cell was closed by applying a torque of 0.6 N m to four screws. Subsequently, the cell was ready for testing, and a continuous flow of N<sub>2</sub> at a rate of 1 L/min was bubbled into the electrolyte (either 0.1 M KOH or ultra-pure water) in a closed-loop system. This was done to remove dissolved CO<sub>2</sub> from the water, prevent the formation of precipitates, and maintain the chemical and mechanical integrity of the membrane. However, it should be noted that contact with ambient air/CO<sub>2</sub> cannot be completely eliminated during the cell assembly preparation and activation steps.

The electrochemical characterization was conducted using a Zahner Zennium Pro electrochemical workstation (potentiostat/galvanostat), with a Zahner PP24 booster employed to achieve currents over 4 A. The cell was initially conditioned in-situ in a 0.1 M KOH solution at 60°C. The potential was monitored as a function of current density, with dwell times of 120 s and small current increments of 50 mA cm<sup>-2</sup> and then 150 mA cm<sup>-2</sup> until reaching 1 A cm<sup>-2</sup>. Five polarization curves were obtained in potentiostatic mode, ranging from 1.3 V to 2.5 V, using a scan rate of 20 mV s<sup>-1</sup> in the 0.1 M KOH electrolyte at 60 °C. An electrochemical impedance spectrum (EIS) was recorded in galvanostatic mode at 200 mA cm<sup>-2</sup>, using an amplitude of 20 mA in the frequency range of 100 MHz to 1 kHz. The cell assembly was then purged with pure water flowing for 30 minutes, and the electrochemical characterization steps were repeated at 60°C using ultra-pure water (UPW) as the electrolyte at a neutral pH.

## 4. Discussion

### 4.1 Conductivities of Piperidinium/Pyrrolidinium Functionalized Membranes Based on SEBS

In this paper, SEBS copolymer is chosen as the backbone for the preparation of AEMs. SEBS copolymer contains ethylene and butadiene as the flexible blocks as well as styrene as the rigid blocks. Therefore, SEBS-based AEMs have high alkaline stability (ether free) and good flexibility which is quite important character to the AEMs. However, AEMs based on ammonium functionalized SEBS always possess lower conductivity due to the relatively low degree of functionalization and respectively low IEC. In the past, to improve the conductivity, several strategies have been tried, such as building a comb-shaped structure, having multi-cation side chains, and crosslinking with backbones being additionally functionalized. Among them, using a comb-shaped structured polymers could induce formation of the micro-phase separation which often enhances the conductivity of the membrane. In our first part, a piperidinium-functionalized flexible ethylene oxide spacer structure was applied as a crosslinker in the presence of trimethylamine to convert the chloromethyl group to a functional membrane. By polymer modification, several polymer structures were designed and synthesized to build the phase separation structure. Polymer modification in this part of work comprises two parts: chloromethylation and quaternization. For the chloromethylation, the chloromethylation rate of SEBS is 83.5%. Subsequently, cmSEBS reacted with some side chain agents such as mP2C6 and trimethylamine. Finally, SEBS-based AEMs have relatively high alkaline conductivity reaching 20.8 mS cm<sup>-1</sup> at room temperature with an IEC of 1.05 mmol g<sup>-1</sup>.

However, this strategy also brought some drawbacks. Firstly, the crosslinkers reduce the IECs of the membranes rapidly and thus lose the advantage of the multi-cation side-chain structure. Secondly, functionalization by post treatment may decrease the mechanical stability of the membrane and make the membrane brittle. And third, benzyl ammonium group is known to have inferior stability which may lead to the degradation in alkaline solution. Therefore, in second part of membrane work we chose a functionalized flexible ethylene oxide spacer structure with a pre-functionalized end (of which one end of the diamines was quaternized by iodomethane before) and removed all the benzyl ammonium groups in the structure. The whole synthesis process was listed below: the first diamines (P2C6 and P2O6) were reacted with iodomethane to get unsymmetrical one-end quaternate amine-ammonium precursors (pre-functionalized end) (mP2C6/mP2O6). Subsequently, both cmSEBS and mP2C6/mP2O6 were dissolved to prepare the final membrane. The IECs of the membranes SEBS-P2C6 and SEBS-P2O6 are higher than the membranes SEBS-P2C6-TMA and SEBS-P2O6-TMA. However, the IECs of SEBS-P2C6 and SEBS-P2O6 are much lower than the fully functionalized membranes (IEC in theory is 2.7 mmol g<sup>-1</sup>), which is probably due to charge repulsion between the charged side chains and the charged polymer product, even though the amine-ammonium precursors are in excess. Due to the higher IEC, the conductivity of the SEBS-

P2C6 and P2O6 improved a lot, reaching  $17.5 \text{ mS cm}^{-1}$  and  $25 \text{ mS cm}^{-1}$  at RT, which is higher than SEBS-based piperidinium-functionalized membrane published before.

Table 4.1 State of the art literature reports of AEM IEC and ion conductivity

Membranes	IEC (Meq g <sup>-1</sup> )	Ion Conductivity (mS cm <sup>-1</sup> )
Fumasep® FAA-3-30	1.7-2.1	4-7 (Cl <sup>-</sup> )
A201	1.8	42 (OH <sup>-</sup> )
Aemion™	2.1-2.5	>80 (OH <sup>-</sup> )
AF1-HNN8-50-X		
Sustanion® 37-50	NA	80 (OH <sup>-</sup> )
Orion TM1	2.19	19(Cl <sup>-</sup> ) 54 (OH <sup>-</sup> )
SEBS-TMHA	2.01	9(Cl <sup>-</sup> ) 39(OH <sup>-</sup> )
SEBS-Pi	1.19	10.09 (OH <sup>-</sup> )
SEBS-P2O6*	1.05	11.7 (Cl <sup>-</sup> ) 20.8 (OH <sup>-</sup> )
SEBS-Py2O6*	1.4	14.1 (Cl <sup>-</sup> ) 27.8 (OH <sup>-</sup> )

As is shown in Table 4.1, For all membranes in this dissertation (SEBS-P2O6 and SEBS-Py2O6), Cl<sup>-</sup> conductivity is about twice lower than OH<sup>-</sup> conductivity, which is due to larger and heavier Cl<sup>-</sup> ion compared to OH<sup>-</sup>. In this dissertation, the ratios of OH<sup>-</sup> to Cl<sup>-</sup> conductivities are slightly lower than the reported Cl<sup>-</sup> and OH<sup>-</sup> conductivity ratio ( $\sigma_{\text{OH}^-}/\sigma_{\text{Cl}^-} \sim 2.7$ ) in the literature. However, this difference may be accounted by residual CO<sub>2</sub> present in our case for the OH<sup>-</sup> value although care was taken to perform the test immediately after removal from KOH solution. That is the reason why SEBS-Py2O6 has highest Cl<sup>-</sup> conductivity in all SEBS membranes but much lower OH<sup>-</sup> conductivity than SEBS-TMHA.

To investigate the relationship between AEM with different side chain structures and their properties, different side chain structures were designed, synthesized and investigated in this dissertation. SEBS-P2O6 and SEBS-Py2O6, containing long flexible and hydrophilic side chains, their hydrophobic and hydrophilic domains formed broader continuous phases than those in SEBS-P2C6 and SEBS-Py2C6, the broader and better interconnected hydrophilic domains of SEBS-P2O6 and SEBS-Py2O6 facilitate the formation of continuous ion channels of relatively constant size, which enables efficient ion transport and exhibits higher conductivity.

Comparing with commercial membranes, the conductivity of SEBS based AEMs including our work, were still lower than most of commercial membranes, such as Aemion™ AF1-HNN8-50-X and Sustanion® 37-50. But the conductivity has been improved a lot recently and considering their good alkaline stability and flexibility, SEBS based AEMs are a promising candidate for AEM electrolysis.

## 4.2 AEM Water Electrolysis Measurements

Considering the benefits of using piperidinium/pyrrolidinium based ethylene oxide spacers side chain and balancing the conductivity and chemical stability of the membranes, SEBS-P2O6 and SEBS-Py2O6 membranes are expected to achieve improved AEM water electrolysis performance and durability. In this dissertation, SEBS-Py2O6/SEBS-P2O6 based membranes and the ionomer were tested in a AEMWE cell using commercially available PGM catalyst (first part) or OXYGN-N, H2GEN-M catalysts (second and third part), respectively. In the whole dissertation, the cell performance at 60°C in 0.1 M KOH was measured via polarization curves after performing a potentiostatic conditioning. In first part, the cell was thorough purged with UPW and a current density of 275 mA cm<sup>-2</sup> at 2 V was reached. In the following degradation test, current density fell at a rate of 140 μA h<sup>-1</sup> cm<sup>-2</sup>, which is the lowest reported up to know. During the test, degradation was caused solely by an increase in HFR resistance, leading to the conclusion, that the reduction of current density is largely caused by ionomer and AEM breakdown, or other phenomena affecting the HFR resistance only. In a separate test in first part, cell performance and degradation at 60°C in 0.1 M KOH was evaluated. A steady-state was reached quickly and largely linear degradation (approximately 1 mA h<sup>-1</sup> cm<sup>-2</sup>) ensued. Initially, a current density of 680 mA cm<sup>-2</sup> was reached at 2 V, significantly outpacing published results recorded using similar materials in AEMWE. It is proved that the physical breakdown of the catalyst layer mainly dictates cell behavior in 0.1 KOH, not the breakdown of the ionic conductivity of the AEM and ionomer.

In second part, a current density of 520 mA cm<sup>-2</sup> was reached at 2 V, which unveils a potential for future applications of the SEBS-Py2O6 membrane and SEBS-TMA ionomer for AEMWE with PGM-free catalysts. Although the use of PGM-free materials in UPW operation is the most wanted option to improve AEM electrolysis competitively, new challenges arise, primarily concerning the lower conductivity of membranes and considerably slower kinetics of the catalysts at neutral pH. In this regard, the AEMWE was tested using UPW as liquid electrolyte to unveil the effect of the spacer addition on the retention capacity of the hydroxyl ion of the membrane and ionomer. After retrieving several polarization curves, the cell did not display any signs of performance decay since no hysteresis could be seen; remarkably, a stable current density of 171 mA cm<sup>-2</sup> could be achieved at 2 V and 60°C with UPW feed. This result is promising since the AEMWE cell outperforms previously reported AEMWE with piperidinium-functionalized SEBS. It is possible that the overall hydroxyl ion conductivity and retention could be increased by the addition of the flexible ethylene oxide spacers in the formulation developed herein. Therefore, it could be confirmed that the SEBS-Py2O6-based AEM/AEI is able to retain its OH<sup>-</sup> conductivity at not only high temperatures, i.e., at 60°C, in 0.1 M KOH but also in pH-neutral media, which poses a versatile option in AEM electrolysis since the possibility of eliminating KOH-based electrolytes is highly anticipated to lower operation expenditure of the technology.

## 5. Conclusion

This cumulative dissertation presents a comprehensive investigation of the new membrane electrode assembly (MEA) design and cell components for AEM electrolysis applications. The work comprises two sections focusing on different AEMs and optimization of cell components, including MEA fabrication methods. The objective of the dissertation is to select optimized materials for our AEM electrolysis cell tests, with the potential for future implementation at an industrial level.

In the first part of this research, a novel flexible ethylene oxide spacer side chain SEBS AEM functionalized with double piperidinium groups was designed, synthesized, and applied as a membrane for AEMWE applications. To improve the membrane conductivity, a comb-shaped structure with multifunctional groups was incorporated, and it was found that a longer spacer (-C6H12-) between functional groups provided a relatively balanced conductivity and chemical stability. Additionally, the substitution of quaternary ammonium with piperidinium groups enhanced the membrane's chemical stability. The flexible ethylene oxide spacer in the side chain promoted water uptake and microphase separation, resulting in improved conductivity. Ultimately, the SEBS-P2O6 membrane achieved a conductivity of  $20.8 \text{ mS cm}^{-1}$  ( $\text{OH}^-$ ) at room temperature, surpassing previously published SEBS piperidinium membranes.

In single-cell AEM water electrolysis tests, conducted at  $60^\circ\text{C}$  with a cell potential of 2 V, current densities of  $275 \text{ mA cm}^{-2}$  and  $680 \text{ mA cm}^{-2}$  were achieved in ultra-pure water (UPW) and 0.1 M KOH, respectively. These results demonstrate that the SEBS-P2O6 membrane outperforms other SEBS-based materials reported in the literature, highlighting SEBS as a promising candidate for AEM electrolysis cells.

In the second part of the dissertation, a novel piperidinium-functionalized flexible ethylene oxide spacer side-chain SEBS AEM was designed, synthesized, and utilized as a membrane for AEMWE. To enhance the membrane conductivity, a comb-shaped structure with multifunctional flexible ethylene oxide spacer side chains was synthesized and investigated. It was discovered that the inclusion of flexible ethylene oxide side chains as spacers in the comb-like structures promoted microphase separation in the membrane morphology, optimizing water uptake and enhancing ion conductivity.

Furthermore, the introduction of pre-functionalized ends on each side chain positively affected the ion exchange capacity (IEC) of the AEM, thereby improving ion conductivity. AEMs with piperidinium-end flexible ethylene oxide spacer side chains exhibited relatively higher conductivity ( $25 \text{ mS cm}^{-1}$ ,  $\text{OH}^-$  form at room temperature) and chemical stability (nearly 95% conductivity retention after 720 hours in 1 M KOH). Additionally, pyrrolidinium functional groups were introduced to enhance alkaline stability. SEBS-Py2O6 achieved a conductivity of  $27.8 \text{ mS cm}^{-1}$  ( $\text{OH}^-$ ) at room temperature, surpassing previously published SEBS piperidinium/pyrrolidinium membranes.

In single-cell AEM water electrolysis tests with PGM-free catalysts (OXYGN-N and H2GEN-M) at  $60^\circ\text{C}$ , current densities of  $171 \text{ mA cm}^{-2}$  at 2 V cell potential and  $520 \text{ mA cm}^{-2}$  at 2 V in ultra-pure water (UPW) and 0.1 M KOH, respectively, were achieved. These results demonstrate that the SEBS-Py2O6 membrane outperforms SEBS-based membranes reported in the literature for AEMWE in pure water. Additionally, when combined with PGM-free electrodes in AEMWE cells, SEBS-Py2O6 exhibits promising potential as a candidate for AEM water electrolysis cells.

In the third part of the dissertation, a novel MEA fabrication strategy was introduced, enabling effective  $\text{OH}^-$  transport pathways during AEMWE cell operation by extending the electrical contact with the aqueous electrolyte and potentially enhancing ion capacity retention. The study revealed several crucial observations:

Firstly, stainless steel felts-based CCSs outperformed CCM configurations, likely due to the loss of mechanical integrity during CCM preparation using conventional gun spraying at  $50^\circ\text{C}$  on pre-heated plates.

Secondly, I/C ratios of 20% were found to be pivotal in extending the number of triple-phase boundaries and improving AEMWE performance.

Thirdly, cell operations at  $85^\circ\text{C}$  delivered higher performances but exhibited less stability compared to operations at  $60^\circ\text{C}$  during long-term tests.

The best performance in ultra-pure water (UPW) was achieved using  $\text{IrO}_2|\text{Pt}/\text{C}$  catalysts with SEBS-Py2O6 AEM and AEI at  $1\text{ A cm}^{-2}$  and  $2\text{ V}$  at  $60^\circ\text{C}$ , surpassing commercial Sustainion-based MEAs. An entirely PGM-free cell achieved unprecedented current densities of approximately  $0.8\text{ A cm}^{-2}$  at  $2\text{ V}$  and  $60^\circ\text{C}$  in UPW with the novel membrane configuration.

Lastly, the most stable AEMWE cell in UPW reported in this study utilized PGM-free catalysts ( $\text{NiFeOx}|\text{Mo}_2\text{C}$ ) along with the novel SEBS-Py2O6 membrane and ionomer. It exhibited the lowest degradation rate, approximately  $3\text{ mV h}^{-1}$  for equivalent systems, and demonstrated stability for approximately 85 hours in pH-neutral operation.

These findings underscore the potential to optimize this system and enhance hydrogen production efficiency through sustainable approaches.



## 6. General Outlook

The aforementioned studies and experiences prompt us to discuss potential improvements in AEM electrolyzer MEA and cell components in order to achieve higher performance and durability.

In the first part of the dissertation, a SEBS-based piperidinium-functionalized AEM was synthesized and utilized for AEM electrolysis. The cell demonstrated satisfactory performance in both alkaline and pure water conditions. However, during practical application, several weaknesses were identified in the membrane synthesis and fabrication process. To address these issues, improvements were attempted in the second part of the thesis. Firstly, in the initial approach, piperidinium-functionalized ethylene oxide spacers were designed as crosslinkers, with both ends attached to the backbone. This design resulted in a limited IEC of the AEM. Consequently, in the second part, a pre-functionalized end structure was devised to increase the IEC of the AEM. Secondly, a portion of the functional groups used was benzyl trimethyl ammonium, which was found to be relatively unstable. In the second part, all the benzyl trimethyl ammonium groups were replaced with more stable piperidinium/pyrrolidinium groups. Thirdly, functionalization was initially performed through post-treatment. However, it was observed that the mechanical properties of the AEM might deteriorate during this process. Therefore, an alternative approach was explored, involving functionalization of the membrane during the solvent evaporation process. By addressing these concerns and implementing the proposed improvements, we aim to enhance the overall performance and reliability of AEM electrolyzers.

By implementing the improvements mentioned above, the AEMs in the second part demonstrated better performance compared to those in the first part. Throughout all three parts, AEM electrolysis exhibited great potential with PGM-free catalysts in both alkaline and pure water conditions. However, to become a more competitive product in the AEM electrolysis market, further research is needed to address certain aspects of SEBS-based piperidinium/pyrrolidinium functionalized AEMs.

Firstly, regarding the SEBS backbone, its solubility remains a significant limitation. In most cases, once ionized, SEBS-based membranes are hardly soluble in any solvents. Therefore, it is necessary to explore alternative methods for attaching the side chain or identify solvent/solvent mixtures capable of dissolving the functionalized SEBS AEM. Secondly, the piperidinium/pyrrolidinium functional group presents a challenge due to its relatively low pKa, which results in lower conductivity. Conductivity improvement can be achieved through further research on modifying the piperidinium/pyrrolidinium structure to maintain high alkaline stability while significantly increasing the pKa. Additionally, in the synthesis of SEBS-based piperidinium/pyrrolidinium functionalized AEMs, the current approach involves chloromethylation followed by ionization. However, it has been observed that the reaction rate between chloromethylated SEBS and piperidine/pyrrolidine is not very high. In future studies, it is recommended to employ bromomethylated SEBS as it would likely exhibit better reactivity with piperidine/pyrrolidine.

Addressing these areas of research will contribute to the advancement of SEBS-based piperidinium/pyrrolidinium functionalized AEMs and improve their suitability for AEM electrolysis applications.

In addition to the AEM, the ionomer for the catalyst layer is another crucial component in AEM electrolysis. Currently, researchers primarily focus on the alkaline stability of the ionomer while overlooking its anti-radical ability, which has gained increasing importance in recent studies. C-H bonds are known to be less stable against radical attacks, and C-F bonds are less stable in alkaline solutions. Consequently, aromatic structures have emerged as the preferred choice for AEM ionomers.

For other components of AEM electrolysis cells, there is a significant demand for high-performance and durable PGM-free OER and HER catalysts. Regarding MEA fabrication, this thesis observed that CCMs (catalyst-coated membranes) appeared brittle. However, further research can potentially address this issue, as CCMs are believed to have lower ohmic resistance.

Last but not least, traditional cell testing has predominantly been conducted using 1 M KOH. However, there is a gradual shift in operational conditions. Many researchers have started using less concentrated KOH, such as 0.1 M KOH, to reduce the requirements for alkaline stability of the membrane and ionomers. Pure water electrolysis is still in the early stages of research, but it has demonstrated great potential. The biggest challenge faced by AEM pure water electrolysis is isolating the system from CO<sub>2</sub>, preventing the AEM and ionomer in the OH<sup>-</sup> form from converting to HCO<sub>3</sub><sup>-</sup> or CO<sub>3</sub><sup>2-</sup>.

## 7. References

- [1] <bp-stats-review-2019-full-report.pdf>.
- [2] B. Zhang, The Effect of Aerosols to Climate Change and Society, *Journal of Geoscience and Environment Protection* 08(08) (2020) 55-78. <https://doi.org/10.4236/gep.2020.88006>.
- [3] C.D. Thomas, A. Cameron, R.E. Green, M. Bakkenes, L.J. Beaumont, Y.C. Collingham, B.F.N. Erasmus, M.F. de Siqueira, A. Grainger, L. Hannah, L. Hughes, B. Huntley, A.S. van Jaarsveld, G.F. Midgley, L. Miles, M.A. Ortega-Huerta, A. Townsend Peterson, O.L. Phillips, S.E. Williams, Extinction risk from climate change, *Nature* 427(6970) (2004) 145-148. <https://doi.org/10.1038/nature02121>.
- [4] S.J. Peighambardoust, S. Rowshanzamir, M. Amjadi, Review of the proton exchange membranes for fuel cell applications, *International Journal of Hydrogen Energy* 35(17) (2010) 9349-9384. <https://doi.org/https://doi.org/10.1016/j.ijhydene.2010.05.017>.
- [5] Y. Wang, K.S. Chen, J. Mishler, S.C. Cho, X.C. Adroher, A review of polymer electrolyte membrane fuel cells: Technology, applications, and needs on fundamental research, *Applied Energy* 88(4) (2011) 981-1007. <https://doi.org/https://doi.org/10.1016/j.apenergy.2010.09.030>.
- [6] The U.S. Department of Energy's (DOE's) Energy Hydrogen Earthshot.
- [7] P. Millet, N. Mbemba, S.A. Grigoriev, V.N. Fateev, A. Aukauloo, C. Etievant, Electrochemical performances of PEM water electrolysis cells and perspectives, *International Journal of Hydrogen Energy* 36(6) (2011) 4134-4142. <https://doi.org/https://doi.org/10.1016/j.ijhydene.2010.06.105>.
- [8] M. Carmo, D.L. Fritz, J. Mergel, D. Stolten, A comprehensive review on PEM water electrolysis, *International Journal of Hydrogen Energy* 38(12) (2013) 4901-4934. <https://doi.org/https://doi.org/10.1016/j.ijhydene.2013.01.151>.
- [9] P. Millet, R. Ngameni, S.A. Grigoriev, N. Mbemba, F. Brisset, A. Ranjbari, C. Etievant, PEM water electrolyzers: From electrocatalysis to stack development, *International Journal of Hydrogen Energy* 35(10) (2010) 5043-5052. <https://doi.org/https://doi.org/10.1016/j.ijhydene.2009.09.015>.
- [10] C. European, E. Directorate-General for, Transport, R. Directorate-General for, Innovation, Hydrogen energy and fuel cells : a vision of our future : final report of the High Level Group, Publications Office2003.
- [11] H.A. Miller, K. Bouzek, J. Hnat, S. Loos, C.I. Bernäcker, T. Weißgärber, L. Röntzsch, J. Meier-Haack, Green hydrogen from anion exchange membrane water electrolysis: a review of recent developments in critical materials and operating conditions, *Sustainable Energy & Fuels* 4(5) (2020) 2114-2133. <https://doi.org/10.1039/C9SE01240K>.
- [12] I. Vincent, D. Bessarabov, Low cost hydrogen production by anion exchange membrane electrolysis: A review, *Renewable and Sustainable Energy Reviews* 81 (2018) 1690-1704. <https://doi.org/https://doi.org/10.1016/j.rser.2017.05.258>.
- [13] A.Y. Faid, S. Sunde, Anion Exchange Membrane Water Electrolysis from Catalyst Design to the Membrane Electrode Assembly, *Energy Technology* 10(9) (2022) 2200506. <https://doi.org/https://doi.org/10.1002/ente.202200506>.
- [14] J.R. Varcoe, P. Atanassov, D.R. Dekel, A.M. Herring, M.A. Hickner, P.A. Kohl, A.R. Kucernak, W.E. Mustain, K. Nijmeijer, K. Scott, T. Xu, L. Zhuang, Anion-exchange membranes in electrochemical energy systems, *Energy & Environmental Science* 7(10) (2014) 3135-3191. <https://doi.org/10.1039/C4EE01303D>.
- [15] T.-H. Tsai, A.M. Maes, M.A. Vandiver, C. Versek, S. Seifert, M. Tuominen, M.W. Liberatore, A.M.

- Herring, E.B. Coughlin, Synthesis and structure–conductivity relationship of polystyrene-block-poly(vinyl benzyl trimethylammonium) for alkaline anion exchange membrane fuel cells, *Journal of Polymer Science Part B: Polymer Physics* 51(24) (2013) 1751-1760. <https://doi.org/https://doi.org/10.1002/polb.23170>.
- [16] J. Zhou, J. Guo, D. Chu, R. Chen, Impacts of anion-exchange-membranes with various ionic exchange capacities on the performance of H<sub>2</sub>/O<sub>2</sub> fuel cells, *Journal of Power Sources* 219 (2012) 272-279. <https://doi.org/https://doi.org/10.1016/j.jpowsour.2012.07.051>.
- [17] W. Lu, Z.-G. Shao, G. Zhang, Y. Zhao, B. Yi, Crosslinked poly(vinylbenzyl chloride) with a macromolecular crosslinker for anion exchange membrane fuel cells, *Journal of Power Sources* 248 (2014) 905-914. <https://doi.org/https://doi.org/10.1016/j.jpowsour.2013.08.141>.
- [18] D.W. Seo, M.A. Hossain, D.H. Lee, Y.D. Lim, S.H. Lee, H.C. Lee, T.W. Hong, W.G. Kim, Anion conductive poly(arylene ether sulfone)s containing tetra-quaternary ammonium hydroxide on fluorenyl group for alkaline fuel cell application, *Electrochimica Acta* 86 (2012) 360-365. <https://doi.org/https://doi.org/10.1016/j.electacta.2012.04.065>.
- [19] Q. Zhang, Q. Zhang, J. Wang, S. Zhang, S. Li, Synthesis and alkaline stability of novel cardo poly(aryl ether sulfone)s with pendent quaternary ammonium aliphatic side chains for anion exchange membranes, *Polymer* 51(23) (2010) 5407-5416. <https://doi.org/https://doi.org/10.1016/j.polymer.2010.09.049>.
- [20] X. Li, Y. Yu, Y. Meng, Novel Quaternized Poly(arylene ether sulfone)/Nano-ZrO<sub>2</sub> Composite Anion Exchange Membranes for Alkaline Fuel Cells, *ACS Applied Materials & Interfaces* 5(4) (2013) 1414-1422. <https://doi.org/10.1021/am302844x>.
- [21] A. Katzfuß, V. Gogel, L. Jörissen, J. Kerres, The application of covalently cross-linked BrPPO as AEM in alkaline DMFC, *Journal of Membrane Science* 425-426 (2013) 131-140. <https://doi.org/https://doi.org/10.1016/j.memsci.2012.09.022>.
- [22] S. Gu, J. Skovgard, Y.S. Yan, Engineering the Van der Waals Interaction in Cross-Linking-Free Hydroxide Exchange Membranes for Low Swelling and High Conductivity, *ChemSusChem* 5(5) (2012) 843-848. <https://doi.org/https://doi.org/10.1002/cssc.201200057>.
- [23] Y. Wu, C. Wu, J.R. Varcoe, S.D. Poynton, T. Xu, Y. Fu, Novel silica/poly(2,6-dimethyl-1,4-phenylene oxide) hybrid anion-exchange membranes for alkaline fuel cells: Effect of silica content and the single cell performance, *Journal of Power Sources* 195(10) (2010) 3069-3076. <https://doi.org/https://doi.org/10.1016/j.jpowsour.2009.11.118>.
- [24] X. Yan, S. Gu, G. He, X. Wu, W. Zheng, X. Ruan, Quaternary phosphonium-functionalized poly(ether ether ketone) as highly conductive and alkali-stable hydroxide exchange membrane for fuel cells, *Journal of Membrane Science* 466 (2014) 220-228. <https://doi.org/https://doi.org/10.1016/j.memsci.2014.04.056>.
- [25] D.W. Seo, Y.D. Lim, M.A. Hossain, S.H. Lee, H.C. Lee, H.H. Jang, S.Y. Choi, W.G. Kim, Anion conductive poly(tetraphenyl phthalazine ether sulfone) containing tetra quaternary ammonium hydroxide for alkaline fuel cell application, *International Journal of Hydrogen Energy* 38(1) (2013) 579-587. <https://doi.org/https://doi.org/10.1016/j.ijhydene.2012.07.044>.
- [26] D. Pan, P.M. Bakvand, T.H. Pham, P. Jannasch, Improving poly(arylene piperidinium) anion exchange membranes by monomer design, *Journal of Materials Chemistry A* 10(31) (2022) 16478-16489. <https://doi.org/10.1039/D2TA03862E>.
- [27] F. Xu, Y. Chen, B. Lin, J. Li, K. Qiu, J. Ding, Highly Durable Ether-Free Polyfluorene-Based Anion Exchange Membranes for Fuel Cell Applications, *ACS Macro Letters* 10(10) (2021) 1180-1185.

<https://doi.org/10.1021/acsmacrolett.1c00506>.

[28] O.I. Deavin, S. Murphy, A.L. Ong, S.D. Poynton, R. Zeng, H. Herman, J.R. Varcoe, Anion-exchange membranes for alkaline polymer electrolyte fuel cells: comparison of pendent benzyltrimethylammonium- and benzylmethylimidazolium-head-groups, *Energy & Environmental Science* 5(9) (2012) 8584-8597. <https://doi.org/10.1039/C2EE22466F>.

[29] M. Zhang, H.K. Kim, E. Chalkova, F. Mark, S.N. Lvov, T.C.M. Chung, New Polyethylene Based Anion Exchange Membranes (PE-AEMs) with High Ionic Conductivity, *Macromolecules* 44(15) (2011) 5937-5946. <https://doi.org/10.1021/ma200836d>.

[30] H.A.I.V. Kostalik, T.J. Clark, N.J. Robertson, P.F. Mutolo, J.M. Longo, H.D. Abruña, G.W. Coates, Solvent Processable Tetraalkylammonium-Functionalized Polyethylene for Use as an Alkaline Anion Exchange Membrane, *Macromolecules* 43(17) (2010) 7147-7150. <https://doi.org/10.1021/ma101172a>.

[31] M. Niu, C. Zhang, G. He, F. Zhang, X. Wu, Pendent piperidinium-functionalized blend anion exchange membrane for fuel cell application, *International Journal of Hydrogen Energy* 44(29) (2019) 15482-15493. <https://doi.org/https://doi.org/10.1016/j.ijhydene.2019.04.172>.

[32] Z. Yin, Y. Wu, B. Shi, C. Yang, Y. Kong, Y. Liu, H. Wu, Z. Jiang, Alkaline stable piperidinium-based biphenyl polymer for anion exchange membranes, *Solid State Ionics* 383 (2022) 115969. <https://doi.org/https://doi.org/10.1016/j.ssi.2022.115969>.

[33] B.-S. Ko, J.-Y. Sohn, J. Shin, Radiation-induced synthesis of solid alkaline exchange membranes with quaternized 1,4-diazabicyclo[2,2,2] octane pendant groups for fuel cell application, *Polymer* 53(21) (2012) 4652-4661. <https://doi.org/https://doi.org/10.1016/j.polymer.2012.08.002>.

[34] J. Wang, S. Gu, R.B. Kaspar, B. Zhang, Y. Yan, Stabilizing the Imidazolium Cation in Hydroxide-Exchange Membranes for Fuel Cells, *ChemSusChem* 6(11) (2013) 2079-2082. <https://doi.org/https://doi.org/10.1002/cssc.201300285>.

[35] O.M.M. Page, S.D. Poynton, S. Murphy, A. Lien Ong, D.M. Hillman, C.A. Hancock, M.G. Hale, D.C. Apperley, J.R. Varcoe, The alkali stability of radiation-grafted anion-exchange membranes containing pendent 1-benzyl-2,3-dimethylimidazolium head-groups, *RSC Advances* 3(2) (2013) 579-587. <https://doi.org/10.1039/C2RA22331G>.

[36] X. Lin, X. Liang, S.D. Poynton, J.R. Varcoe, A.L. Ong, J. Ran, Y. Li, Q. Li, T. Xu, Novel alkaline anion exchange membranes containing pendant benzimidazolium groups for alkaline fuel cells, *Journal of Membrane Science* 443 (2013) 193-200. <https://doi.org/https://doi.org/10.1016/j.memsci.2013.04.059>.

[37] B. Xing, O. Savadogo, Hydrogen/oxygen polymer electrolyte membrane fuel cells (PEMFCs) based on alkaline-doped polybenzimidazole (PBI), *Electrochemistry Communications* 2(10) (2000) 697-702. [https://doi.org/https://doi.org/10.1016/S1388-2481\(00\)00107-7](https://doi.org/https://doi.org/10.1016/S1388-2481(00)00107-7).

[38] L.-c. Jheng, S.L.-c. Hsu, B.-y. Lin, Y.-l. Hsu, Quaternized polybenzimidazoles with imidazolium cation moieties for anion exchange membrane fuel cells, *Journal of Membrane Science* 460 (2014) 160-170. <https://doi.org/https://doi.org/10.1016/j.memsci.2014.02.043>.

[39] L. Işikel Şanlı, S. Alkan Gürsel, Synthesis and characterization of novel graft copolymers by radiation-induced grafting, *Journal of Applied Polymer Science* 120(4) (2011) 2313-2323. <https://doi.org/https://doi.org/10.1002/app.33419>.

[40] M. Sudoh, S. Niimi, N. Takaoka, M. Watanabe, Design of Direct Methanol Alkaline Fuel Cell with Anion Conductive Membrane Prepared by Plasma Polymerization, *ECS Transactions* 25(13) (2010) 61. <https://doi.org/10.1149/1.3315173>.

[41] S.D. Sajjad, Y. Hong, F. Liu, Synthesis of guanidinium-based anion exchange membranes and their

- stability assessment, *Polymers for Advanced Technologies* 25(1) (2014) 108-116. <https://doi.org/https://doi.org/10.1002/pat.3211>.
- [42] C.H. Zhao, Y. Gong, Q.L. Liu, Q.G. Zhang, A.M. Zhu, Self-crosslinked anion exchange membranes by bromination of benzylmethyl-containing poly(sulfone)s for direct methanol fuel cells, *International Journal of Hydrogen Energy* 37(15) (2012) 11383-11393. <https://doi.org/https://doi.org/10.1016/j.ijhydene.2012.04.163>.
- [43] Q. Zhang, S. Li, S. Zhang, A novel guanidinium grafted poly(aryl ether sulfone) for high-performance hydroxide exchange membranes, *Chemical Communications* 46(40) (2010) 7495-7497. <https://doi.org/10.1039/C0CC01834A>.
- [44] L. Jiang, X. Lin, J. Ran, C. Li, L. Wu, T. Xu, Synthesis and Properties of Quaternary Phosphonium-based Anion Exchange Membrane for Fuel Cells, *Chinese Journal of Chemistry* 30(9) (2012) 2241-2246. <https://doi.org/https://doi.org/10.1002/cjoc.201200649>.
- [45] S. Maurya, S.-H. Shin, M.-K. Kim, S.-H. Yun, S.-H. Moon, Stability of composite anion exchange membranes with various functional groups and their performance for energy conversion, *Journal of Membrane Science* 443 (2013) 28-35. <https://doi.org/https://doi.org/10.1016/j.memsci.2013.04.035>.
- [46] X. Kong, K. Wadhwa, J.G. Verkade, K. Schmidt-Rohr, Determination of the Structure of a Novel Anion Exchange Fuel Cell Membrane by Solid-State Nuclear Magnetic Resonance Spectroscopy, *Macromolecules* 42(5) (2009) 1659-1664. <https://doi.org/10.1021/ma802613k>.
- [47] B. Zhang, S. Gu, J. Wang, Y. Liu, A.M. Herring, Y. Yan, Tertiary sulfonium as a cationic functional group for hydroxide exchange membranes, *RSC Advances* 2(33) (2012) 12683-12685. <https://doi.org/10.1039/C2RA21402D>.
- [48] Y. Zha, M.L. Disabb-Miller, Z.D. Johnson, M.A. Hickner, G.N. Tew, Metal-Cation-Based Anion Exchange Membranes, *Journal of the American Chemical Society* 134(10) (2012) 4493-4496. <https://doi.org/10.1021/ja211365r>.
- [49] V. Neagu, I. Bunia, I. Plesca, Ionic polymers VI. Chemical stability of strong base anion exchangers in aggressive media, *Polymer Degradation and Stability* 70(3) (2000) 463-468. [https://doi.org/https://doi.org/10.1016/S0141-3910\(00\)00142-7](https://doi.org/https://doi.org/10.1016/S0141-3910(00)00142-7).
- [50] P. Yu Xu, T. Yi Guo, C. Hui Zhao, I. Broadwell, Q. Gen Zhang, Q.L. Liu, Anion exchange membranes based on poly(vinyl alcohol) and quaternized polyethyleneimine for direct methanol fuel cells, *Journal of Applied Polymer Science* 128(6) (2013) 3853-3860. <https://doi.org/https://doi.org/10.1002/app.38592>.
- [51] W. Lu, Z.-G. Shao, G. Zhang, Y. Zhao, J. Li, B. Yi, Preparation and characterization of imidazolium-functionalized poly(ether sulfone) as anion exchange membrane and ionomer for fuel cell application, *International Journal of Hydrogen Energy* 38(22) (2013) 9285-9296. <https://doi.org/https://doi.org/10.1016/j.ijhydene.2013.05.070>.
- [52] J.B. Edson, C.S. Macomber, B.S. Pivovar, J.M. Boncella, Hydroxide based decomposition pathways of alkyltrimethylammonium cations, *Journal of Membrane Science* 399-400 (2012) 49-59. <https://doi.org/https://doi.org/10.1016/j.memsci.2012.01.025>.
- [53] T. Sata, M. Tsujimoto, T. Yamaguchi, K. Matsusaki, Change of anion exchange membranes in an aqueous sodium hydroxide solution at high temperature, *Journal of Membrane Science* 112(2) (1996) 161-170. [https://doi.org/https://doi.org/10.1016/0376-7388\(95\)00292-8](https://doi.org/https://doi.org/10.1016/0376-7388(95)00292-8).
- [54] S. Chempath, J.M. Boncella, L.R. Pratt, N. Henson, B.S. Pivovar, Density Functional Theory Study of Degradation of Tetraalkylammonium Hydroxides, *The Journal of Physical Chemistry C* 114(27) (2010) 11977-11983. <https://doi.org/10.1021/jp9122198>.

- [55] E.N. Komkova, D.F. Stamatialis, H. Strathmann, M. Wessling, Anion-exchange membranes containing diamines: preparation and stability in alkaline solution, *Journal of Membrane Science* 244(1) (2004) 25-34. <https://doi.org/https://doi.org/10.1016/j.memsci.2004.06.026>.
- [56] L. Zeng, T.S. Zhao, High-performance alkaline ionomer for alkaline exchange membrane fuel cells, *Electrochemistry Communications* 34 (2013) 278-281. <https://doi.org/https://doi.org/10.1016/j.elecom.2013.07.015>.
- [57] R. Janarthanan, S. Kishore Pilli, J.L. Horan, D.A. Gamarra, M.R. Hibbs, A.M. Herring, A Direct Methanol Alkaline Fuel Cell Based on Poly(phenylene) Anion Exchange Membranes, *Journal of The Electrochemical Society* 161(9) (2014) F944. <https://doi.org/10.1149/2.1041409jes>.
- [58] K.M. Hugar, H.A.I.V. Kostalik, G.W. Coates, Imidazolium Cations with Exceptional Alkaline Stability: A Systematic Study of Structure–Stability Relationships, *Journal of the American Chemical Society* 137(27) (2015) 8730-8737. <https://doi.org/10.1021/jacs.5b02879>.
- [59] D. Chen, M.A. Hickner, Degradation of Imidazolium- and Quaternary Ammonium-Functionalized Poly(fluorenyl ether ketone sulfone) Anion Exchange Membranes, *ACS Applied Materials & Interfaces* 4(11) (2012) 5775-5781. <https://doi.org/10.1021/am301557w>.
- [60] C.G. Arges, V. Ramani, Two-dimensional NMR spectroscopy reveals cation-triggered backbone degradation in polysulfone-based anion exchange membranes, *Proceedings of the National Academy of Sciences* 110(7) (2013) 2490-2495. <https://doi.org/10.1073/pnas.1217215110>.
- [61] C. Fujimoto, D.-S. Kim, M. Hibbs, D. Wroblewski, Y.S. Kim, Backbone stability of quaternized polyaromatics for alkaline membrane fuel cells, *Journal of Membrane Science* 423-424 (2012) 438-449. <https://doi.org/https://doi.org/10.1016/j.memsci.2012.08.045>.
- [62] S.A. Nuñez, M.A. Hickner, Quantitative <sup>1</sup>H NMR Analysis of Chemical Stabilities in Anion-Exchange Membranes, *ACS Macro Letters* 2(1) (2013) 49-52. <https://doi.org/10.1021/mz300486h>.
- [63] D. Marx, A. Chandra, M.E. Tuckerman, Aqueous Basic Solutions: Hydroxide Solvation, Structural Diffusion, and Comparison to the Hydrated Proton, *Chemical Reviews* 110(4) (2010) 2174-2216. <https://doi.org/10.1021/cr900233f>.
- [64] T. Kimura, Y. Yamazaki, Effects of CO<sub>2</sub> Concentration and Electric Current on the Ionic Conductivity of Anion Exchange Membranes for Fuel Cells, *Electrochemistry* 79(2) (2011) 94-97. <https://doi.org/10.5796/electrochemistry.79.94>.
- [65] I.T. Lucas, S. Durand-Vidal, E. Dubois, J. Chevalet, P. Turq, Surface Charge Density of Maghemite Nanoparticles: Role of Electrostatics in the Proton Exchange, *The Journal of Physical Chemistry C* 111(50) (2007) 18568-18576. <https://doi.org/10.1021/jp0743119>.
- [66] L. Gubler, Polymer Design Strategies for Radiation-Grafted Fuel Cell Membranes, *Advanced Energy Materials* 4(3) (2014) 1300827. <https://doi.org/https://doi.org/10.1002/aenm.201300827>.
- [67] S. Zhang, C. Li, X. Xie, F. Zhang, Novel cross-linked anion exchange membranes with diamines as ionic exchange functional groups and crosslinking groups, *International Journal of Hydrogen Energy* 39(25) (2014) 13718-13724. <https://doi.org/https://doi.org/10.1016/j.ijhydene.2014.03.122>.
- [68] Q. Li, L. Liu, Q. Miao, B. Jin, R. Bai, A novel poly(2,6-dimethyl-1,4-phenylene oxide) with trifunctional ammonium moieties for alkaline anion exchange membranes, *Chemical Communications* 50(21) (2014) 2791-2793. <https://doi.org/10.1039/C3CC47897A>.
- [69] K.A. Mauritz, R.B. Moore, State of Understanding of Nafion, *Chemical Reviews* 104(10) (2004) 4535-4586. <https://doi.org/10.1021/cr0207123>.
- [70] M.E. Tuckerman, D. Marx, M. Parrinello, The nature and transport mechanism of hydrated hydroxide ions in aqueous solution, *Nature* 417(6892) (2002) 925-929.

<https://doi.org/10.1038/nature00797>.

[71] J. Pan, C. Chen, Y. Li, L. Wang, L. Tan, G. Li, X. Tang, L. Xiao, J. Lu, L. Zhuang, Constructing ionic highway in alkaline polymer electrolytes, *Energy & Environmental Science* 7(1) (2014) 354-360.

<https://doi.org/10.1039/C3EE43275K>.

[72] L. Zhu, J. Pan, Y. Wang, J. Han, L. Zhuang, M.A. Hickner, Multication Side Chain Anion Exchange Membranes, *Macromolecules* 49(3) (2016) 815-824. <https://doi.org/10.1021/acs.macromol.5b02671>.

[73] Y. Zhu, L. Ding, X. Liang, M.A. Shehzad, L. Wang, X. Ge, Y. He, L. Wu, J.R. Varcoe, T. Xu, Beneficial use of rotatable-spacer side-chains in alkaline anion exchange membranes for fuel cells, *Energy & Environmental Science* 11(12) (2018) 3472-3479. <https://doi.org/10.1039/C8EE02071J>.

[74] J.Y. Jeon, S. Park, J. Han, S. Maurya, A.D. Mohanty, D. Tian, N. Saikia, M.A. Hickner, C.Y. Ryu, M.E. Tuckerman, S.J. Paddison, Y.S. Kim, C. Bae, Synthesis of Aromatic Anion Exchange Membranes by Friedel–Crafts Bromoalkylation and Cross-Linking of Polystyrene Block Copolymers, *Macromolecules* 52(5) (2019) 2139-2147. <https://doi.org/10.1021/acs.macromol.8b02355>.

[75] A. Ursúa, E.L. Barrios, J. Pascual, I. San Martín, P. Sanchis, Integration of commercial alkaline water electrolyzers with renewable energies: Limitations and improvements, *International Journal of Hydrogen Energy* 41(30) (2016) 12852-12861. <https://doi.org/https://doi.org/10.1016/j.ijhydene.2016.06.071>.

[76] K. Zeng, D. Zhang, Recent progress in alkaline water electrolysis for hydrogen production and applications, *Progress in Energy and Combustion Science* 36(3) (2010) 307-326. <https://doi.org/https://doi.org/10.1016/j.pecs.2009.11.002>.

[77] M. Schalenbach, O. Kasian, K.J.J. Mayrhofer, An alkaline water electrolyzer with nickel electrodes enables efficient high current density operation, *International Journal of Hydrogen Energy* 43(27) (2018) 11932-11938. <https://doi.org/https://doi.org/10.1016/j.ijhydene.2018.04.219>.

[78] A. Midilli, M. Ay, I. Dincer, M.A. Rosen, On hydrogen and hydrogen energy strategies: I: current status and needs, *Renewable and Sustainable Energy Reviews* 9(3) (2005) 255-271. <https://doi.org/https://doi.org/10.1016/j.rser.2004.05.003>.

[79] C.C. Pavel, F. Cecconi, C. Emiliani, S. Santiccioli, A. Scaffidi, S. Catanorchi, M. Comotti, Highly Efficient Platinum Group Metal Free Based Membrane-Electrode Assembly for Anion Exchange Membrane Water Electrolysis, *Angewandte Chemie International Edition* 53(5) (2014) 1378-1381. <https://doi.org/https://doi.org/10.1002/anie.201308099>.

[80] J. Parrondo, C.G. Arges, M. Niedzwiecki, E.B. Anderson, K.E. Ayers, V. Ramani, Degradation of anion exchange membranes used for hydrogen production by ultrapure water electrolysis, *RSC Advances* 4(19) (2014) 9875-9879. <https://doi.org/10.1039/C3RA46630B>.

[81] L. Xiao, S. Zhang, J. Pan, C. Yang, M. He, L. Zhuang, J. Lu, First implementation of alkaline polymer electrolyte water electrolysis working only with pure water, *Energy & Environmental Science* 5(7) (2012) 7869-7871. <https://doi.org/10.1039/C2EE22146B>.

[82] A. Lim, H.-j. Kim, D. Henkensmeier, S. Jong Yoo, J. Young Kim, S. Young Lee, Y.-E. Sung, J.H. Jang, H.S. Park, A study on electrode fabrication and operation variables affecting the performance of anion exchange membrane water electrolysis, *Journal of Industrial and Engineering Chemistry* 76 (2019) 410-418. <https://doi.org/https://doi.org/10.1016/j.jiec.2019.04.007>.

[83] X. Wu, K. Scott, A Li-doped Co<sub>3</sub>O<sub>4</sub> oxygen evolution catalyst for non-precious metal alkaline anion exchange membrane water electrolyzers, *International Journal of Hydrogen Energy* 38(8) (2013) 3123-3129. <https://doi.org/https://doi.org/10.1016/j.ijhydene.2012.12.087>.

[84] D. Xu, M.B. Stevens, M.R. Cosby, S.Z. Oener, A.M. Smith, L.J. Enman, K.E. Ayers, C.B. Capuano, J.N.



- Renner, N. Danilovic, Y. Li, H. Wang, Q. Zhang, S.W. Boettcher, Earth-Abundant Oxygen Electrocatalysts for Alkaline Anion-Exchange-Membrane Water Electrolysis: Effects of Catalyst Conductivity and Comparison with Performance in Three-Electrode Cells, *ACS Catalysis* 9(1) (2019) 7-15. <https://doi.org/10.1021/acscatal.8b04001>.
- [85] S.H. Ahn, B.-S. Lee, I. Choi, S.J. Yoo, H.-J. Kim, E. Cho, D. Henkensmeier, S.W. Nam, S.-K. Kim, J.H. Jang, Development of a membrane electrode assembly for alkaline water electrolysis by direct electrodeposition of nickel on carbon papers, *Applied Catalysis B: Environmental* 154-155 (2014) 197-205. <https://doi.org/https://doi.org/10.1016/j.apcatb.2014.02.021>.
- [86] M. Faraj, M. Boccia, H. Miller, F. Martini, S. Borsacchi, M. Geppi, A. Pucci, New LDPE based anion-exchange membranes for alkaline solid polymeric electrolyte water electrolysis, *International Journal of Hydrogen Energy* 37(20) (2012) 14992-15002. <https://doi.org/https://doi.org/10.1016/j.ijhydene.2012.08.012>.
- [87] Y. Leng, G. Chen, A.J. Mendoza, T.B. Tighe, M.A. Hickner, C.-Y. Wang, Solid-State Water Electrolysis with an Alkaline Membrane, *Journal of the American Chemical Society* 134(22) (2012) 9054-9057. <https://doi.org/10.1021/ja302439z>.
- [88] X. Su, L. Gao, L. Hu, N.A. Qaisrani, X. Yan, W. Zhang, X. Jiang, X. Ruan, G. He, Novel piperidinium functionalized anionic membrane for alkaline polymer electrolysis with excellent electrochemical properties, *Journal of Membrane Science* 581 (2019) 283-292. <https://doi.org/https://doi.org/10.1016/j.memsci.2019.03.072>.
- [89] T. Pandiarajan, L. John Berchmans, S. Ravichandran, Fabrication of spinel ferrite based alkaline anion exchange membrane water electrolyzers for hydrogen production, *RSC Advances* 5(43) (2015) 34100-34108. <https://doi.org/10.1039/C5RA01123J>.
- [90] Y.X. Chen, A. Lavacchi, H.A. Miller, M. Bevilacqua, J. Filippi, M. Innocenti, A. Marchionni, W. Oberhauser, L. Wang, F. Vizza, Nanotechnology makes biomass electrolysis more energy efficient than water electrolysis, *Nature Communications* 5(1) (2014) 4036. <https://doi.org/10.1038/ncomms5036>.
- [91] I. Vincent, A. Kruger, D. Bessarabov, Development of efficient membrane electrode assembly for low cost hydrogen production by anion exchange membrane electrolysis, *International Journal of Hydrogen Energy* 42(16) (2017) 10752-10761. <https://doi.org/https://doi.org/10.1016/j.ijhydene.2017.03.069>.
- [92] G. Gupta, K. Scott, M. Mamlouk, Performance of polyethylene based radiation grafted anion exchange membrane with polystyrene-b-poly (ethylene/butylene)-b-polystyrene based ionomer using NiCo<sub>2</sub>O<sub>4</sub> catalyst for water electrolysis, *Journal of Power Sources* 375 (2018) 387-396. <https://doi.org/https://doi.org/10.1016/j.jpowsour.2017.07.026>.
- [93] X. Wu, K. Scott, F. Xie, N. Alford, A reversible water electrolyser with porous PTFE based OH-conductive membrane as energy storage cells, *Journal of Power Sources* 246 (2014) 225-231. <https://doi.org/https://doi.org/10.1016/j.jpowsour.2013.07.081>.
- [94] B.K. Kakati, D. Sathiyamoorthy, A. Verma, Electrochemical and mechanical behavior of carbon composite bipolar plate for fuel cell, *International Journal of Hydrogen Energy* 35(9) (2010) 4185-4194. <https://doi.org/https://doi.org/10.1016/j.ijhydene.2010.02.033>.
- [95] E.J. Park, C.B. Capuano, K.E. Ayers, C. Bae, Chemically durable polymer electrolytes for solid-state alkaline water electrolysis, *Journal of Power Sources* 375 (2018) 367-372. <https://doi.org/https://doi.org/10.1016/j.jpowsour.2017.07.090>.
- [96] D. Li, E.J. Park, W. Zhu, Q. Shi, Y. Zhou, H. Tian, Y. Lin, A. Serov, B. Zulevi, E.D. Baca, C. Fujimoto, H.T. Chung, Y.S. Kim, Highly quaternized polystyrene ionomers for high performance anion exchange

membrane water electrolyzers, *Nature Energy* 5(5) (2020) 378-385. <https://doi.org/10.1038/s41560-020-0577-x>.

[97] J. Hnát, M. Plevová, J. Žitka, M. Paidar, K. Bouzek, Anion-selective materials with 1,4-diazabicyclo[2.2.2]octane functional groups for advanced alkaline water electrolysis, *Electrochimica Acta* 248 (2017) 547-555. <https://doi.org/https://doi.org/10.1016/j.electacta.2017.07.165>.



## Novel piperidinium-functionalized crosslinked anion exchange membrane with flexible spacers for water electrolysis

Ziqi Xu<sup>a,b</sup>, Vincent Wilke<sup>a</sup>, Jagoda Justyna Chmielarz<sup>a</sup>, Morawietz Tobias<sup>a,c</sup>, Vladimir Atanasov<sup>b</sup>, Aldo Saul Gago<sup>a,\*</sup>, Kaspar Andreas Friedrich<sup>a,d,\*\*</sup>

<sup>a</sup> German Aerospace Center (DLR), Institute of Engineering Thermodynamics, Pfaffenwaldring 38-40, 70569, Stuttgart, Germany

<sup>b</sup> Institute of Chemical Process Engineering, University of Stuttgart, Böblinger Straße 78, 70199, Stuttgart, Germany

<sup>c</sup> Faculty of Science, Energy and Building Services, Esslingen University of Applied Sciences, Kanalstraße 33, 73728 Esslingen am Neckar, Germany

<sup>d</sup> Institute of Building Energetics, Thermal Engineering and Energy Storage (IGTE), University of Stuttgart, Pfaffenwaldring 6, 70569, Stuttgart, Germany

### ARTICLE INFO

#### Keywords:

Alkaline anion exchange membrane  
Flexible ethylene oxide spacers  
Anion exchange membrane water electrolysis  
Styrene-*b*-ethylene-*b*-butylene-*b*-styrene copolymer  
Cell stability

### ABSTRACT

Anion Exchange membranes (AEM) are core components for alkaline electrochemical energy technology, such as the AEM water electrolysis and AEM fuel cell. They are regarded as promising alternatives for proton exchange membrane-based systems due to the possibility of using noble metal-free electrocatalyst. However, chemical stability and conductivity of the membrane are still the main challenge of the electrolyzer system. Here in we highlight an AEM with styrene-*b*-ethylene-*b*-butylene-*b*-styrene copolymer (SEBS) as its backbone and piperidinium functionalized flexible ethylene oxide spacer structure as its side-chains (SEBS-P206). This membrane reached  $20.8 \text{ mS cm}^{-1}$  hydroxide ion conductivity at room temperature, which is higher compared to previously obtained piperidinium functionalized SEBS with  $10.09 \text{ mS cm}^{-1}$  [1]. The SEBS-P206 was measured in a single cell AEM electrolysis cell with platinum group metal (PGM) catalyst. Current densities  $275 \text{ mA cm}^{-2}$  and  $680 \text{ mA cm}^{-2}$  at  $60 \text{ }^\circ\text{C}$  and  $2 \text{ V}$  cell potential were achieved in ultra-pure water (UPW) and  $0.1 \text{ M KOH}$ , respectively. Remarkably, in UPW the degradation rate was only  $140 \text{ } \mu\text{A h}^{-1} \text{ cm}^{-2}$ , which is the lowest reported up to know.

### 1. Introduction

Nowadays, the need of green hydrogen for chemical industry, steel manufacturing, transport and heat for achieving the climate goals emphasizes the importance for developing a cost-effective electrolysis technology for green hydrogen production in power supply system [2–5]. Among them, alkaline water electrolysis (AWE) has potentially the advantage of utilizing low-cost catalysts based on non-PGM and great convertibility at industrial level [6,7]. However, the low conductivity diaphragm and high corrosive alkaline electrolyte (30 wt% KOH) have brought a series of problems including carbonate formation and gas emitting impurities and often still PGM containing electrode packages are used [8,9].

To address those issues, anion exchange membranes (AEM) are regarded promising alternatives by allowing concentration reduction of electrolyte in the system and efficiency improvement [7,10–15]. However, there are still no reliable AEMs with the desired conductivity and stability [16–19], which are major challenges for developing high

performance AEMWE. Due to the strong nucleophilic and basic character of the hydroxide, the chemical stability in an alkaline environment at elevated temperature is the most critical issue for AEM. Basically, for the stability of the backbone of AEM, heteroatom groups have to be excluded because they can be easily attacked by hydroxide [20]. When considering the stability of functional group, there are several degradation mechanisms on quaternary ammonium (QA), including the nucleophilic substitution,  $\beta$ -elimination (Hofmann elimination) and rearrangement reaction [21,22]. In a study from Marino and Kreuer [23], the stability against nucleophilic attack of a number of functional groups, such as 1,4-diazabicyclooctane (DABCO), imidazolium, methyl piperazine have been compared. Among them, the 6-membered cycloaliphatic QA has shown a good resistance towards the nucleophilic substitution and  $\beta$ -elimination due to its unfavorable bond angles and lengths in the reaction transition states.

Another challenge for the performance of the AEMs is the moderate conductivity. Numerous effective strategies have been investigated to increase ionic conductivity [18,24]. Although the increase of the ion

\* Corresponding author.

\*\* Corresponding author. German Aerospace Center (DLR), Institute of Engineering Thermodynamics, Pfaffenwaldring 38-40, 70569, Stuttgart, Germany.  
E-mail address: Aldo.Gago@dlr.de (A.S. Gago).

<https://doi.org/10.1016/j.memsci.2022.121302>

Received 7 September 2022; Received in revised form 18 November 2022; Accepted 18 December 2022

Available online 30 December 2022

0376-7388/© 2023 Elsevier B.V. All rights reserved.

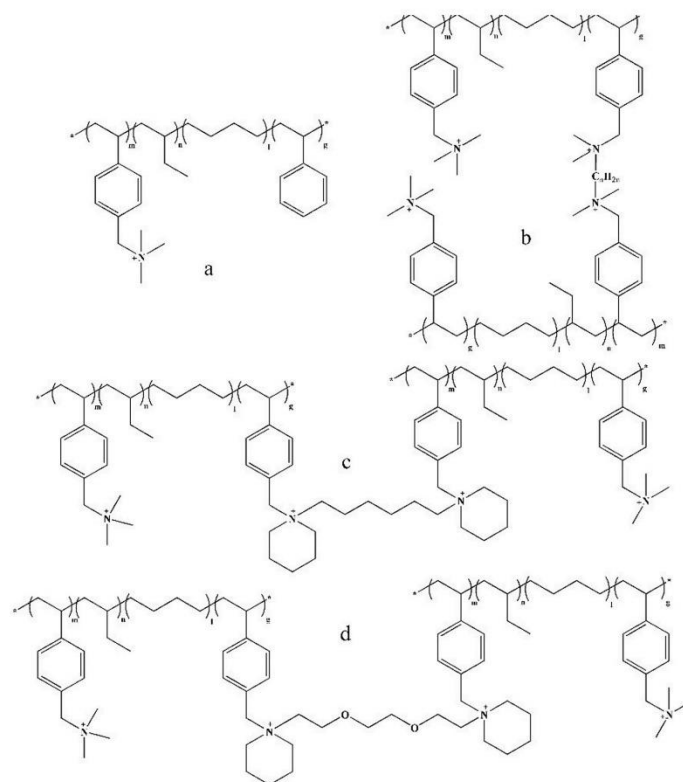


Fig. 1. Different membranes structures obtained in this study: (a)SEBS-TMA (b)SEBS-N2CX (c)SEBS-P2C6 (d)SEBS-P2O6.

exchange capacity (IEC) can contribute directly to the increase of the conductivity, its excessive increase will lead to uncontrolled swelling and membrane destabilization. So, designing a phase separation by the introduction of comb-shaped structures [25,26] and simultaneously increase of cations per chain [27,28] is believed to be more efficient method for membrane stabilization without losing the performance. Cross-linking has been reported to be an effective method for tackling the necessary trade-off between conductivity and stability. Cross-linked AEMs usually display a lower swelling ratio, higher chemical and mechanical properties than un-cross-linked counterparts [29]. A flexible spacer group is expected to improve this mechanical properties but due to the possibility of polymer arrangement helping in the formation of effective conductive channels in the membrane. However, so far to the best of our knowledge, there is no research report on comb-shaped multi-cations in one crosslinker in a combination with the stable 6-membered cycloaliphatic functional group like piperidinium.

In this work, piperidinium-functionalized multi-cation comb-shaped structure is reported. Moreover, more hydrophilic ethylene glycol-based side chains are introduced to gain more flexible-spacer structure and induce microphase separation. A multi-block copolymer styrene-*b*-ethylene-*b*-butylene-*b*-styrene copolymer (SEBS) is chosen as the backbone because of its excellent stability and mechanical integrity. Trimethylamine was selected to be the additional functional group due to its

relatively high stability against nucleophilic displacement [30–33]. Therefore, membrane bearing piperidinium-functionality and with crosslinkers is expected to have both good conductivity and stability. In detail, different structures of the side chain were investigated including the number of cations per chain, carbon chain length between two piperidinium groups and the degree of freedom of the spacer. Membrane properties including conductivity, IEC and alkaline stability were investigated. Moreover, membrane electrode assemblies (MEA) based on those membranes are fabricated. AEMWE performance with both PGM and non-PGM catalyst in pure water and KOH were studied.

## 2. Experimental section

### 2.1. Materials

SEBS (30%wt styrene, Taipol 6152) was provided by TSRC cooperation. Chlorotrimethylsilane, 1,3-dibromopropane, 1,4-dibromobutane, sodium chloride and potassium hydroxide were purchased from TCI Europe. Trioxane, tin (IV) chloride, 1,6-dibromohexane, Pt/C (40%), iridium black, chloroform, xylene, dimethyl sulfoxide, water solution of trimethylamine (33%), ethanol, dichloromethane and tetrahydrofuran were all purchased from Merck. All chemicals were used as received without further purification.

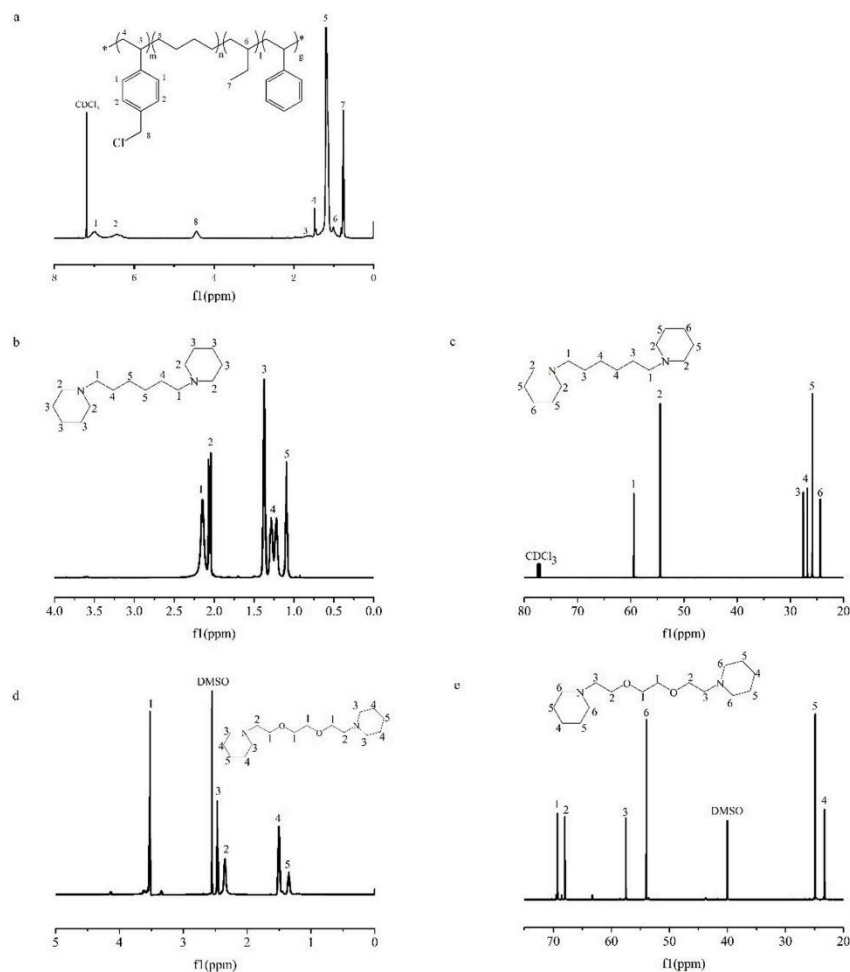


Fig. 2. (a)  $^1\text{H}$ NMR spectra of CMSEBS; (b), (c)  $^1\text{H}$ NMR and  $^{13}\text{C}$ NMR spectra of P2C6; (d), (e)  $^1\text{H}$ NMR and  $^{13}\text{C}$ NMR spectra of P2O6.

## 2.2. Synthesis and membrane preparation

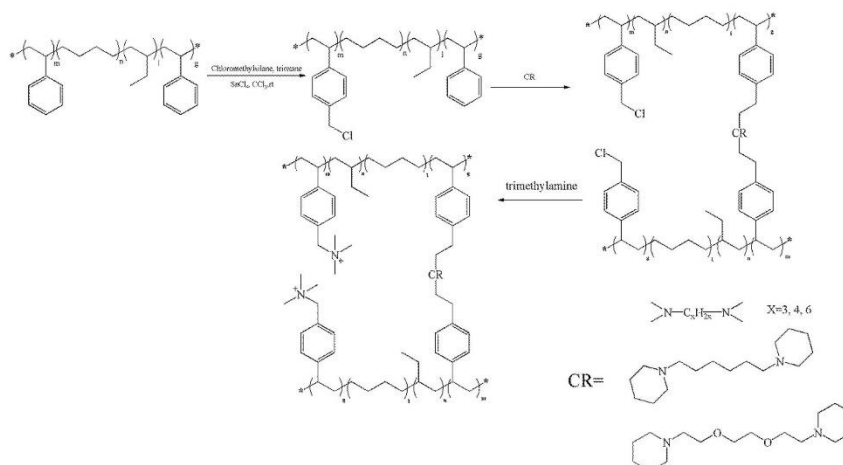
### 2.2.1. Synthesis of chloromethylated SEBS (CMSEBS)

The detailed CMSEBS synthesis procedures have been reported previously [31]. Chloroform (250 mL) was added to SEBS polymer (4 g, 25 mmol) in argon-purged three-neck round-bottom flask. The mixture was stirred at room temperature for 4 h. After dissolution of the polymer, trioxane (5.4 g, 60 mmol) was added and the flask was then immersed in ice bath until the temperature of the mixture decreased to 1 °C. Chlorotrimethylsilane (22.8 mL, 37.5 mmol) and then tin chloride (3 mL, 3 mmol) was injected in the reaction mixture with a syringe. The mixture was kept stirring at lower than 5 °C for 30 min, and then at room temperature for 24 h. To stop the reaction at the end of the reaction time, the

mixture was poured into a beaker filled with 300 mL of ethanol/water (50%v/v) mixture. After filtration to collect the solid, the product was twice precipitated from chloroform solution into ethanol/water (50% v/v) mixture. The final product was dried in vacuum oven overnight at 50 °C.

### 2.2.2. CMSEBS membrane preparation

CMSEBS (0.7 g) was dissolved into 10 mL xylene at 50 °C for 2 h to form 5 wt% solution. The membrane was cast from the solution on a PTFE square dish (15 cm  $\times$  15 cm) and dried at 50 °C in vacuum for 24 h. Finally, the CMSEBS membrane was detached from the PTFE dish.



Scheme 1. Polymer synthesis and crosslinking process obtained in this study.

### 2.2.3. 1,6-Bis(piperidin-1-yl) hexane preparation

Piperidine (26 mL, 250 mmol) was dissolved in acetone (150 mL) under argon and the mixture was stirred at room temperature for 30 min. After cooling down in an ice bath to  $T < 5\text{ }^{\circ}\text{C}$ , 1,6-dibromohexane (16 mL, 100 mmol) was added dropwise to the solution. Afterwards, anhydrous potassium carbonate (20 g, 152 mmol) was added and the reaction mixture is stirred at room temperature for 48 h. After filtration to remove the unwanted precipitates, vacuum evaporation was used to remove the solvent. Dichloromethane (60 mL) was added to the residue to extract the product, rinsed with deionized water ( $5 \times 100\text{ mL}$ ) and then dried at  $60\text{ }^{\circ}\text{C}$  for 10 h, resulting in a viscous yellowish liquid. The  $^1\text{H}$  NMR spectrum of 1,6-bis(piperidin-1-yl) hexane is shown in Fig. 2 (b).

### 2.2.4. 1,2-Bis(2-piperidinylethoxy) ethane preparation

Piperidine (26 mL, 250 mmol) was dissolved in acetonitrile (150 mL) under argon and the mixture was stirred at room temperature for 30 min. 1,2-Bis(ethoxy)ethane (14 mL, 100 mmol) was then added dropwise to the solution. Afterwards, anhydrous potassium carbonate (20 g, 0.145 mol) was added in and kept stirring at  $60\text{ }^{\circ}\text{C}$  for 48 h. After filtration to remove the unwanted precipitate, ethyl acetate was added to the residue to extract the product and remove the water phase. Finally, the rest was put into the vacuum oven at  $60\text{ }^{\circ}\text{C}$  for 24 h, resulting in a viscous dark yellow liquid. The  $^1\text{H}$  NMR spectrum of 1,2-Bis(2-piperidinylethoxy) ethane is shown in Fig. 2(d).

### 2.2.5. Membrane amination process

For SEBS-TMA preparation, CMSEBS membrane was immersed into water solution of trimethylamine (33%wt) at room temperature for 2 days. For SEBS-N2C6 preparation, first the CMSEBS was put into the 1,6-diaminohexane solution,  $60\text{ }^{\circ}\text{C}$  stirring for 24 h and then immersed into a water solution of trimethylamine at room temperature for 48 h. For SEBS-P2C6 and SEBS-P2O6 preparation was similar to that of SEBS-N2C6, but using 1,6-bis(piperidin-1-yl) hexane instead of 1,6-diaminohexane. By controlling the amount of crosslinkers, crosslinking rate is fixed. The chloromethyl and crosslinking process is shown in Scheme 1 in detail.

## 2.3. Instrumental

### 2.3.1. Nuclear magnetic resonance (NMR) spectroscopy and fourier-transform infrared spectroscopy (FT-IR)

$^1\text{H}$  and  $^{13}\text{C}$  NMR spectroscopy were recorded at room temperature on Bruker Avance III HD 400 NanoBay NMR spectrometer in either  $\text{DMSO}-d_6$  or  $\text{CDCl}_3$  as solvents whereas the internal reference was tetramethylsilane (TMS). FT-IR spectra of the membranes were recorded comprising 64 scans in the wave number range from  $4000$  to  $400\text{ cm}^{-1}$  using a Nicolet iS5 (ThermoFisher Scientific, Karlsruhe, Germany) and a diamond attenuated total reflectance (ATR) module.

### 2.3.2. Atomic force microscope (AFM)

Atomic force microscopy measurements were performed on a Multimode 8 AFM (Bruker Karlsruhe, Germany) in PeakForce Tapping Mode [34] measuring the nanomechanical properties of the membranes. The AFM modulus recorded force-distance curves at every measurement point and evaluates these online. Besides height information adhesion, stiffness and deformation were recorded simultaneously. Tap150 tips (Budgetsensors) with a tip radius  $< 10\text{ nm}$  and Bruker SNL10-C tips ( $k = 0.24\text{ N/m}$ ) with a nominal tip radius of  $2\text{ nm}$  were used (Measurements of SEBS-P2O6 in SI). The membranes were glued with adhesive carbon tape (Plano) to  $12\text{ mm}$  AFM steel-discs and were measured at ambient conditions at 45% RH. Image size was  $1\text{ }\mu\text{m}^2$  measured at  $0.966\text{ Hz}$  with  $512 \times 512$  pixels for all membranes. Other magnifications can be found in the SI for SEBS-P2O6.

### 2.3.3. Membrane conductivity

Membrane resistances were measured by electrochemical impedance spectroscopy using a Zahner elektrik IM6 device (Zahner-elektrok GmbH, Kronach, Germany) in  $1\text{ M NaCl}$  solution or  $1\text{ M KOH}$  at room temperature [35]. The resistance was read from intercepting the impedance with the real x-axis in a frequency range of  $200\text{ kHz} - 8\text{ MHz}$ . Four samples per membrane were measured. The through-plan conductivity was calculated using the following equation (Equation (1)).

$$\sigma = \frac{1}{R_{sp}} = \frac{d}{R \times A} \quad (1)$$

where  $\sigma$  is the conductivity (S/cm),  $R_{sp}$  is the resistivity ( $\Omega$  cm),  $d$  is the thickness of membrane (cm),  $R$  is the ohmic resistance ( $\Omega$ ), and  $A$  is the electrode area ( $\text{cm}^2$ ).

### 2.3.4. Water uptake and swelling degree

The water uptake (WU) and the swelling degree (SD) of the membranes in  $\text{Cl}^-$  form are calculated from the weight and dimension differences of membranes after soaking in deionized water for 48 h at room temperature and after drying in a vacuum oven at 60 °C for 24 h. The WU is calculated by equation (2) as follows:

$$WU\% = (m_{wet} - m_{dry}) / m_{dry} \times 100 \quad (2)$$

where  $m_{wet}$  and  $m_{dry}$  are the weight of wet and dry membranes in  $\text{Cl}^-$  forms in grams, respectively.

The SD was calculated by equation (3) as follows:

$$SD\% = (l_{wet} - l_{dry}) / l_{dry} \quad (3)$$

where  $l_{wet}$  and  $l_{dry}$  are the geometric length of the wet and dry membranes in  $\text{Cl}^-$  forms, respectively.

### 2.3.5. Ion exchange capacity (IEC)

IEC was calculated by the back-titration method. Accordingly, the membrane sample was put into the 1 M NaOH solution, then washed with DI water, afterwards immersed in a saturated sodium chloride solution at room temperature for 1 day. Hydrochloric acid (3 mL, 0.1 M) standard solution was added, and the mixture was stirred at room temperature for 1 day. The resulting solution was titrated with standard 0.1 M sodium hydroxide solution. The membrane was rinsed intensely with DI water and dried overnight at 90 °C. The dry weight of the membrane was then determined on a balance. The IEC was calculated using the following equation (Equation (4)).

$$IEC = \frac{C_{HCl} \times V_{HCl} - C_{NaOH} \times V_{NaOH}}{m_{dry}} \quad (4)$$

where IEC is the ion exchange capacity ( $\text{OH}^-$  form,  $\text{mmol g}^{-1}$ ),  $C_{HCl}$  is the concentration of the hydrochloric acid solution ( $\text{mmol mL}^{-1}$ ),  $V_{HCl}$  is the volume of the hydrochloric acid solution used (mL),  $C_{NaOH}$  is the concentration of the sodium hydroxide solution ( $\text{mmol mL}^{-1}$ ),  $V_{NaOH}$  is the added volume of the sodium hydroxide solution (mL), and  $m_{dry}$  is the dry weight of the membrane (g).

### 2.3.6. Chemical stability of the membranes

Chemical stability was determined in 1 M KOH at 90 °C for 30 days. Before being dried at 90 °C in an oven, several pieces of membranes were washed repeatedly with water for 1 day. In test, every 5 days a small piece of membrane was taken out and new KOH solution was exchanged. Subsequently, the membranes should be thoroughly washed by deionized water and afterwards, the  $\text{OH}^-$  conductivity of membrane was tested ( $\sigma_1$ ). The conductivity retention rate (CR%) of the membrane was calculated using the following equation.

$$CR\% = \frac{\sigma_1}{\sigma} \times 100 \quad (5)$$

where  $\sigma$  is the conductivity of the membrane before treatment in KOH.

## 2.4. Fabrication of SEBS P2O6 MEAs for AEMWE testing

For cell testing, Chloromethylated SEBS (cmSEBS) was used as the ionomer precursor and dissolved in THF to obtain the catalyst ink. After spraying we put the whole CCS into trimethylamine solution to functionalize the cmSEBS. In detail, the membrane electrode assembly (MEA) was prepared via the catalyst coated substrate approach (CCS), to simplify the wet spraying process and prevent swelling of the AEM that

can occur using the catalyst coated membrane (CCM) approach. Both CCM and CCS approach MEAs have been shown to produce adequate AEMWE performance [36]. As electrode substrates, 0.2 mm thick Spectracarb 1050-2050A graphite paper for the cathode side and 0.23 mm thick 316L stainless-steel felt (Bekeart, Bekipor ST 40 type 40 BL3) for the anode were selected. Pt/C (HISPEC4000, Alfa) and Ir-Black (Umicore), both widely employed reference catalysts, were used as cathode and anode catalyst, respectively. The target electrode catalyst loading was 1  $\text{mg}_{Pt} \text{cm}^{-2}$  and 2  $\text{mg}_{Ir} \text{cm}^{-2}$ ; the ionomer content was 30 wt % for both the electrodes. In order to manufacture the CCSs, firstly, a catalyst ink, with appropriate rheological properties had to be formulated. After combining the desired amount of catalyst with a CMSEBS-THF solution, i.e., 25  $\text{mg}_{Pt/C} \text{mL}^{-1}$  and 10  $\text{mg}_{Ir-Black} \text{mL}^{-1}$ , the ink was dispersed in an ultrasonic bath (Bandelin Sonocool SC255) at 100% power for 1 h at 5 °C. Next followed the catalysts deposition using a generic spray gun with a 0.5 mm nozzle using compressed nitrogen at 2 bar over-pressure. The electrode substrates were placed on a hot plate set to 60 °C to accelerate the solvent evaporation and prevent substrate flooding. After coating, to crosslink the ionomer phase in the electrode layers, the CCS were submerged in a large excess of 30 wt % aqueous triethylamine solution at room temperature for 24 h, then thoroughly rinsed and left again overnight in a DI water bath to remove all triethylamine. Finally, prior to cell assembly, the crosslinked and rinsed CCSs and AEM were activated in 100 mL each of a 1 M aqueous KOH solution, for 72 h at room temperature.

### 2.5. SEBS-P2O6 AEMWE cell test

The AEMWE cell tests carried out in this study were performed at atmospheric pressure and 60 °C using a small single cell with a 4  $\text{cm}^2$  active surface, feeding supporting electrolyte or water to both the anode and cathode compartment. During operation, the complete testing setup was sealed against the atmosphere to prevent any carbon dioxide intrusion only allowing hydrogen and oxygen to escape through a gas washing apparatus, to avoid corrosion, titanium grade 1 polar plates without flow fields and titanium grade 1 GKN Sinter Metals SIKA-HY PTLs were employed on both anode and cathode. The SIKA-HY PTLs, designed in cooperation with the DLR, have been shown to allow operation without mass transport limitation free operation at up to 6 A  $\text{cm}^{-2}$  [37]. The cells were constructed with the CCSs and AEM in contact to 1 M KOH solution, applying an effective MEA compression of approximately 85 N  $\text{cm}^{-2}$ . Immediately after assembly the feed was changed to 0.1 M KOH and an activation process was carried, applying 1.4 V, 1.6 V, 1.8 V, each for 5 min, and finally 2 V, until current density started to decrease again. The last step lasted approximately 15 min. In case of the ultra-pure water (UPW) test, the cell was then carefully and thoroughly rinsed with 2 L of carbon dioxide free (ion exchange resin plus nitrogen bubbling) ultra-pure water (Milli-Q 18.2  $\text{M}\Omega \text{cm}^{-1}$ ), completely drained, and refilled with 2 L of fresh carbon dioxide free ultra-pure water. This step was not present for the measurement in 0.1 M KOH. Subsequently the cell was cycled between 1 and 2 V (10  $\text{mV s}^{-1}$ ) twelve times until the peak current density was largely stable, albeit slowly decreasing due to cell degradation (initial steady state, dubbed "initial"). Subsequently, after recording an electrochemical impedance spectrum, a constant cell potential of 2 V was applied, recording current density over 330 h. This potentiostatic operation was interrupted each time recording three consecutive IV-curves (1–2 V, 10  $\text{mV s}^{-1}$ ) and an impedance spectrum. In each group of IV-curves, the third is considered to be representative of the cell condition and presented in the following. All impedance spectra were recorded at 25  $\text{mA cm}^{-2}$  using an amplitude of 2.5  $\text{mA cm}^{-2}$  scanning from 100 kHz to 100 mHz. EIS and IV-curves were recorded using a Zahner Zennium X potentiostat coupled with a Zahner PP241 booster.

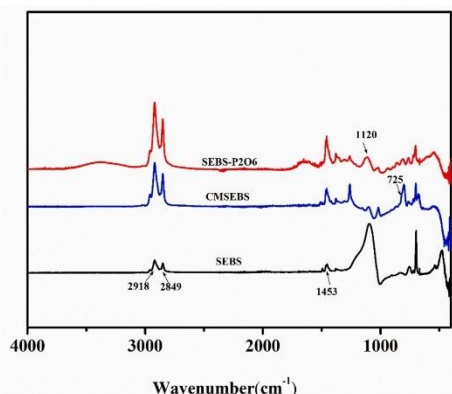


Fig. 3. FT-IR spectra of SEBS, CMSEBS and SEBS-P2O6 membranes.

### 3. Results and discussion

#### 3.1. Synthesis and preparation

In this paper SEBS was used as polymer educt for preparation of AEM. This block copolymer possesses both flexible blocks as ethylene and butadiene and some aromatic ring containing blocks as styrene. The last was used for polymer post-modification via (i) chloroalkylation and (ii) amination of the polymer to obtain quaternary ammonium functional groups. Initial chloromethylation of SEBS showed functionalization degree of about 74.6%. In the next step, beside reactions with TMA in the absence of cross-linkers (Fig. 1a), some crosslinking agents such as diaminoalkanes (N2CX) (Fig. 1(b)), 1,6-bis(piperidin-1-yl) hexane (P2C6) (Fig. 1(c)) and 1,2-Bis(2-piperidinylethoxy) ethane (P2O6) (Fig. 1(d)) were used to study their impact on the stabilization of the membrane, swelling reduction and conductivity improvement.

In order to prove the functionalization and crosslinking degree and thus clarify the composition and the chemical structure, CMSEBS was characterized by  $^1\text{H}$  NMR (Fig. 2(a)). The resonance peak with chemical shift was 0.75–0.86 ppm ( $-\text{CH}_3$  in butane), 0.95–1.14 ppm (methylene in butane), 1.15–1.33 ppm ( $-\text{CH}_2-$  in ethylene), 1.54–1.59 ppm (methylene in styrene), 1.75–1.90 ppm ( $-\text{CH}_2-$  in styrene) and 6.3–7.25 ppm (benzene in styrene). They belong to the backbone structure of the polymer. The peaks at 4.5 ppm which can be ascribed to  $-\text{CH}_2\text{Cl}$  on benzene, indicate that chloromethylation reaction proceeded smoothly [38,39]. Comparing the integral ratio of the  $-\text{CH}_2\text{Cl}$  (peak 8) to Ar-H (peaks 1 and 2) in Figs. 2 (a), 74.6 mol% styrene units were found to be chloromethylated (11.9 mol% for the whole polymer).

For the structure of 1,6-bis(piperidin-1-yl) hexane (P2C6), the  $^1\text{H}$ NMR chemical shift and  $^{13}\text{C}$ NMR spectra are shown in Fig. 2(b) and (c) and those for 1,2-Bis(2-piperidinylethoxy) ethane (P2O6) in Fig. 2(d)

and (e). In both structures the absence of peaks for  $\text{Br}-\text{CH}_2-$  and the corresponding integral ratios between the  $\text{N}-\text{CH}_2-$  and the rest of the protons in the structure, confirms the successful preparation of those crosslinker molecules.

For those samples that were insoluble due to crosslinking, FT-IR was carried out to reveal the crosslinking of CMSEBS by the cross-linker P2O6. Comparing with the FT-IR of pristine SEBS, a new peak appeared at  $725\text{ cm}^{-1}$  (Fig. 3). This peak corresponds to C-Cl stretching vibration of the chloromethyl group. For the case of CMSEBS, the membrane was immersed into the P2O6 solution, which lead to appearance of a new peak in the FT-IR at  $1120\text{ cm}^{-1}$ . This wave numbers are the typical for C-O stretching vibration, which indicates that the CMSEBS was efficiently crosslinked by P2O6.

#### 3.2. Ionic conductivity, dimensional and chemical stability of the membranes

##### 3.2.1. SEBS-N2CX membranes

Commonly, AEMs based on ammonium functionalized SEBS possess lower conductivity [40,41], therefore improving the conductivity of the SEBS based membranes is a challenge. In earlier researches, several strategies have been followed to improve the conductivity of SEBS based membrane, such as building a comb-shaped structure [42], putting multi-cation in one side chain [43] and crosslinking with other backbones [44]. Among them, building a comb-shaped structure in the membrane is a common way to increase the conductivity of the membrane by enhancing the microphase separation. In this work, we applied the concept of comb-shaped macromolecules to membranes based on SEBS-TMA and simultaneously stabilize the membrane via crosslinking with various crosslinkers. To do so, we first crosslinked CMSEBS with crosslinkers (N2CX or P2C/O6) and then converted the rest of benzyl chlorides into ammonium functional groups by reaction with trimethylamine. Some of the most important properties of so prepared CMSEBS membranes crosslinked with diaminopropane, diaminobutane and diaminohexane in respect to their application are presented in Table 1. Among SEBS-N2CX membranes, SEBS-N2C3 reached  $16.2\text{ mS cm}^{-1}$  hydroxide conductivity at room temperature, which is higher than that of SEBS-N2C4 ( $12.4\text{ mS cm}^{-1}$ ) and SEBS-N2C6 ( $10.2\text{ mS cm}^{-1}$ ). The higher conductivity of SEBS-N2C3 might be attributed to higher swelling and water uptake while IEC for all SEBS-N2CX samples is similar to each other. The conductivities of SEBS-N2C4 and SEBS-N2C6 at room temperature are similar to piperidinium functionalized SEBS-pi-73% ( $10.09\text{ mS cm}^{-1}$  at  $1.19\text{ mmol g}^{-1}$  IEC), that has been published before [1]. For mechanical properties of all membranes, due to low relative styrene polymer changes we do not expect significant tensile stress variation between the membranes. The Stress-strain relations are expected to be similar to Yang et al. J [32].

In order to check the alkaline stability, the membranes were immersed into the  $1\text{ M KOH}$  at  $90\text{ }^\circ\text{C}$  for more than 200 h. At these conditions the membrane SEBS-N2C3 became very brittle and did not survive further conductivity measurements. At the same time, after immersing SEBS-N2C6 in  $1\text{ M KOH}$  at  $90\text{ }^\circ\text{C}$  for more than 700 h, the conductivity of the membrane dropped down from  $10.2\text{ mS cm}^{-1}$  to  $8.2\text{ mS cm}^{-1}$  ( $\text{OH}^-$  form). This is 81.6% conductivity retention, which can be ascribable to the degradation of benzyl ammonium in harsh hot

Table 1

IEC, conductivity, swelling ratio and water uptake of the membrane at  $25\text{ }^\circ\text{C}$  (IECa is the IEC after membrane crosslinking and IECb is the final IEC).

	IECa ( $\text{mmol g}^{-1}$ )	IECb ( $\text{mmol g}^{-1}$ )	Conductivity ( $\text{Cl}^-$ ) ( $\text{mS cm}^{-1}$ )	Conductivity ( $\text{OH}^-$ ) ( $\text{mS cm}^{-1}$ )	Swelling ratio (%)	Water Uptake ( $\text{Cl}^-$ ) (%)
SEBS-TMA			$4.6 \pm 0.31$	$8.8 \pm 0.50$	$3.8 \pm 1.22$	$12.5 \pm 4.14$
SEBS-N2C6	$0.44 \pm 0.01$	$0.96 \pm 0.03$	$5.7 \pm 0.44$	$10.2 \pm 0.24$	$5.5 \pm 1.61$	$17.2 \pm 5.61$
SEBS-N2C3	$0.47 \pm 0.02$	$1.05 \pm 0.04$	$8.9 \pm 0.40$	$16.2 \pm 0.50$	$7.3 \pm 2.20$	$28.6 \pm 8.30$
SEBS-N2C4	$0.46 \pm 0.01$	$1.04 \pm 0.03$	$6.6 \pm 0.47$	$12.4 \pm 0.53$	$6.8 \pm 2.41$	$22.4 \pm 6.00$
SEBS-P2C6	$0.40 \pm 0.01$	$1.10 \pm 0.01$	$6.45 \pm 0.30$	$12.5 \pm 0.42$	$6.5 \pm 2.79$	$20.1 \pm 8.43$
SEBS-P2O6	$0.42 \pm 0.01$	$1.05 \pm 0.04$	$11.7 \pm 0.54$	$20.8 \pm 0.74$	$9.2 \pm 4.81$	$36.8 \pm 7.35$
Tokuyama A201 [45]	–	1.7	12	–	–	19



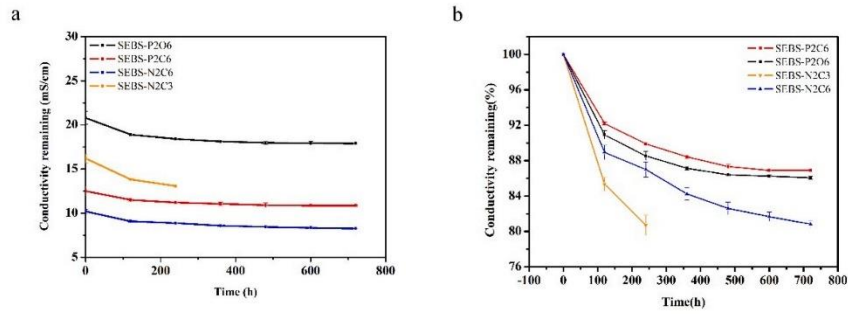


Fig. 4. (a) Ionic conductivity at room temperature, (b) conductivity retention of SEBS-P2O6 membranes after stability test in KOH at 90 °C.

alkaline environment [21]. Considering both the conductivity and stability, longer chains ( $-C_6H_{12}-$ ) between the functional groups showed relatively balanced conductivity and stability and these systems were mainly investigated further on in this work.

### 3.2.2. SEBS-P2C6 and SEBS-P2O6 membranes

Basically, piperidinium group is expected to be one of the most stable functional groups for AEM, due to lower ring strain and high energy barrier to transition originating from favorable non-anti-periplanar conformation caused by the unique ring structure [1,23]. In order to

stabilize the membrane—especially the side chain, piperidinium group is selected to replace the quaternary ammonium in the side chain. After replacing the quaternary ammonium to piperidinium group in the crosslinking chain, the conductivity remained at similar level at room temperature.

Comparing the results for piperidinium crosslinkers SEBS-P2C6 and SEBS-P2O6 with SEBS-N2CX (Table 1), the highest hydroxide conductivity of  $20.8 \text{ mS cm}^{-1}$  was obtained for SEBS-P2O6. Both SEBS-P2C6 and -P2O6 showed similar IEC compared to SEBS-N2CX membranes, however, the swelling and the water uptake of SEBS-P2O6 was 1.5–3

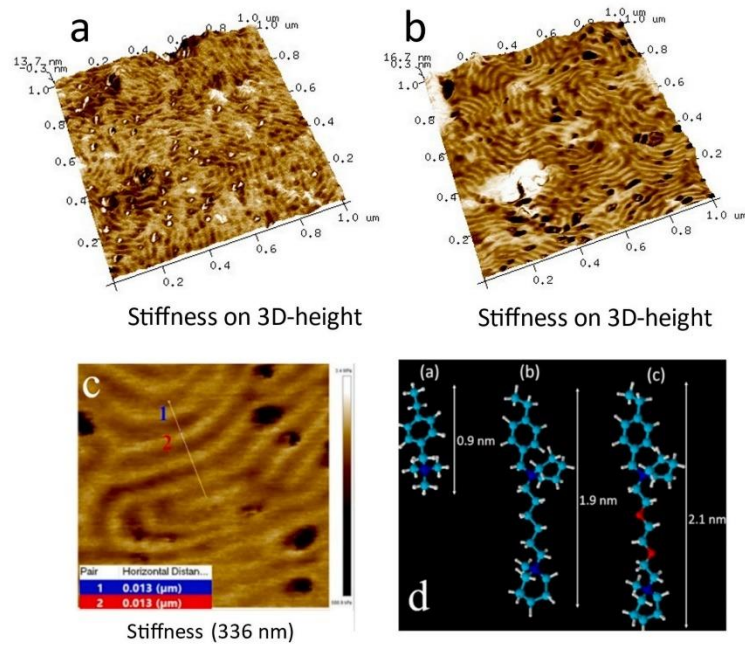


Fig. 5. AFM 3D-height images with superposed stiffness data of the membranes for (a) SEBS-P2C6 and (b, c) SEBS-P2O6; (d) 3D structures and their corresponding length of a monomer unit with trimethyl ammonium (a), P2C6 (b) and P2O6 (c) functional groups.

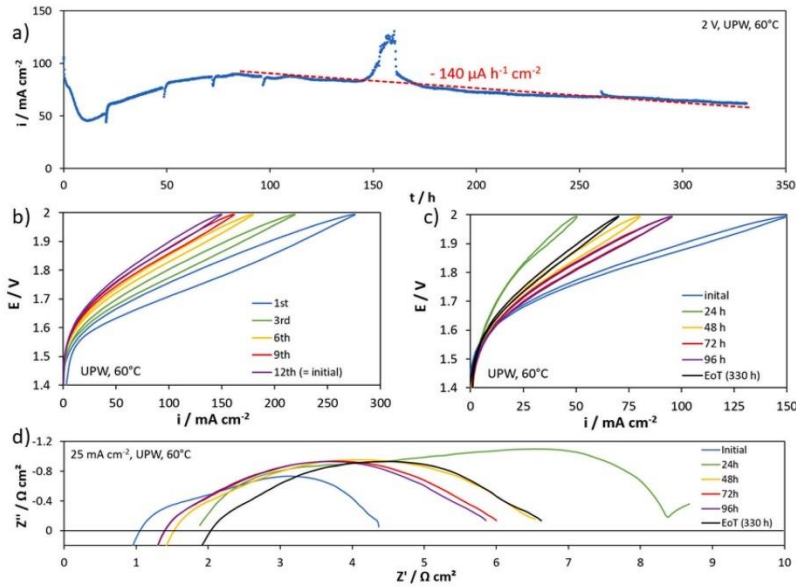


Fig. 6. AEM water electrolysis test results measured in 60 °C UPW, a) degradation at 2 V, b) IV-curves recorded after switching to UPW from 0.1 M KOH, c) following IV-curves recorded during the degradation test and d) EIS recorded during the degradation test.

times higher than for the other membranes. This could be the most probable reason for the higher conductivity of the SEBS-P2O6 membranes. In all cases  $\text{Cl}^-$  conductivity is about twice lower than the  $\text{OH}^-$  conductivity, which is due to larger and heavier  $\text{Cl}^-$  ion compared to  $\text{OH}^-$ . The ratios of  $\text{OH}^-$  to  $\text{Cl}^-$  conductivities are slightly lower than the reported  $\text{Cl}^-$  and  $\text{OH}^-$  conductivity ratio ( $\sigma_{\text{OH}^-}/\sigma_{\text{Cl}^-} \sim 2.7$ ) in the literature [46]. However, this difference may be accounted by residual  $\text{CO}_2$  present in our case for the  $\text{OH}^-$  value although care was taken to perform the test immediately after removal from KOH solution.

In addition, the chemical stability of SEBS-P2C6 and SEBS-P2O6 were superior compared to SEBS-N2CX, demonstrated in a stability test in 1 M KOH for more than 700 h (Fig. 4). The conductivity of SEBS-P2C6 membrane dropped down from  $12.5 \text{ mS cm}^{-1}$  to  $10.9 \text{ mS cm}^{-1}$  with 86.9% conductivity retention. Similarly, the conductivity of SEBS-P2O6 decreased from  $20.8$  to  $17.9 \text{ mS cm}^{-1}$  with conductivity retention about 85.9%. In both cases relatively quick conductivity decay is observed after the first 50 h, followed by stabilization and low conductivity decay rate of about 1 and  $1.5 \mu\text{S cm}^{-1} \text{ h}^{-1}$ . Thus, the membrane SEBS-P2O6, bearing long, flexible, hydrophilic side-chain, showed high conductivity and chemical stability. Expected stability differences between SEBS-P2O6 and SEBS-P2C6 are not significant within the measurement time and future work will aim at clarifying this point. Similarly, in a study from Zhu et al., an improvement of AEM ion conductivity and a good chemical stability has been reported by incorporating hydrophilic and flexible ethylene oxide spacers into the ionic side-chains, hence forming a flexible-spacer structure [29].

### 3.3. Membranes morphology study on SEBS-P2O6 and SEBS-P2C6

To investigate the structural arrangement and hydrophobic/hydrophilic nano-phase separation geometry of SEBS-P2O6 and SEBS-P2C6 membranes, nanomechanical AFM measurements were performed.

DMT modulus stiffness mappings of SEBS-P2O6 and SEBS-P2C6 membranes surface are shown in Fig. 5(a) and (b), respectively. The bright (stiffer) regions correspond to hydrophobic polymer backbone aggregation and the dark regions to hydrophilic side-chain assembly. A significant separation of hydrophilic and hydrophobic phases was found for both SEBS-P2O6 and SEBS-P2C6 membranes. For SEBS-P2O6, containing long flexible and hydrophilic side chains, the hydrophobic and hydrophilic domains formed broader continuous phases than those in SEBS-P2C6. The width scale of the lamellar structuring for SEBS-P2O6 is about 13 nm. Estimations of the length of the monomer units bearing trimethyl ammonium as well as P2C6 and P2O6 are shown in Fig. 5(d). These structures were obtained after minimization of the energy by ACD 3D Viewer software to reach a local minimum after at least 50 iterations. The estimated lengths are about 1 nm for the trimethyl ammonium and about 2 nm for P2C6 and P2O6 functionalized monomer units. A rough comparison revealed a factor 6 larger hydrophilic domains compared to the length of the crosslinkers. Therefore, it can be assumed that crosslinking occurs primarily in the hydrophobic domains and the spacers with side functional groups are well unzipped. The broader and better interconnected hydrophilic domains of SEBS-P2O6 facilitate the formation of continuous ion channels of relatively constant size, which enables efficient ion transport [47,48].

### 3.4. AEM water electrolysis measurements

Considering the benefits of using cross-linking piperidinium based ethylene oxide spacers side chain, SEBS-P2O6 membranes are expected to achieve improved AEM water electrolysis performance and durability. Here we chose to operate at 60 °C rather than 80 °C because at present no commercial AEMWE (which operate with UPW) can operate at 80 °C [31] due to the poor stability of the ion exchange resin.

Commonly, MEAs tested in AEM electrolysis cells are not only

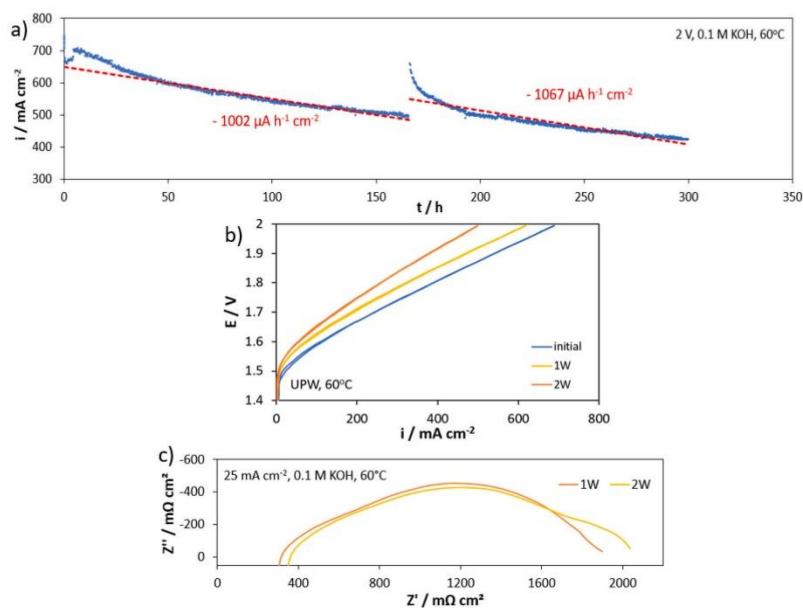


Fig. 7. AEM water electrolysis test results measured weekly (W) in 60 °C 0.1 M KOH, a) degradation at 2 V, b) IV-curves recorded during the degradation test and c) EIS recorded during the degradation test.

activated ex-situ in an alkaline solution, but are also activated in-situ, feeding an alkaline solution to the cell, carrying out an activation protocol, before the ultra-pure water is introduced, leading to increased performance. As shown by Lindquist et al., there is a benefit to this additional activation step in KOH, which is elevated performance in ultra-pure water operation and only some of this performance improvement is reversible, presumably because of remaining KOH in the MEA [49]. Even after thorough UPW purging, performance remains elevated initially, supposedly due to a more complete AEM and ionomer activation or lower AEM and ionomer swelling in KOH, which revert quickly after starting operation in UPW, leading to a short term improvement of catalyst/ionomer interaction. Moreover, it may also be caused by the adsorption of KOH in the layers, which means the UPW purging is not effective. Adsorbed KOH ( $K^+$ ,  $OH^-$ ) maybe not be removed simply by diffusion (i.e., surrounding the layer with UPW) but convectively after starting cell operation in UPW. The actual underlying mechanisms remain unclear.

After in-situ activation in 0.1 M KOH, the cell was thorough purged with UPW a current density of 275  $\text{mA cm}^{-2}$  at 2 V was reached (Fig. 6 (b)). After nine IV-cycles, peak-to-peak degradation became linear, which led to the conclusion, that the cell had entered a gradual degradation regime, not connected to the reversible in-situ activation. After cycling twelve times, now reaching 150  $\text{mA cm}^{-2}$  at 2 V, the cell was considered to have reached the initial UPW steady-state. Overall, the UPW performance reached here exceeds previous results achieved with SEBS AEMs and ionomers in AEMWE [1,31].

In the following potentiostatic degradation test (Fig. 6(a)), performance first rapidly deteriorated over 20 h, before recovering to a significant degree over the following 70 h. This unexpected behavior has not been reported in previous publications. As becomes apparent in Fig. 6(d), the recovery process (24 h–96 h) was not dominated by ohmic

contribution but almost exclusively due to a reduction of kinetic resistance, being the sum of hydrogen evolution reaction (HER), oxygen evolution reaction (OER) and mass transport loss (MTL). The High frequency resistance (HFR)-resistance was not significantly affected. This suggests, that the changes are connected to the catalyst layer structure, i.e., available catalyst surface and permeability of the catalyst surface, not to the ionomer and membrane itself. It can be speculated that a first excessive ionomer content (30 wt.-%) was improved after some ionomer breakdown during operation. The low swelling and water permeability of the ionomer may lead to an initial blocking of catalyst surface.

In the following linear degradation regime, current density fell at a rate of 140  $\mu\text{A h}^{-1} \text{cm}^{-2}$ . A spike in current density was caused by an accidental overheating of the cell to 85 °C, not resulting in any irreversible degradation. Between hour 96 h and the end of test (EoT), degradation was caused solely by an increase in HFR resistance, leading to the conclusion, that the reduction of current density is largely caused by ionomer and AEM breakdown, or other phenomena affecting the HFR resistance only.

In a separate test, cell performance and degradation at 60 °C in 1 M KOH was evaluated (Fig. 7). A steady-state was reached quickly and largely linear degradation (approximately  $-1 \text{ mA h}^{-1} \text{cm}^{-2}$ ) ensued. Initially, a current density of 680  $\text{mA cm}^{-2}$  was reached at 2 V, significantly outpacing published results recorded using similar materials in AEMWE [1,31]. Inspection of the EIS and IV-curves recorded (Fig. 7(b) and (c)) shows an initial increase of HFR-free cell resistance (initial to week 1, IV-curve is shifted upwards), followed by an increase of low frequency impedance, likely connected to an increase of MTL resistances (week 1 to week 2, visible in the Nyquist plots). The HFR resistance remains largely unchanged (initial to 1 W, slope at higher densities, in the linear regime). These results give evidence, that in 0.1 M KOH, the physical breakdown of the catalyst layer dictates cell behavior, not the

breakdown of the ionic conductivity of the AEM and ionomer. This doesn't mean necessarily that the ionomer and AEM are not degrading, but that this degradation is not reflected in the electrochemical behavior of the cell. If conductive liquid electrolyte is present, typically degradation of AEM and ionomer are somewhat masked by that.

#### 4. Conclusions

Novel double piperidinium functionalized flexible ethylene oxide spacer side chain SEBS AEM was designed, synthesized and applied as membrane for AEMWE application. In order to improve the conductivity of the membrane, comb-shaped multi-functional groups structure was assigned and investigated revealing that longer spacer ( $-C_6H_{12}-$ ) between functional groups had relatively balanced conductivity and chemical stability. In the next approach the quaternary ammonium was substituted by piperidinium groups to enhance the chemical stability of the membrane. Furthermore, flexible ethylene oxide spacer structure in side chain could enhance the water uptake of the membrane and thus promote the microphase separation resulting in enhanced conductivity. Finally, SEBS-P2O6 reached conductivity of  $20.8 \text{ mS cm}^{-1} (\text{OH}^-)$  at room temperature, which is higher than SEBS piperidinium membrane published in the past. In single cell AEM water electrolysis tests, at  $60^\circ\text{C}$  and 2 V cell potential, current densities  $275 \text{ mA cm}^{-2}$  and  $680 \text{ mA cm}^{-2}$  were reached in UPW and 0.1 M KOH, respectively. We have shown that the SEBS P2O6 membrane outperforms other SEBS based materials presented in literature [1,31] and that SEBS is a promising candidate for AEM electrolysis cells. The results suggest, that further optimization of the electrode structure is needed to increase mechanical stability and that via improvement of ink formulation, layer deposition and cell setup parameters to increase mechanical stability.

#### Author statement

Ziqi Xu: Conceptualization, Methodology, membrane synthesis, membrane characterization and manuscript writing. Vincent Wilke: cell tests, manuscript writing (cell part) and manuscript reviewing. Jagoda Justyna Chmielarz: cell tests, manuscript writing (cell part) and manuscript reviewing. Tobias Morawietz: AFM test and manuscript reviewing. Vladimir Atanasov: membrane supervision and manuscript reviewing. Aldo Saul Gago: supervision and manuscript reviewing. Kaspar Andreas Friedrich: supervision and manuscript reviewing.

#### Declaration of competing interest

The authors declare that they have no known competing financial interests or personal relationships that could have appeared to influence the work reported in this paper.

#### Data availability

Data will be made available on request.

#### Acknowledgments

This work was supported by the European project NEWELY, which received funding from the Fuel Cells and Hydrogen 2 Joint Undertaking (now Clean Hydrogen Partnership) under Grant Agreement No 875118 and the Chinese Scholarship Council (201706060199). We also thank TSRC for offering the SEBS polymer.

#### References

- [1] X. Su, L. Gao, L. Hu, N.A. Qaisrani, X. Yan, W. Zhang, X. Jiang, X. Ruan, G. He, Novel piperidinium functionalized anionic membrane for alkaline polymer electrolysis with excellent electrochemical properties, *J. Membr. Sci.* 581 (2019) 283–292, <https://doi.org/10.1016/j.memsci.2019.03.072>.

- [2] Y. Leng, G. Chen, A.J. Mendoza, T.B. Tighe, M.A. Hickner, C.-Y. Wang, Solid-state water electrolysis with an alkaline membrane, *J. Am. Chem. Soc.* 134 (22) (2012) 9054–9057, <https://doi.org/10.1021/ja302439z>.
- [3] J. Chu, H. Yu, Water electrolysis based on renewable energy for hydrogen production, *Chin. J. Catal.* 39 (3) (2018) 390–394, [https://doi.org/10.1016/S1872-2067\(17\)62949-8](https://doi.org/10.1016/S1872-2067(17)62949-8).
- [4] W.L. Li Xu, Y.O.U. Yan, Shaoping Zhang, Z.H.A.O. Yingchun, Polysulfone and zirconia composite separators for alkaline water electrolysis, *Front. Chem. Sci. Eng.* 7 (2) (2013) 154–161, <https://doi.org/10.1007/s11705-013-1331-8>.
- [5] I. Vincent, D. Bessarabov, Low cost hydrogen production by anion exchange membrane electrolysis: a review, *Renew. Sustain. Energy Rev.* 81 (2018) 1690–1704, <https://doi.org/10.1016/j.rser.2017.05.258>.
- [6] F. Razmjooei, A. Farooqui, R. Reissner, A.S. Gago, S.A. Ansar, K.A. Friedrich, Elucidating the performance limitations of alkaline electrolyte membrane electrolysis: dominance of anion concentration in membrane electrode assembly, *ChemElectrochem* 7 (19) (2020) 3951–3960, <https://doi.org/10.1002/celec.202000605>.
- [7] H.A. Miller, K. Buzek, J. Hnat, S. Loos, C.I. Bernicker, T. Weißgürber, I. Röntsch, J. Meier-Haack, Green hydrogen from anion exchange membrane water electrolysis: a review of recent developments in critical materials and operating conditions, *Sustain. Energy Fuels* 4 (5) (2020) 2114–2133, <https://doi.org/10.1039/C9SE01240K>.
- [8] D. Burnat, M. Schlupp, A. Wichser, B. Lothenbach, M. Gorbar, A. Züttel, U.F. Vogt, Composite membranes for alkaline electrolysis based on polysulfone and mineral fillers, *J. Power Sources* 291 (2015) 163–172, <https://doi.org/10.1016/j.jpowsour.2015.04.066>.
- [9] N. Lee, D.T. Duong, D. Kim, Cyclic ammonium grafted poly(arylene ether ketone) hydroxide ion exchange membranes for alkaline water electrolysis with high chemical stability and cell efficiency, *Electrochim. Acta* 271 (2018) 150–157, <https://doi.org/10.1016/j.electacta.2018.03.117>.
- [10] H.J. Kaezi, Y. Yang, Z. Liu, S.D. Sajjad, R.I. Masel, Carbon dioxide and water electrolysis using new alkaline stable anion membranes, *Front. Chem.* 6 (263) (2018), <https://doi.org/10.3389/fchem.2018.00263>.
- [11] P. Fortin, T. Khoza, X. Cao, S.Y. Martinsen, A. Oyaree Barnett, S. Holdcroft, High-performance alkaline water electrolysis using Aemion™ anion exchange membranes, *J. Power Sources* 451 (2020), 227814, <https://doi.org/10.1016/j.jpowsour.2020.227814>.
- [12] I.V. Pushkareva, A.S. Pushkarev, S.A. Grigoriev, P. Modisha, D.G. Bessarabov, Comparative study of anion exchange membranes for low-cost water electrolysis, *Int. J. Hydrogen Energy* 45 (49) (2020) 26070–26079, <https://doi.org/10.1016/j.ijhydene.2019.11.011>.
- [13] N.C. Buggy, Y. Du, M.-C. Kuo, K.A. Ahrens, J.S. Wilkinson, S. Seifert, E.B. Coughlin, A.M. Herring, A polyethylene-based triblock copolymer anion exchange membrane with high conductivity and practical mechanical properties, *ACS Applied Polymer Materials* 2 (3) (2020) 1294–1303, <https://doi.org/10.1021/acscppm.9b01182>.
- [14] M. David, C. Ocampo-Martínez, R. Sánchez-Peña, Advances in alkaline water electrolyzers: a review, *J. Energy Storage* 23 (2019) 392–403, <https://doi.org/10.1016/j.est.2019.03.001>.
- [15] T.H. Pham, J.S. Olsson, P. Jannasch, Poly(arylene alkylene)s with pendant N-spirocyclic quaternary ammonium cations for anion exchange membranes, *J. Mater. Chem.* 6 (34) (2018) 16537–16547, <https://doi.org/10.1039/C8TA04699A>.
- [16] J.R. Varcoe, P. Atanasov, D.R. Dekel, A.M. Herring, M.A. Hickner, P.A. Kohl, A. R. Kucernak, W.E. Mustain, K. Nijmeijer, K. Scott, T. Xu, L. Zhuang, Anion-exchange membranes in electrochemical energy systems, *Energy Environ. Sci.* 7 (10) (2014) 3135–3191, <https://doi.org/10.1039/C4EE01303D>.
- [17] C. Yang, S. Wang, L. Jlang, J. Hu, W. Ma, G. Sun, 1,2-Dimethylimidazolium-functionalized cross-linked alkaline anion exchange membranes for alkaline direct methanol fuel cells, *Int. J. Hydrogen Energy* 40 (5) (2015) 2363–2370, <https://doi.org/10.1016/j.ijhydene.2014.12.050>.
- [18] L. Zhu, X. Peng, S.-L. Shang, M.T. Kwasny, T.J. Zimudzi, X. Yu, N. Saikia, J. Pan, Z.-K. Liu, G.N. Tew, W.E. Mustain, M. Yandrasits, M.A. Hickner, High performance anion exchange membrane fuel cells enabled by fluoropoly(olefin) membranes, *Adv. Funct. Mater.* 29 (26) (2019), 1902059, <https://doi.org/10.1002/adfm.201902059>.
- [19] J.Y. Jeon, S. Park, J. Han, S. Maurya, A.D. Mohanty, D. Tian, N. Saikia, M. A. Hickner, C.Y. Ryu, M.E. Tuckerman, S.J. Paddison, Y.S. Kim, C. Bae, Synthesis of aromatic anion exchange membranes by Friedel-Crafts bromoalkylation and cross-linking of polystyrene block copolymers, *Macromolecules* 52 (5) (2019) 2139–2147, <https://doi.org/10.1021/acs.macromol.8b02355>.
- [20] C.G. Argers, V. Ramanil, Two-dimensional NMR spectroscopy reveals cation-triggered backbone degradation in polysulfone-based anion exchange membranes, *Proc. Natl. Acad. Sci. USA* 110 (7) (2013) 2490, <https://doi.org/10.1073/pnas.1217215110>.
- [21] J.B. Edson, C.S. Macomber, B.S. Pivovar, J.M. Boncella, Hydroxide based decomposition pathways of alkyltrimethylammonium cations, *J. Membr. Sci.* 399–400 (2012) 49–59, <https://doi.org/10.1016/j.memsci.2012.01.025>.
- [22] H. Long, K. Kim, B.S. Pivovar, Hydroxide degradation pathways for substituted trimethylammonium cations: a dft study, *J. Phys. Chem. C* 116 (17) (2012) 9419–9426, <https://doi.org/10.1021/jp3014964>.
- [23] M.G. Marino, K.D. Kreuer, Alkaline stability of quaternary ammonium cations for alkaline fuel cell membranes and ionic liquids, *ChemSusChem* 8 (3) (2015) 513–523, <https://doi.org/10.1002/cssc.201403022>.
- [24] J.S. Olsson, T.H. Pham, P. Jannasch, Tuning poly(arylene piperidinium) anion-exchange membranes by copolymerization, partial quaternization and

- crosslinking, *J. Membr. Sci.* 578 (2019) 183–195, <https://doi.org/10.1016/j.memsci.2019.01.036>.
- [25] J. Pan, C. Chen, Y. Li, L. Wang, L. Tan, G. Li, X. Tang, L. Xiao, J. Lu, L. Zhuang, Constructing ionic highway in alkaline polymer electrolytes, *Energy Environ. Sci.* 7 (1) (2014) 354–360, <https://doi.org/10.1039/C3EE43275K>.
- [26] N. Li, T. Yan, Z. Li, T. Thurn-Albrecht, W.H. Binder, Comb-shaped polymers to enhance hydroxide transport in anion exchange membranes, *Energy Environ. Sci.* 5 (7) (2012) 7888–7892, <https://doi.org/10.1039/C2EE22050D>.
- [27] L. Zhu, J. Pan, Y. Wang, J. Han, L. Zhuang, M.A. Hickner, Multication side chain anion exchange membranes, *Macromolecules* 49 (3) (2016) 815–824, <https://doi.org/10.1021/acs.macromol.5b02671>.
- [28] J. Han, L. Zhu, J. Pan, T.J. Zimudzi, Y. Wang, Y. Peng, M.A. Hickner, L. Zhuang, Elastic long-chain multication cross-linked anion exchange membranes, *Macromolecules* 50 (8) (2017) 3323–3332, <https://doi.org/10.1021/acs.macromol.6b01140>.
- [29] Y. Zhu, L. Ding, X. Liang, M.A. Shehzad, L. Wang, X. Ge, Y. He, L. Wu, J.R. Varcoe, T. Xu, Beneficial use of rotatable-spacer side-chains in alkaline anion exchange membranes for fuel cells, *Energy Environ. Sci.* 11 (12) (2018) 3472–3479, <https://doi.org/10.1039/C8EE02071J>.
- [30] X. Gao, H. Yu, J. Jia, J. Hao, F. Xie, J. Chi, B. Qin, L. Fu, W. Song, Z. Shao, High performance anion exchange ionomer for anion exchange membrane fuel cells, *RSC Adv.* 7 (31) (2017) 19153–19161, <https://doi.org/10.1039/C7RA01980G>.
- [31] G. Gupta, K. Scott, M. Mamlouk, Performance of polyethylene based radiation grafted anion exchange membrane with polystyrene-*b*-poly (ethylene/butylene)-*b*-polystyrene based ionomer using NiCo2O4 catalyst for water electrolysis, *J. Power Sources* 375 (2018) 387–396, <https://doi.org/10.1016/j.jpowsour.2017.07.026>.
- [32] C. Yang, S. Wang, W. Ma, S. Zhao, Z. Xu, G. Sun, Highly stable poly(ethylene glycol)-grafted alkaline anion exchange membranes, *J. Mater. Chem.* 4 (10) (2016) 3886–3892, <https://doi.org/10.1039/C6TA00200E>.
- [33] A.D. Mohanty, C.Y. Ryu, Y.S. Kim, C. Bae, Stable elastomeric anion exchange membranes based on quaternary ammonium-tethered polystyrene-*b*-poly (ethylene-co-butylene)-*b*-polystyrene triblock copolymers, *Macromolecules* 48 (19) (2015) 7085–7095, <https://doi.org/10.1021/acs.macromol.5b01382>.
- [34] T. Morawietz, M. Handl, C. Oldani, K.A. Friedrich, R. Hiesgen, Influence of water and temperature on ionomer in catalytic layers and membranes of fuel cells and electrolyzers evaluated by AFM, *Fuel Cell* 18 (3) (2018) 239–250, <https://doi.org/10.1002/fuce.201700113>.
- [35] H. Cho, V. Atanasov, H.M. Krieg, J.A. Kerres, Novel anion exchange membrane based on poly(pentafluorostyrene) substituted with mercaptotetrazole pendant groups and its blend with polybenzimidazole for vanadium redox flow battery applications, *Polymers* 12 (4) (2020), <https://doi.org/10.3390/polym12040915>.
- [36] N. Du, C. Roy, R. Peach, M. Turnbull, S. Thiele, C. Bock, Anion-Exchange Membrane Water Electrolyzers, *Chem Rev.* 2022, <https://doi.org/10.1021/acs.chemrev.1c00854>.
- [37] S. Stüber, H. Balzer, A. Wierhake, F.J. Winkert, J. Roth, U. Rost, M. Brodmann, J. K. Lee, A. Bazyłak, W. Waiblinger, A.S. Gago, K.A. Friedrich, Porous transport layers for proton exchange membrane electrolysis under extreme conditions of current density, temperature, and pressure, *Adv. Energy Mater.* 11 (33) (2021), 2100630, <https://doi.org/10.1002/aenm.202100630>.
- [38] P. Dai, Z.-H. Mo, R.-W. Xu, S. Zhang, Y.-X. Wu, Cross-linked quaternized poly (styrene-*b*-(ethylene-co-butylene)-*b*-styrene) for anion exchange membrane: synthesis, characterization and properties, *ACS Appl. Mater. Interfaces* 8 (31) (2016) 20329–20341, <https://doi.org/10.1021/acsami.6b04590>.
- [39] J. Hao, X. Gao, Y. Jiang, H. Zhang, J. Luo, Z. Shao, B. Yi, Crosslinked high-performance anion exchange membranes based on poly(styrene-*b*-(ethylene-co-butylene)-*b*-styrene), *J. Membr. Sci.* 551 (2018) 66–75, <https://doi.org/10.1016/j.memsci.2018.01.033>.
- [40] N. Yu, J. Dong, H. Li, T. Wang, J. Yang, Improving the performance of quaternized SEBS based anion exchange membranes by adjusting the functional group and side chain structure, *Eur. Polym. J.* 154 (2021), 110528, <https://doi.org/10.1016/j.eurpolymj.2021.110528>.
- [41] F. Wang, C. Li, J. Sang, Y. Cui, H. Zhu, Synthesis and characterization of a long side-chain double-cation crosslinked anion-exchange membrane based on poly (styrene-*b*-(ethylene-co-butylene)-*b*-styrene), *Int. J. Hydrogen Energy* 46 (73) (2021) 36301–36313, <https://doi.org/10.1016/j.ijhydene.2021.08.172>.
- [42] A.Z. Al Munsur, I. Hossain, S.Y. Nam, J.E. Chae, T.-H. Kim, Hydrophobic-hydrophilic comb-type quaternary ammonium-functionalized SEBS copolymers for high performance anion exchange membranes, *J. Membr. Sci.* 599 (2020), 117829, <https://doi.org/10.1016/j.memsci.2020.117829>.
- [43] Z. Li, C. Li, C. Long, J. Sang, L. Tian, F. Wang, Z. Wang, H. Zhu, Elastic and durable multi-cation-crosslinked anion exchange membrane based on poly(styrene-*b*-(ethylene-co-butylene)-*b*-styrene), *J. Polym. Sci.* 58 (16) (2020) 2181–2196, <https://doi.org/10.1002/pol.20200290>.
- [44] S. Sung, J.E. Chae, K. Min, H.-J. Kim, S.Y. Nam, T.-H. Kim, Preparation of crosslinker-free anion exchange membranes with excellent physicochemical and electrochemical properties based on crosslinked PPO-SEBS, *J. Mater. Chem.* 9 (2) (2021) 1062–1079, <https://doi.org/10.1039/D0TA10194J>.
- [45] C.G. Morandi, R. Peach, H.M. Krieg, J. Kerres, Novel imidazolium-functionalized anion-exchange polymer PBI blend membranes, *J. Membr. Sci.* 476 (2015) 253–263, <https://doi.org/10.1016/j.memsci.2014.11.049>.
- [46] T.P. Pandey, H.N. Sarode, Y. Yang, Y. Yang, K. Vozzò, V.D. Noto, S. Seifert, D. M. Knauss, M.W. Liberatore, A.M. Herring, A highly hydroxide conductive, chemically stable anion exchange membrane, poly(2,6-dimethyl 1,4-phenylene oxide)-*b*-Poly(vinyl benzyl trimethyl ammonium), for electrochemical applications, *J. Electrochem. Soc.* 163 (7) (2016) H513–H520, <https://doi.org/10.1149/2.0421607jes>.
- [47] M. Zhang, C. Shan, L. Liu, J. Liao, Q. Chen, M. Zhu, Y. Wang, L. An, N. Li, Facilitating anion transport in polyolefin-based anion exchange membranes via bulky side chains, *ACS Appl. Mater. Interfaces* 8 (35) (2016) 23321–23330, <https://doi.org/10.1021/acsami.6b06426>.
- [48] D.W. Shin, S.Y. Lee, C.H. Lee, K.-S. Lee, C.H. Park, J.E. McGrath, M. Zhang, R. B. Moore, M.D. Lingwood, L.A. Madsen, Y.T. Kim, I. Hwang, Y.M. Lee, Sulfonated poly(arylene sulfide sulfone nitrile) multiblock copolymers with ordered morphology for proton exchange membranes, *Macromolecules* 46 (19) (2013) 7797–7804, <https://doi.org/10.1021/ma400889t>.
- [49] G.A. Lindquist, S.Z. Oener, R. Krivina, A.R. Motz, A. Keane, C. Capuano, K.E. Ayers, S.W. Boettcher, Performance and durability of pure-water-fed anion exchange membrane electrolyzers using baseline materials and operation, *ACS Appl. Mater. Interfaces* (2021), <https://doi.org/10.1021/acsami.1c06053>.

## Article II



Article

# Novel Pyrrolidinium-Functionalized Styrene-*b*-ethylene-*b*-butylene-*b*-styrene Copolymer Based Anion Exchange Membrane with Flexible Spacers for Water Electrolysis

Ziqi Xu <sup>1,\*</sup>, Sofia Delgado <sup>2,†</sup>, Vladimir Atanasov <sup>3</sup>, Tobias Morawietz <sup>1,4</sup>, Aldo Saul Gago <sup>1,\*</sup> and Kaspar Andreas Friedrich <sup>1,5</sup>

<sup>1</sup> German Aerospace Center (DLR), Institute of Engineering Thermodynamics, Pfaffenwaldring 38-40, 70569 Stuttgart, Germany

<sup>2</sup> Laboratory for Process Engineering, Environmental, Biotechnology and Energy (LEPABE), Faculty of Engineering of University of Porto, Rua Roberto Frias S/n, 4200-465 Porto, Portugal

<sup>3</sup> Institute of Chemical Process Engineering, University of Stuttgart, Boeblingen-Strasse 78, 70199 Stuttgart, Germany

<sup>4</sup> Faculty of Science, Energy and Building Services, Esslingen University of Applied Sciences, Kanalstraße 33, 73728 Esslingen am Neckar, Germany

<sup>5</sup> Institute of Building Energetics, Thermal Engineering and Energy Storage (IGTE), University of Stuttgart, Pfaffenwaldring 6, 70569 Stuttgart, Germany

\* Correspondence: xu.ziqi@dlr.de (Z.X.); aldo.gago@dlr.de (A.S.G.)

† These authors contributed equally to this study.



**Citation:** Xu, Z.; Delgado, S.; Atanasov, V.; Morawietz, T.; Gago, A.S.; Friedrich, K.A. Novel Pyrrolidinium-Functionalized Styrene-*b*-ethylene-*b*-butylene-*b*-styrene Copolymer Based Anion Exchange Membrane with Flexible Spacers for Water Electrolysis. *Membranes* **2023**, *13*, 328. <https://doi.org/10.3390/membranes13030328>

Academic Editor: Dirk Henkensmeier

Received: 17 February 2023

Revised: 9 March 2023

Accepted: 10 March 2023

Published: 13 March 2023



**Copyright:** © 2023 by the authors. Licensee MDPI, Basel, Switzerland. This article is an open access article distributed under the terms and conditions of the Creative Commons Attribution (CC BY) license (<https://creativecommons.org/licenses/by/4.0/>).

**Abstract:** Anion exchange membranes (AEM) are core components for alkaline electrochemical energy technologies, such as water electrolysis and fuel cells. They are regarded as promising alternatives for proton exchange membranes (PEM) due to the possibility of using platinum group metal (PGM)-free electrocatalysts. However, their chemical stability and conductivity are still of great concern, which is appearing to be a major challenge for developing AEM-based energy systems. Herein, we highlight an AEM with styrene-*b*-ethylene-*b*-butylene-*b*-styrene copolymer (SEBS) as a backbone and pyrrolidinium or piperidinium functional groups tethered on flexible ethylene oxide spacer side-chains (SEBS-Py2O6). This membrane reached  $27.8 \text{ mS cm}^{-1}$  hydroxide ion conductivity at room temperature, which is higher compared to previously obtained piperidinium-functionalized SEBS reaching up to  $10.09 \text{ mS cm}^{-1}$ . The SEBS-Py2O6 combined with PGM-free electrodes in an AWE water electrolysis (AEMWE) cell achieves  $520 \text{ mA cm}^{-2}$  at 2 V in 0.1 M KOH and  $171 \text{ mA cm}^{-2}$  in ultra-pure water (UPW). This high performance indicates that SEBS-Py2O6 membranes are suitable for application in water electrolysis.

**Keywords:** anion exchange membrane; anion exchange membrane water electrolysis; flexible oxide spacers; conductivity; chemical stability

## 1. Introduction

Transitioning to a net-zero world is one of the greatest challenges that humankind has faced in modern society. To fulfill this goal, the need of creating a cost-effective electrolysis method for green hydrogen production in power supply systems is highly emphasized by the demand in industry [1–4]. Compared with proton exchange membrane (PEM) electrolysis, alkaline water electrolysis (AWE) has risen to prominence because of its ability to use low-cost PGM-free catalysts and high industrial convertibility [5,6]. However, the high corrosive alkaline electrolyte (30 wt% KOH) is responsible for several issues, including carbonate formation, the need for electrolyte circulation, and gas-emitting impurities [7,8].

Anion exchange membranes (AEM) are regarded as potential solutions to these challenges since they facilitate the reduction of electrolyte concentration [6,9–14] and improve

gas purity and electrical efficiency. However, no dependable commercial AEMs with the requisite conductivity and stability exist [15–18], posing considerable obstacles in the development of high-performance AEMWEs. Due to the hydroxide's strong nucleophilic and basic character, the chemical stability in an alkaline environment at elevated temperature is the most essential challenge for AEM. In detail, for the backbone of AEM, heteroatoms, e.g., oxygen and sulfur, must be avoided because they can be quickly destroyed by the hydroxide [19]. When it comes to the stability of functional groups on quaternary ammonium (QA), there are many degradation processes that include nucleophilic substitution, elimination (Hofmann elimination), and rearrangement reactions [20,21]. Marino and Kreuer [22] evaluated the stability of a range of functional groups against nucleophilic attack, including 1,4-diazabicyclooctane (DABCO), imidazolium, and methyl piperazine. Due to their unfavorable bond angles and lengths in the chemical transition states, the 6-membered and 5-membered cycloaliphatic QAs have exhibited good resistance to nucleophilic substitution and elimination.

The moderate conductivity of the AEMs is also a hurdle for their performance [17,23]. To improve ionic conductivity, several effective approaches have been investigated. Although an increase in ion exchange capacity (IEC) can contribute significantly to an increase in conductivity, an overabundance of IEC can result in uncontrolled swelling and membrane instability. Constructing a phase separation by introducing comb-shaped structures [24,25] while simultaneously increasing the number of cations per chain [26,27] is a more efficient technique for conductivity improvement without compromising dimensional stability.

A piperidinium/pyrrolidinium-functionalized multi-cation comb-shaped polymer structure is discussed in this paper. Because of its high stability and mechanical integrity, a multi-block copolymer SEBS was selected as the backbone. More hydrophilic ethylene glycol-based side chains are also added to achieve a more flexible spacer structure and induce microphase separation [28]. As a result, a membrane with piperidinium/pyrrolidinium functionality and flexible ethylene oxide spacers has good conductivity and stability [29–32]. Different functional groups (piperidinium/pyrrolidinium) and architectures of the side chain, such as the pre-functionalized end of the spacer, are discussed in detail. The properties of the membrane, such as conductivity, IEC, and alkaline stability were studied.

## 2. Materials and Methods

### 2.1. Materials

SEBS (30 wt% styrene, Taipol 6152) was provided by TSRC cooperation. Commercial catalysts H2GEN-M (which contains Mo and C) and OXYGN-N (which mainly contains Ni and Fe) from CENmat were used for fabrication of the cathode and anode, respectively, for the AEM electrolyzer tests. These catalysts are platinum group metal (PGM)-free. Chlorotrimethylsilane, 1,3-dibromopropane, 1,4-dibromobutane, sodium chloride, and potassium hydroxide were purchased from TCI Europe. Trioxane, tin (IV) chloride, 1,6-dibromohexane, chloroform, xylene, dimethyl sulfoxide, water solution of trimethylamine (33%), ethanol, dichloromethane, and tetrahydrofuran were all purchased from Merck. All chemicals were used as received without further purification.

### 2.2. Synthesis and Membrane Preparation

#### 2.2.1. Synthesis of Chloromethylated SEBS (cmSEBS)

The cmSEBS synthesis in detail has already been published elsewhere [33]. In an argon-purged three-neck round-bottom flask, chloroform (250 mL) was added to SEBS polymer (4 g, 25 mmol). Then, the mixture was stirred at room temperature for 4 h. After the polymer dissolution, trioxane (5.4 g, 60 mmol) was added and the flask was placed in an ice bath until the temperature of the mixture dropped down to 1 °C. Chlorotrimethylsilane (22.8 mL, 37.5 mmol) was injected to the reaction mixture and subsequently tin (IV) chloride (3 mL, 3 mmol) into the reaction mixture. The mixture was stirred at a temperature at less than 5 °C for 30 min and then at room temperature for 24 h. Afterwards, the mixture

was transferred into a beaker filled with 300 mL of ethanol/water (50 % *v/v*) mixture to terminate the reaction at the end of the reaction time. The product was twice precipitated from chloroform solution into ethanol/water (50 % *v/v*) mixture after filtering to collect the solid. The final product was dried in a vacuum oven at 50 °C overnight. The <sup>1</sup>H NMR spectrum was shown in Figure 1a.

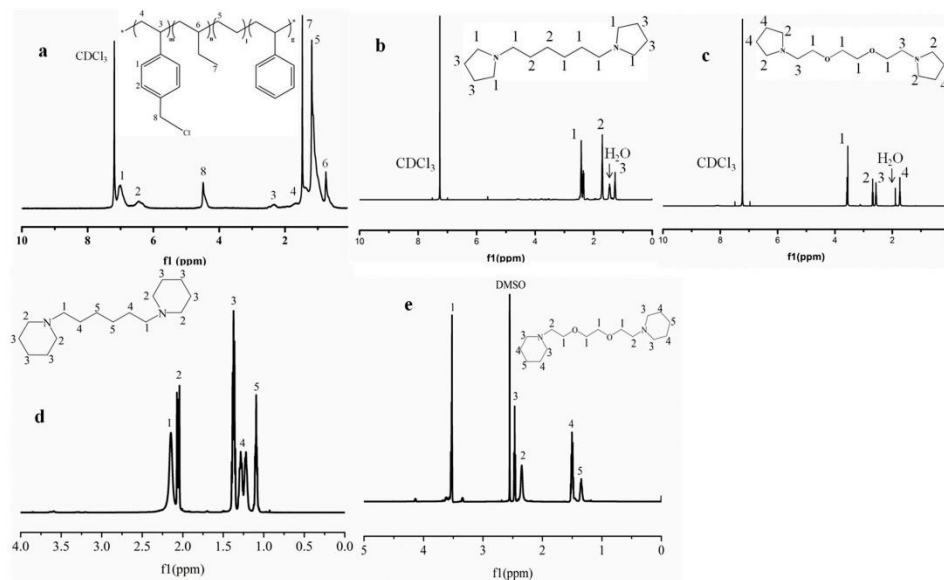


**Figure 1.** (a) <sup>1</sup>H NMR spectrum of cmSEBS; (b–e) <sup>1</sup>H NMR spectra of Py2C6, Py2O6, P2C6, and P2O6.

### 2.2.2. Synthesis of 1,6-Bis(piperidin-1-yl) Hexane (P2C6) and 1,6-Bis(pyrrolidin-1-yl) Hexane (Py2C6)

Piperidine (26 mL, 250 mmol) was dissolved in 150 mL acetone under argon and stirred for 30 min at room temperature. 1,6-dibromohexane (16 mL, 100 mmol) was added dropwise to the piperidine solution after cooling in an ice bath at  $T < 5$  °C. The reaction mixture was then stirred at room temperature for 48 h after adding anhydrous potassium carbonate (20 g, 152 mmol). Once removing the undesirable precipitates using filtration (solid phase removed), the solvent was removed using vacuum evaporation. To extract the product, 60 mL dichloromethane was added to the residue, which was then rinsed with deionized water ( $5 \times 100$  mL) and dried at 60 °C for 10 h, leaving a thick yellowish liquid (16.4 g, about 65 mmol). Figure 2d shows the <sup>1</sup>H NMR spectrum of P2C6.

For the synthesis of Py2C6, the same synthetic procedure as for P2C6 was followed using pyrrolidine instead of piperidine. The <sup>1</sup>H NMR spectrum is shown in Figure 2b.



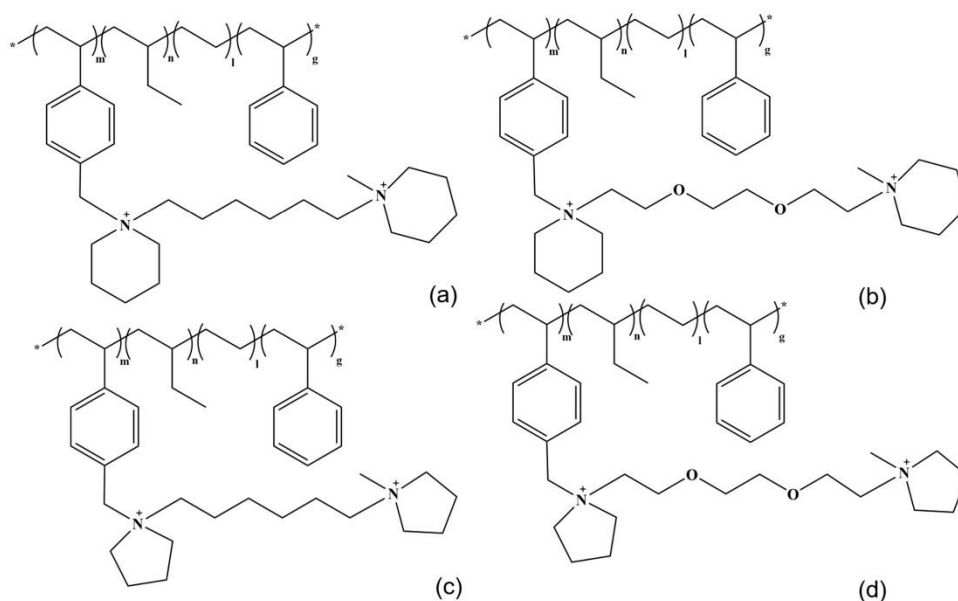


**Figure 2.** Different membranes structures obtained in this study: (a) SEBS-P2C6, (b) SEBS-P2O6, (c) SEBS-Py2C6, (d) SEBS-Py2O6.

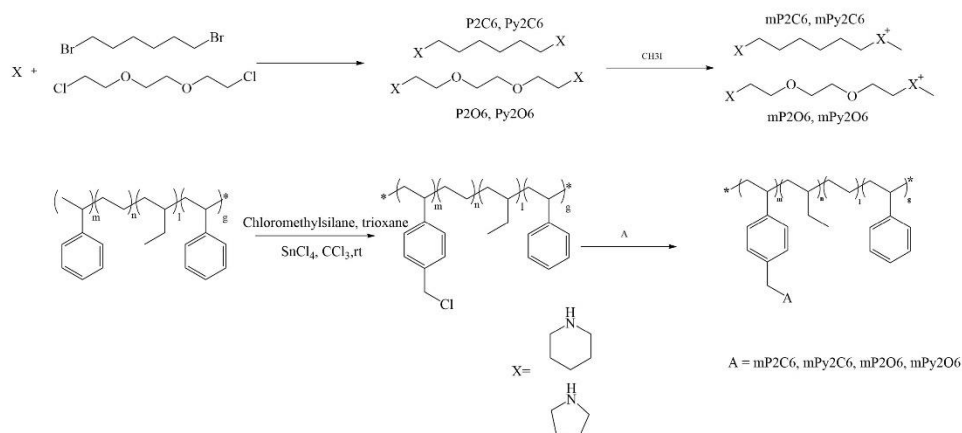
#### 2.2.3. Synthesis of 1,2-Bis(2-piperidinylethoxy) Ethane (P2O6) and 1,2-Bis(2-pyrrolidinylethoxy) Ethane (Py2O6)

Piperidine (26 mL, 250 mmol) was dissolved in 150 mL acetonitrile under argon and stirred for 30 min at room temperature. 1,2-bis(2-chloroethoxy)ethane (14 mL, 100 mmol) was then mixed dropwise to piperidine solution. After that, anhydrous potassium carbonate (20 g, 0.145 mol) was added and stirred for 48 h at 60 °C. After removing the undesirable precipitate using filtration (solid phase removed), 100 mL water was added in. Later, the solution was treated with ethyl acetate to extract the product and ethyl acetate phase was obtained. Rotating evaporation was taken afterwards to remove the ethyl acetate. Finally, the remainder was put into the vacuum oven at 60 °C for 24 h, yielding a viscous dark yellow liquid (9.4 g, about 33 mmol). Figure 2e shows the  $^1\text{H}$  NMR spectrum of P2O6.

For the synthesis of Py2O6, the same synthetic procedure as for P2O6 was followed using pyrrolidine instead of piperidine. The  $^1\text{H}$  NMR spectrum are shown in Figure 2c.

#### 2.2.4. Membrane Preparation

Different membrane structures obtained in this study were shown in Figure 2 and the overall membrane preparation process in Scheme 1. For SEBS-P2C6 membrane preparation, cmSEBS (0.7 g) was dissolved into 25 mL chloroform at 50 °C for 2 h to form nearly 2 wt% solution. Then 1 mL of P2C6 (around 0.003 mol) was added in 25 mL chloroform and 0.2 mL iodomethane dropped in, with continued stirring for 2 h to have mP2C6. Subsequently, two solutions mixed together, and the membrane was cast from the solution on a PTFE square dish (15 cm  $\times$  15 cm) and dried first at 50 °C for 4 h and then 100 °C for 20 h in vacuum. Finally, the SEBS-P2C6 membrane was detached from the PTFE dish. SEBS-P2C6 membrane was boiled in water to remove the remaining solvent. For SEBS-Py2C6, SEBS-P2O6, and SEBS-Py2O6, preparation methods were similar to that of SEBS-P2C6 but used Py2C6, P2O6, or Py2O6 instead of P2C6.



**Scheme 1.** Membranes and other synthesis process obtained in this study.

### 2.3. Instrumental

#### 2.3.1. NMR Spectroscopy and Fourier-Transform Infrared Spectroscopy (FT-IR)

Bruker Avance III HD 400 NanoBay NMR spectrometer was used to measure the  $^1\text{H}$  and  $^{13}\text{C}$  NMR spectroscopy of the polymer at room temperature in either  $\text{DMSO-d}_6$  or  $\text{CDCl}_3$  as solvents, with tetramethylsilane as the internal reference (TMS). A Nicolet iS5 (ThermoFisher Scientific, Karlsruhe, Germany) and a diamond attenuated total reflectance (ATR) module was used to record FT-IR spectra of the membranes with 64 scans in the wave number range of  $4000$  to  $400\text{ cm}^{-1}$ .

#### 2.3.2. Atomic Force Microscope (AFM)

Icon XR (Bruker Karlsruhe, Germany) was used to perform the atomic force microscopy on in PeakForce Tapping Mode to measure the nanomechanical properties of the membranes. At each measurement point, the AFM modus records and evaluates force-distance curves. Along with height adhesion, stiffness and deformation were measured at the same time. Bruker Scanasyt-Air tips ( $k = 0.4\text{ N m}^{-1}$ ) with a tip radius of  $2\text{ nm}$  were used. The membranes were glued to  $15\text{ mm}$  AFM steel-discs with adhesive carbon tape (Plano) and measured at ambient conditions. For all membranes, the image size for the AFM test was set to  $1\text{ }\mu\text{m}$  and they were measured at  $0.977\text{ Hz}$  with  $512 \times 512$  pixels.

#### 2.3.3. Membrane Conductivity

A Teflon contact cell and four electrode methods were used to measure the through plane conductivity of the membrane. Electrodes are made of Au and a Zahner-elektrok IM6 device (Zahner-elektrok GmbH, Kronach, Germany) was used to record the electrochemical impedance spectroscopy by measuring membrane resistances in  $1\text{ M NaCl}$  solution or  $1\text{ M KOH}$  at room temperature. In a frequency range of  $200\text{ KHz}$ – $8\text{ MHz}$ , by intersecting the impedance with the true x-axis, the resistance was calculated. Since we do not have a setup to remove  $\text{CO}_2$ ,  $\text{OH}^-$  conductivity was measured immediately after the membrane was changed to  $\text{OH}^-$  form. For each membrane, four samples were collected. The conductivity was calculated by the equation below (Equation (1)).

$$\sigma = \frac{1}{R_{sp}} = \frac{d}{R \times A} \quad (1)$$

where  $\sigma$  is the conductivity ( $S\text{ cm}^{-1}$ ),  $R_{sp}$  is the resistivity ( $\Omega\text{ cm}$ ),  $d$  is the thickness of membrane (cm),  $R$  is the ohmic resistance ( $\Omega$ ), and  $A$  is the electrode area ( $\text{cm}^2$ )

#### 2.3.4. Water Uptake and Swelling Ratio

The weight and dimension differences of membranes after soaking in deionized water for 48 h at room temperature and drying in a vacuum oven at  $60\text{ }^\circ\text{C}$  for 24 h are measured to calculate the water uptake (WU) and swelling ratio (SR) in  $\text{Cl}^-$  form. The WU is calculated by the Equation (2) as follows:

$$WU\% = \frac{(m_{wet} - m_{dry})}{m_{dry}} \times 100 \quad (2)$$

where  $m_{wet}$  and  $m_{dry}$  are the weight of wet and dry membranes in  $\text{Cl}^-$  forms in grams, respectively.

The SD was calculated by the Equation (3) as follows:

$$SD\% = \frac{(l_{wet} - l_{dry})}{l_{dry}} \times 100 \quad (3)$$

where  $l_{wet}$  and  $l_{dry}$  are the geometric length of the wet and dry membranes in  $\text{Cl}^-$  forms, respectively.

#### 2.3.5. Ion Exchange Capacity (IEC)

IEC was determined by a back-titration strategy. The membrane sample was immersed in 1M NaOH solution, then washed with DI water before being immersed in a soaked sodium chloride arrangement at room temperature for 1 day. Afterwards, membranes were taken out from the solution. Hydrochloric acid (3 mL, 0.1 M) standard arrangement was added and the mixture was stirred at room temperature for 1 day. The following arrangement was titrated with a standard 0.1 M sodium hydroxide solution. The membrane was thoroughly washed with DI water and dried overnight at  $90\text{ }^\circ\text{C}$ . On a balance, the dry weight of the membrane was determined. The IEC was calculated by Equation (4).

$$IEC = \frac{C_{HCl} \times V_{HCl} - C_{NaOH} \times V_{NaOH}}{m_{dry}} \quad (4)$$

where IEC is the ion exchange capacity ( $\text{Cl}^-$  form, mmol/g),  $C_{HCl}$  is the concentration of the hydrochloric acid solution (mmol/mL),  $V_{HCl}$  is the volume of the hydrochloric acid solution used (mL),  $C_{NaOH}$  is the concentration of the sodium hydroxide solution (mmol/mL),  $V_{NaOH}$  is the added volume of the sodium hydroxide solution (mL), and  $m_{dry}$  is the dry weight of the membrane (g).

#### 2.3.6. Chemical Stability of the Membranes

Chemical stability was determined in 1 M KOH at  $90\text{ }^\circ\text{C}$  for 30 days. Several pieces of membrane were washed repeatedly with water for 1 day before being put into the alkaline solution at  $90\text{ }^\circ\text{C}$  in an oven. Every 5 days during the test, a small piece of membrane was cut to test the conductivity, and new KOH solution was exchanged. Following that, the membranes were thoroughly washed with deionized water before being tested for  $\text{OH}^-$  conductivity. The conductivity retention rate (CR%) of the membrane was calculated using the following equation.

$$CR\% = \frac{\sigma_1}{\sigma} \times 100 \quad (5)$$

where  $\sigma$  is the conductivity of the membrane before treatment in KOH.

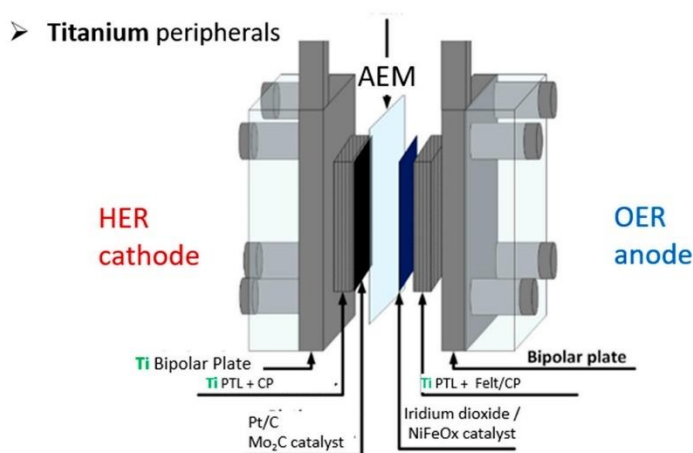
#### 2.4. Fabrication of Membrane Electrode Assemblies (MEAs) for AEMWEs

Catalyst coated substrates (CCS) were prepared by dispersing the H2GEN-M and OXYGN-N catalysts on carbon paper substrates from Sigracarb using a manual spraying technique [34]. Initially, chloromethylated SEBS (cmSEBS) was used as the ionomer precursor and dissolved in tetrahydrofuran.

Thereupon, the catalyst suspensions were prepared using isopropanol (Merck, Darmstadt, Germany) and ultra-pure water (Millipore, Burlington, MA, USA) as solvents and by maintaining an ionomer to catalyst ratio of 3:7, and 4 cm<sup>2</sup> active area CCSs of 4 mg cm<sup>-2</sup> (anode composed of OXYGEN-N and cathode composed of H2GEN-M catalyst) was fabricated and immersed into a 500 mL trimethylamine solution to functionalize the cmSEBS binder overnight. Then, CCSs were thoroughly washed with ultra-pure water and then submerged in a 1 M KOH solution for 15 h at room temperature to convert the chloride anion into the hydroxide anion. The membranes were finally rinsed with water prior to their assembly. A similar approach was performed to prepare CCS to be tested in UPW; for that, previous in situ activated CCS in 0.1 M KOH was flushed for half an hour in UPW until reaching a neutral pH at the outlet of the AEMWE.

#### 2.5. AEMWE Cell Test

The whole AEM electrolysis setup in this work was shown in Scheme 2. The AEMWE cell consisted of titanium bipolar plates (BPPs) and porous transport layers (PTL) of Ti porous sintered layer (PSL) on Ti mesh (PSL/mesh-PTL) [35] (GKN Sinter Metals) and also carbon paper inside for both cathode and anode. The different cell assemblies were accomplished by cramming the CCSs together with the SEBS-Py206 membrane which was as well immersed for 15 h in 1 M KOH solution and then thoroughly rinsed with deionized water. A torque of 0.6 Nm was applied on 4 screws, which allowed closing of the cell [35]. The cell was then ready to test, and 1 L/min N<sub>2</sub> was continuously bubbled into the electrolyte, either 0.1 M KOH or ultra-pure water, in a closed-loop system to remove the CO<sub>2</sub> dissolved in the water and thus avoid the generation of precipitates and to maintain the chemical/mechanical integrity of the membrane. Nevertheless, contact with ambient air/CO<sub>2</sub> cannot be entirely disregarded throughout the cell assembly preparation and activation steps. The electrochemical characterization was accomplished using a Zahner Zennium Pro electrochemical workstation (potentiostat/galvanostat) and a Zahner PP24 booster was employed to reach currents over 4 A. The cell was initially conditioned in situ in a 0.1 M KOH solution at 60 °C by monitoring the potential as function of the current density using a dwell time of 120 s and with small current increments of 50 mA cm<sup>-2</sup> and then 150 mA cm<sup>-2</sup> until reaching 1 A cm<sup>-2</sup>. Five polarization curves were retrieved in potentiostatic mode, from 1.3 V to 2.5 V using a scan rate of 20 mV s<sup>-1</sup> in the 0.1 M KOH electrolyte at 60 °C. An electrochemical impedance spectrum (EIS) was recorded in galvanostatic mode at 200 mA cm<sup>-2</sup> using an amplitude of 20 mA in the frequency range of 100 mHz to 1 kHz. The cell assembly was then purged with pure water flowing for 30 min and the electrochemical characterization steps were repeated at 60 °C using ultra-pure water (UPW) as electrolyte at neutral pH.



### Nomenclature: PEM Cell

Scheme 2. AEM electrolysis setup in this work.

## 3. Results and Discussion

### 3.1. Synthesis and Preparation

In this paper, SEBS copolymer is chosen as the backbone for the preparation of the AEM. SEBS copolymer contains ethylene and butadiene as the flexible blocks as well as styrene as the rigid blocks. The polymer modification comprises two parts: chloromethylation and quaternization. For the chloromethylation, as shown in Figure 2a, the chloromethylation rate of SEBS is 83.5%. Subsequently, cmSEBS reacted with some side chain agents such as mP2C6 and mP2O6 (Scheme 1) and the impact of side chain agents on the chemical stabilization via functionalization of the membrane, swelling changes and proton conductivity were studied in this work.

In detail, <sup>1</sup>H NMR was recorded on cmSEBS to investigate the grafting rate and chemical composition. The resonance peak with chemical shift of 4.5 ppm belongs to -CH<sub>2</sub>Cl of benzyl chloride and the signals at 6.3–7.25 ppm belongs to aromatic protons of the styrene [36,37]. By comparing the ratio of these two peaks, -CH<sub>2</sub>Cl (peak 8) to Ar-H (peaks 1 and 2) in Figure 2a, 83.3% of the styrene part was chloromethylated (25.4% of the whole polymer).

For the structures of 1,6-bis(pyrrolidin-1-yl) hexane (Py2C6) and 1,6-bis(piperidin-1-yl) hexane (P2C6), the <sup>1</sup>H NMR spectra chemical shifts are shown in Figure 2b,d and those for 1,2-bis(2-pyrrolidinylethoxy) ethane (Py2O6) and 1,2-bis(2-piperidinylethoxy) ethane (P2O6) are shown in Figure 2c,e. Due to the absence of CH<sub>2</sub>Br signals in all structures and the corresponding integral ratios between the N-CH<sub>2</sub>- and the rest of the protons in the structure, we are able to conclude the successful synthesis of those side-chain molecules (P2C6, P2O6, Py2O6 and Py2C6).

After the functionalization, the corresponding membrane samples were not soluble in any common organic solvents. Therefore, the membranes were subjected to ATR-FTIR spectroscopy to find out whether the cmSEBS had reacted with the amine side chain (mPy2O6 and mP2O6). Taking SEBS-Py2O6 for example, in the ATR-FTIR spectrum of cmSEBS, a new peak at 725 cm<sup>-1</sup> appeared in comparison to the pristine SEBS (Figure 3). This peak corresponds to C-Cl stretching vibration of the chloromethyl group. After the membrane was cast from the reaction mixture of cmSEBS, Py2O6 and iodomethane, a

new peak appeared in the ATR-FTIR at  $1120\text{ cm}^{-1}$ . This peak is typical for C-O stretching vibration, which indicates the membrane functionalization.

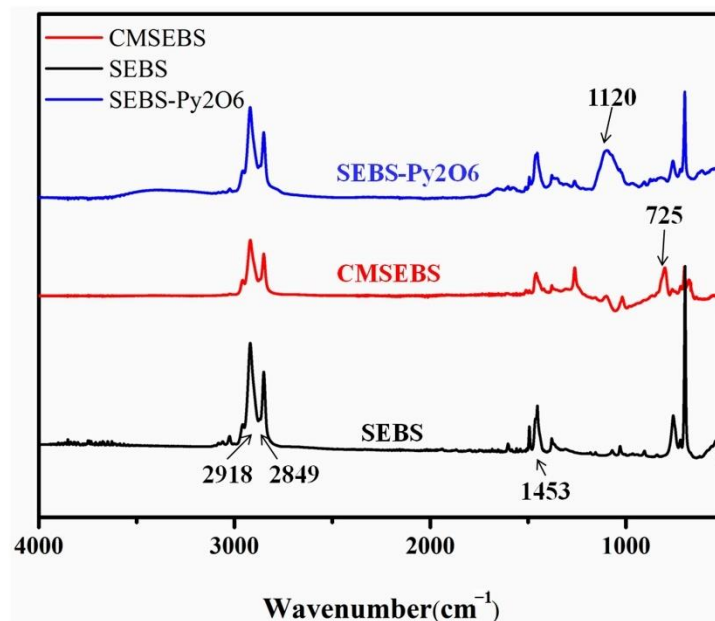


Figure 3. FT-IR spectra of SEBS, CMSEBS and SEBS-Py206 membranes.

### 3.2. Conductivities of Piperidinium/Pyrrolidinium Functionalized Membranes Based on SEBS

Commonly, SEBS-based piperidinium-functionalized AEMs have not shown high conductivity due to the relatively low degree of functionalization and respectively low IEC [38,39]. In the past, to improve the conductivity, several strategies have been tried, such as building a comb-shaped structure [40], having multi-cation side chains [41], and crosslinking with backbones being additionally functionalized [42]. Among them, using a comb-shaped structured polymers could induce formation of the micro-phase separation which often enhances the conductivity of the membrane. In our previous study, a piperidinium-functionalized flexible ethylene oxide spacer structure was applied as a crosslinker in the presence of trimethylamine to convert the chloromethyl group to a functional membrane [43]. However, this strategy also brought some drawbacks. Firstly, the crosslinkers reduce the IECs of the membranes rapidly and thus lose the advantage of the multi-cation side-chain structure. Secondly, functionalization by post treatment may decrease the mechanical stability of the membrane and make the membrane brittle. And third, benzyl ammonium group is known to have inferior stability which may lead to the degradation in alkaline solution. Therefore, in this work we chose a functionalized flexible ethylene oxide spacer structure with a pre-functionalized end (of which one end of the diamines was quaternized by iodomethane before) and removed all the benzyl ammonium groups in the structure. As is shown in Scheme 1, the first diamines (P2C6 and P2O6) were reacted with iodomethane to get unsymmetrical one-end quaternate amine-ammonium precursors (pre-functionalized end) (mP2C6/mP2O6). Subsequently, both cmSEBS and mP2C6/mP2O6 were dissolved to prepare the final membrane. Some of the most important properties relating to their application are shown in Table 1. The IECs of the membranes

SEBS-P2C6 and SEBS-P2O6 are higher than the membranes SEBS-P2C6-TMA and SEBS-P2O6-TMA. However, the IECs of SEBS-P2C6 and SEBS-P2O6 are much lower than the fully functionalized membranes (IEC in theory is  $2.7 \text{ mmol g}^{-1}$ ), which is probably due to charge repulsion between the charged side chains and the charged polymer product, even though the amine-ammonium precursors are in excess. Due to the higher IEC, the conductivity of the SEBS-P2C6 and P2O6 improved a lot, reaching  $17.5 \text{ mS cm}^{-1}$  and  $25 \text{ mS cm}^{-1}$  at RT, which is higher than SEBS-based piperidinium-functionalized membrane published before (piperidinium functionalized SEBS-pi-73%,  $10.09 \text{ mS cm}^{-1}$ ) [1]. In all cases,  $\text{Cl}^-$  conductivity is about twice as low as than the  $\text{OH}^-$  conductivity, which is due to the larger and heavier  $\text{Cl}^-$  ion compared to  $\text{OH}^-$ . This factor is slightly lower than the  $\text{Cl}^-$  and  $\text{OH}^-$  conductivities ( $\sigma_{\text{OH}^-} / \sigma_{\text{Cl}^-} \sim 2.7$ ) that have been reported in the literature [44]. However, the residual  $\text{CO}_2$  present in our case may account to this difference for the  $\text{OH}^-$  value, although the test was performed with care immediately after removal from KOH solution.

**Table 1.** IEC, conductivity, swelling ratio, and water uptake of the membrane at  $25^\circ\text{C}$ .

	IEC ( $\text{mmol g}^{-1}$ )	Conductivity ( $\text{Cl}^-$ ) ( $\text{mS cm}^{-1}$ )	Conductivity ( $\text{OH}^-$ ) ( $\text{mS cm}^{-1}$ )	Swelling Ratio (%)	Water Uptake ( $\text{Cl}^-$ ) (%)	Thickness ( $\mu\text{m}$ )
SEBS-P2C6-TMA	$1.10 \pm 0.01$	$6.45 \pm 0.30$	$12.5 \pm 0.42$	$6.5 \pm 2.79$	$20.1 \pm 8.43$	$70 \pm 2.8$
SEBS-P2O6-TMA	$1.05 \pm 0.04$	$11.7 \pm 0.54$	$20.8 \pm 0.74$	$9.2 \pm 4.81$	$36.8 \pm 7.35$	$68 \pm 4.3$
SEBS-P2C6	$1.35 \pm 0.22$	$9.85 \pm 0.30$	$17.5 \pm 0.72$	$10.5 \pm 4.67$	$32.1 \pm 9.13$	$65 \pm 3.3$
SEBS-P2O6	$1.38 \pm 0.18$	$13.6 \pm 0.86$	$25.0 \pm 1.32$	$14.3 \pm 6.72$	$50.6 \pm 10.30$	$68 \pm 2.8$
SEBS-Py2C6	$1.42 \pm 0.21$	$10.4 \pm 0.60$	$18.6 \pm 0.38$	$8.5 \pm 2.79$	$30.1 \pm 10.41$	$72 \pm 4.8$
SEBS-Py2O6	$1.40 \pm 0.25$	$14.1 \pm 0.67$	$27.8 \pm 0.73$	$12.2 \pm 3.79$	$47.8 \pm 9.35$	$70 \pm 3.3$

Basically, pyrrolidinium is believed to be a very chemically stable functional group in alkaline solution because of its low ring strain and relatively high energy barrier towards E2 elimination [22]. Therefore, in this work, SEBS membranes having pyrrolidinium functional groups were synthesized and studied. In Table 1, SEBS-Py2C6 and SEBS-Py2O6 have shown relatively high conductivity being  $17.6 \text{ mS cm}^{-1}$  and  $27.8 \text{ mS cm}^{-1}$  at RT, respectively. Compared with piperidinium-functionalized membranes (SEBS-P2C6 and SEBS-P2O6), at almost the same IEC, pyrrolidinium-functionalized membranes showed similar conductivities, making them a promising candidate for AEM electrolysis application.

### 3.3. Membranes Morphology Study on SEBS-P2O6 and SEBS-Py2O6

In our previous work, the micro-phase separation of the ethylene oxide spacer structure in crosslinkers was investigated. In the AFM image, the membrane with the ethylene oxide spacer structure showed broader and better connected hydrophilic domains, which was believed would promote better formation of counter ion channels, thus improving the conductivity of membranes which have the ethylene oxide spacer structure crosslinkers [43]. In the literature, other studies were also taken to explain the high conductivity of the ethylene oxide spacer structure [28,32]. Similarly, in this work, membrane morphology was proven by AFM imaging in DMT modulus (Figure 4). The bright (stiffer) regions correspond to hydrophobic polymer backbone agglomeration, while the dark regions stand for hydrophilic side chains. For both SEBS-Py2O6 and SEBS-Py2C6 membranes, a clear phase-separation of hydrophilic and hydrophobic phases was observed. For SEBS-Py2O6 (Figure 4a,b), containing long flexible and hydrophilic side chains, the hydrophilic domains formed were much better connected and broader compared with SEBS-Py2C6 (Figure 4c,d). The broader and better interconnected hydrophilic domains of SEBS-Py2O6 make the ion-channels much better intercalated with relatively constant size, which enables efficient ion transport [45,46].

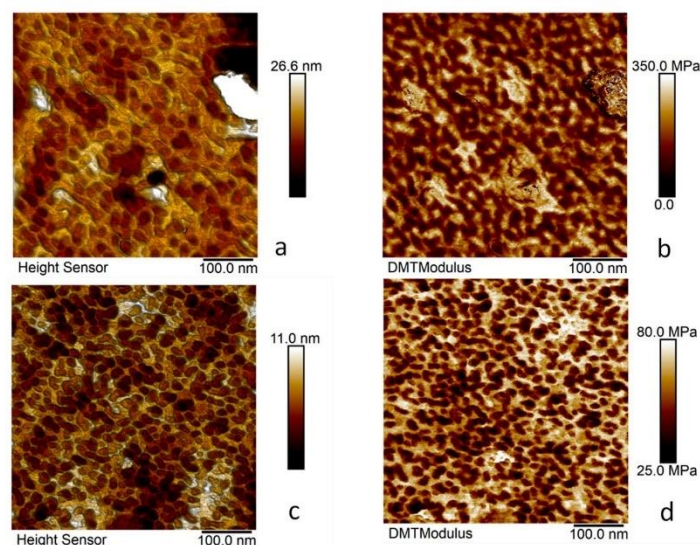


**Figure 4.** AFM stiffness mapping of the membranes for (a,b) SEBS-Py2O6 and (c,d) SEBS-Py2C6.

### 3.4. Chemical Stability of SEBS-Based Piperidinium/Pyrrolidinium-Functionalized Membranes

In order to check the alkaline stability, the membranes were immersed into 1M KOH at 90 °C for more than 700 h. As is shown in Figure 5, AEMs with benzyl trimethyl ammonium groups showed low conductivity retention, which can be ascribable to the degradation of benzyl trimethyl ammonium in hot alkaline environment. At the same time, when adding ethylene oxide spacers to the side chain, there are no significant losses on membrane stability (SEBS-P2C6 and SEBS-P2O6), which has similar results in the literature [32]. Comparing the membranes having piperidinium groups with those having pyrrolidinium groups, after immersing AEMs in 1M KOH at 90 °C for more than 700 h, the conductivity of both SEBS-P2O6 and SEBS-Py2O6 still have nearly 95% conductivity retention, and we can draw the conclusion that replacing the piperidinium with pyrrolidinium cannot significantly change the chemical stability of the membrane. For SEBS-Py2O6, the conductivity only dropped from 27.8 mS cm<sup>-1</sup> to 26.4 mS cm<sup>-1</sup> (OH<sup>-</sup> form), which may due to some benzyl group degradation in harsh hot alkaline environment or some radical attack [20,47]. Considering both the conductivity and stability of the membranes functionalized by piperidinium and pyrrolidinium functional groups suited on flexible ethylene oxide spacer side chains, a well-balanced conductivity and stability have been achieved.

### 3.5. AEM Water Electrolysis Measurements

After balancing the conductivity and chemical stability of the membranes, membranes with ethylene oxide spacer side chains and piperidinium/pyrrolidinium functional groups are necessary to achieve high performance in AEMWE. In this work, SEBS-Py2O6-based membranes and the ionomer were tested in a AEMWE cell using the OXYGN-N and H2GEN-M catalysts for the anode and cathode, respectively. As shown in Figure 6a, the cell performance at 60 °C in 0.1 M KOH was measured via polarization curves after performing a potentiostatic conditioning; see Supplementary Figure S1a,b. A current density of 520 mA cm<sup>-2</sup> was reached at 2 V, which unveils a potential for future applications of the SEBS-Py2O6 membrane and SEBS-TMA ionomer for AEMWE with PGM-free catalysts. In fact, polyethylene-based membranes were attempted in similar AEMWE configurations



(0.1 M KOH and 60 °C), achieving ca. 0.1 A cm<sup>-2</sup> at 1.65 V although using Pt as cathode; nonetheless, the performance of the system attains about half the performance from that obtained with the SEBS-Py2O6 membrane [33]. Still, the reported performances of AEM water electrolyzers are generally high, particularly considering the circulating alkaline electrolyte. For instances, the Sustainion membranes composed of polystyrene backbone and doped with quaternized imidazolium groups allow us to reach 1 A cm<sup>-2</sup> at 1.9 V using 1 M KOH while demonstrating a great stability [9]. However, Sustainion membranes work poorly in pure water, where a significant decrease in conductivity is visible, resulting in over one order of magnitude lower performance in contrast to more mature PEM water electrolyzers, i.e., reaching less than 500 mA cm<sup>-2</sup> at 2 V [48,49].

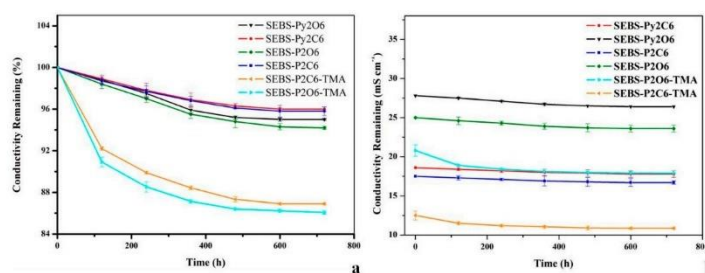


**Figure 5.** (a) Conductivity retention and (b) ionic conductivity of SEBS-P206 membranes after stability test in KOH at 90 °C.

Although the use of PGM-free materials in UPW operation is the most wanted option to improve AEM electrolysis competitively, new challenges arise, primarily concerning the lower conductivity of membranes and considerably slower kinetics of the catalysts at neutral pH.

In this regard, the AEMWE was tested using UPW as liquid electrolyte to unveil the effect of the spacer addition on the retention capacity of the hydroxyl ion of the membrane and ionomer. After retrieving several polarization curves, as shown in Figure 6, the cell did not display any signs of performance decay since no hysteresis could be seen; remarkably, a stable current density of 171 mA cm<sup>-2</sup> could be achieved at 2 V and 60 °C with UPW feed. This result is promising since the AEMWE cell outperforms previously reported AEMWE with piperidinium-functionalized SEBS [47]. It is possible that the overall hydroxyl ion conductivity and retention could be increased by the addition of the flexible ethylene oxide spacers in the formulation developed herein [50].

The Nyquist plots of the EIS shown in Figure 6b demonstrate that although the ohmic resistance of the membrane is nearly 3.6 fold-higher in ultra-pure water operation compared to operation in the OH<sup>-</sup> saturated environment, the overall charge transfer increment associated with both the anode and cathode in neutral pH is rather low (ca. 1.3 fold higher); thereby, it is suggested that a detrimental degradation of the catalyst does not occur in UPW, since most likely the local pH does not trigger the leaching of the earth transition elements composing the catalyst, which are commonly unstable in acid/neutral conditions.

Therefore, it could be confirmed that the SEBS-P206-based AEM/AEI is able to retain its OH<sup>-</sup> conductivity at not only high temperatures, i.e., at 60 °C, in 0.1 M KOH but also in pH-neutral media, which poses a versatile option in AEM electrolysis since the possibility of eliminating KOH-based electrolytes is highly anticipated to lower operation expenditure of the technology.

However, further improvements at the cell level are necessary, namely by optimizing the PTL used at the anode side by increasing the operation temperature and understanding

its effect on chemical/mechanical stability of the SEBS-P206 membrane and ionomer and also by attempting in situ strategies for increasing the long-term  $\text{OH}^-$  retention in UPW.

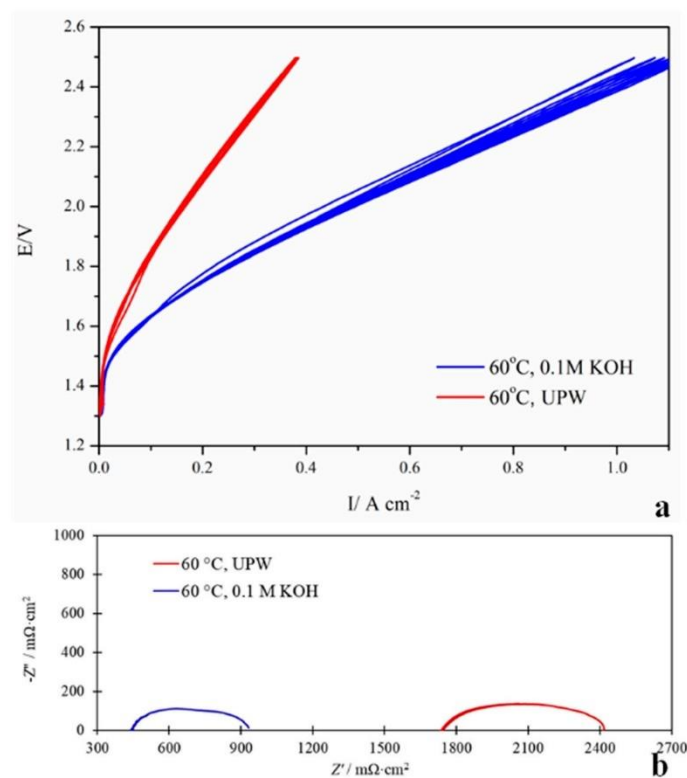


**Figure 6.** (a) AEM water electrolysis test  $IV$  curve results and (b) EIS recorded at  $200\text{ mA cm}^{-2}$  measured at  $60^\circ\text{C}$  in ultra-pure water (UPW) and  $0.1\text{ M KOH}$ .

#### 4. Conclusions

Novel piperidinium-functionalized flexible ethylene oxide spacer side-chain SEBS AEM was designed, synthesized, and applied as a membrane for AEMWE. In order to improve the conductivity of the membrane, a comb-shaped multi-functional flexible ethylene oxide spacer structure on the side chain was synthesized and investigated, revealing that flexible ethylene oxide side chains as spacers in the comb-like structures can promote a microphase separation in the membrane morphology and thus optimize the water uptake and enhanced ion conductivity. Moreover, having a pre-functionalized end of each side chain could also promote the IEC of the AEM and positively affect the ion conductivity so AEMs with piperidinium-end flexible ethylene oxide spacer side chains had relatively higher conductivity ( $25\text{ mS cm}^{-1}$ ,  $\text{OH}^-$  form at room temperature) and chemical stability (nearly 95% conductivity retention after in  $1\text{ M KOH}$  for 720 h). In the next approach, pyrrolidinium was introduced as a functional group for enhancing the alkaline stability. Furthermore, SEBS-Py2O6 reached conductivity of  $27.8\text{ mS cm}^{-1}$  ( $\text{OH}^-$ ) at RT, which is higher than SEBS piperidinium/pyrrolidinium membrane published in the past [47].

Finally, in single-cell AEMs, water electrolysis tests with PGM-free catalyst (OXYGN-N and H2GEN-M) at 60 °C achieved current densities of 171 mA cm<sup>-2</sup> at 2 V cell potential and 520 mA cm<sup>-2</sup> at 2 V in UPW and 0.1 M KOH, respectively. We have shown that the SEBS-P2O6 membrane for AEMWE in pure water outperforms membranes based on SEBS reported in the literature [20,33]. Additionally, the combination with of PGM-free electrodes in a AEMWE cells showed that SEBS-Py2O6 is a promising candidate for AEM water electrolysis cells.

**Supplementary Materials:** The following supporting information can be downloaded at: <https://www.mdpi.com/article/10.3390/membranes13030328/s1>, Figure S1: (a) potentiostatic conditioning in 0.1 M KOH electrolyte; (b) potentiostatic conditioning in UPW.

**Author Contributions:** Z.X.: Conceptualization, methodology, membrane synthesis, membrane characterization, and manuscript writing; S.D.: cell tests, manuscript writing (cell part), and manuscript reviewing; T.M.: AFM testing and manuscript reviewing; V.A.: membrane supervision and manuscript reviewing; A.S.G.: supervision and manuscript reviewing; K.A.F.: supervision and manuscript reviewing. All authors have read and agreed to the published version of the manuscript.

**Funding:** This research was funded by the EU project NEWELY funded by Fuel Cells and Hydrogen 2 Joint Undertaking (now Clean Hydrogen Partnership) under Grant Agreement No. 875118 and Chinese Scholarship Council (201706060199).

**Data Availability Statement:** Data available on request due to privacy restrictions. The data presented in this study are available on request from the corresponding author.

**Acknowledgments:** We thank TSRC for offering us the SEBS polymer.

**Conflicts of Interest:** The authors declare no conflict of interest.

## References

- Leng, Y.; Chen, G.; Mendoza, A.J.; Tighe, T.B.; Hickner, M.A.; Wang, C.-Y. Solid-State Water Electrolysis with an Alkaline Membrane. *J. Am. Chem. Soc.* **2012**, *134*, 9054–9057. [CrossRef]
- Chi, J.; Yu, H. Water electrolysis based on renewable energy for hydrogen production. *Chin. J. Catal.* **2018**, *39*, 390–394. [CrossRef]
- Xu, L.; Li, W.; You, Y.; Zhang, S.; Zhao, Y. Polysulfone and zirconia composite separators for alkaline water electrolysis. *Front. Chem. Sci. Eng.* **2013**, *7*, 154–161. [CrossRef]
- Vincent, L.; Bessarabov, D. Low cost hydrogen production by anion exchange membrane electrolysis: A review. *Renew. Sustain. Energy Rev.* **2018**, *81*, 1690–1704. [CrossRef]
- Razmjooei, F.; Farooqui, A.; Reissner, R.; Gago, A.S.; Ansar, S.A.; Friedrich, K.A. Elucidating the Performance Limitations of Alkaline Electrolyte Membrane Electrolysis: Dominance of Anion Concentration in Membrane Electrode Assembly. *ChemElectroChem* **2020**, *7*, 3951–3960. [CrossRef]
- Miller, H.A.; Bouzek, K.; Hnat, J.; Loos, S.; Bernäcker, C.I.; Weißgärber, T.; Röntzsch, L.; Meier-Haack, J. Green hydrogen from anion exchange membrane water electrolysis: A review of recent developments in critical materials and operating conditions. *Sustain. Energy Fuels* **2020**, *4*, 2114–2133. [CrossRef]
- Burnat, D.; Schlupp, M.; Wichser, A.; Lothenbach, B.; Gorbar, M.; Züttel, A.; Vogt, U.F. Composite membranes for alkaline electrolysis based on polysulfone and mineral fillers. *J. Power Sources* **2015**, *291*, 163–172. [CrossRef]
- Lee, N.; Duong, D.T.; Kim, D. Cyclic ammonium grafted poly (arylene ether ketone) hydroxide ion exchange membranes for alkaline water electrolysis with high chemical stability and cell efficiency. *Electrochim. Acta* **2018**, *271*, 150–157. [CrossRef]
- Kaczur, J.J.; Yang, H.; Liu, Z.; Sajjad, S.D.; Masel, R.I. Carbon Dioxide and Water Electrolysis Using New Alkaline Stable Anion Membranes. *Front. Chem.* **2018**, *6*, 263. [CrossRef]
- Fortin, P.; Khoza, T.; Cao, X.; Martinsen, S.Y.; Oyarcé Barnett, A.; Holdcroft, S. High-performance alkaline water electrolysis using Aemion™ anion exchange membranes. *J. Power Sources* **2020**, *451*, 227814. [CrossRef]
- Pushkareva, I.V.; Pushkarev, A.S.; Grigoriev, S.A.; Modisha, P.; Bessarabov, D.G. Comparative study of anion exchange membranes for low-cost water electrolysis. *Int. J. Hydrogen Energy* **2020**, *45*, 26070–26079. [CrossRef]
- Buggy, N.C.; Du, Y.; Kuo, M.-C.; Ahrens, K.A.; Wilkinson, J.S.; Seifert, S.; Coughlin, E.B.; Herring, A.M. A Polyethylene-Based Triblock Copolymer Anion Exchange Membrane with High Conductivity and Practical Mechanical Properties. *ACS Appl. Polym. Mater.* **2020**, *2*, 1294–1303. [CrossRef]
- David, M.; Ocampo-Martinez, C.; Sánchez-Peña, R. Advances in alkaline water electrolyzers: A review. *J. Energy Storage* **2019**, *23*, 392–403. [CrossRef]
- Pham, T.H.; Olsson, J.S.; Jannasch, P. Poly(arylene alkylene)s with pendant N-spirocyclic quaternary ammonium cations for anion exchange membranes. *J. Mater. Chem. A* **2018**, *6*, 16537–16547. [CrossRef]

15. Varcoe, J.R.; Atanassov, P.; Dekel, D.R.; Herring, A.M.; Hickner, M.A.; Kohl, P.A.; Kucernak, A.R.; Mustain, W.E.; Nijmeijer, K.; Scott, K.; et al. Anion-exchange membranes in electrochemical energy systems. *Energy Environ. Sci.* **2014**, *7*, 3135–3191. [[CrossRef](#)]
16. Yang, C.; Wang, S.; Ma, W.; Zhao, S.; Xu, Z.; Sun, G. Highly stable poly(ethylene glycol)-grafted alkaline anion exchange membranes. *J. Mater. Chem. A* **2016**, *4*, 3886–3892. [[CrossRef](#)]
17. Zhu, L.; Peng, X.; Shang, S.-L.; Kwasny, M.T.; Zimudzi, T.J.; Yu, X.; Saikia, N.; Pan, J.; Liu, Z.-K.; Tew, G.N.; et al. High Performance Anion Exchange Membrane Fuel Cells Enabled by Fluoropoly(olefin) Membranes. *Adv. Funct. Mater.* **2019**, *29*, 1902059. [[CrossRef](#)]
18. Jeon, J.Y.; Park, S.; Han, J.; Maurya, S.; Mohanty, A.D.; Tian, D.; Saikia, N.; Hickner, M.A.; Ryu, C.Y.; Tuckerman, M.E.; et al. Synthesis of Aromatic Anion Exchange Membranes by Friedel–Crafts Bromoalkylation and Cross-Linking of Polystyrene Block Copolymers. *Macromolecules* **2019**, *52*, 2139–2147. [[CrossRef](#)]
19. Arges, C.G.; Ramani, V. Two-dimensional NMR spectroscopy reveals cation-triggered backbone degradation in polysulfone-based anion exchange membranes. *Proc. Natl. Acad. Sci. USA* **2013**, *110*, 2490. [[CrossRef](#)]
20. Edson, J.B.; Macomber, C.S.; Pivovar, B.S.; Boncella, J.M. Hydroxide based decomposition pathways of alkyltrimethylammonium cations. *J. Membr. Sci.* **2012**, *399–400*, 49–59. [[CrossRef](#)]
21. Long, H.; Kim, K.; Pivovar, B.S. Hydroxide Degradation Pathways for Substituted Trimethylammonium Cations: A DFT Study. *J. Phys. Chem. C* **2012**, *116*, 9419–9426. [[CrossRef](#)]
22. Marino, M.G.; Kreuer, K.D. Alkaline Stability of Quaternary Ammonium Cations for Alkaline Fuel Cell Membranes and Ionic Liquids. *ChemSusChem* **2015**, *8*, 513–523. [[CrossRef](#)]
23. Olsson, J.S.; Pham, T.H.; Jannasch, P. Tuning poly(arylene piperidinium) anion-exchange membranes by copolymerization, partial quaternization and crosslinking. *J. Membr. Sci.* **2019**, *578*, 183–195. [[CrossRef](#)]
24. Pan, J.; Chen, C.; Li, Y.; Wang, L.; Tan, L.; Li, G.; Tang, X.; Xiao, L.; Lu, J.; Zhuang, L. Constructing ionic highway in alkaline polymer electrolytes. *Energy Environ. Sci.* **2014**, *7*, 354–360. [[CrossRef](#)]
25. Li, N.; Yan, T.; Li, Z.; Thurn-Albrecht, T.; Binder, W.H. Comb-shaped polymers to enhance hydroxide transport in anion exchange membranes. *Energy Environ. Sci.* **2012**, *5*, 7888–7892. [[CrossRef](#)]
26. Zhu, L.; Pan, J.; Wang, Y.; Han, J.; Zhuang, L.; Hickner, M.A. Multication Side Chain Anion Exchange Membranes. *Macromolecules* **2016**, *49*, 815–824. [[CrossRef](#)]
27. Han, J.; Zhu, L.; Pan, J.; Zimudzi, T.J.; Wang, Y.; Peng, Y.; Hickner, M.A.; Zhuang, L. Elastic Long-Chain Multication Cross-Linked Anion Exchange Membranes. *Macromolecules* **2017**, *50*, 3323–3332. [[CrossRef](#)]
28. Zhu, Y.; Ding, L.; Liang, X.; Shehzad, M.A.; Wang, L.; Ge, X.; He, Y.; Wu, L.; Varcoe, J.R.; Xu, T. Beneficial use of rotatable-spacer side-chains in alkaline anion exchange membranes for fuel cells. *Energy Environ. Sci.* **2018**, *11*, 3472–3479. [[CrossRef](#)]
29. Liu, M.; Hu, X.; Hu, B.; Liu, L.; Li, N. Soluble poly(aryl piperidinium) with extended aromatic segments as anion exchange membranes for alkaline fuel cells and water electrolysis. *J. Membr. Sci.* **2022**, *642*, 119966. [[CrossRef](#)]
30. Yin, Z.; Wu, Y.; Shi, B.; Yang, C.; Kong, Y.; Liu, Y.; Wu, H.; Jiang, Z. Alkaline stable piperidinium-based biphenyl polymer for anion exchange membranes. *Solid State Ion.* **2022**, *383*, 115969. [[CrossRef](#)]
31. Xue, J.; Zhang, J.; Liu, X.; Huang, T.; Jiang, H.; Yin, Y.; Qin, Y.; Guiver, M.D. Toward alkaline-stable anion exchange membranes in fuel cells: Cycloaliphatic quaternary ammonium-based anion conductors. *Electrochem. Energy Rev.* **2022**, *5*, 348–400. [[CrossRef](#)]
32. Zhang, J.; Yu, W.; Liang, X.; Zhang, K.; Wang, H.; Ge, X.; Wei, C.; Song, W.; Ge, Z.; Wu, L.; et al. Flexible Bis-piperidinium Side Chains Construct Highly Conductive and Robust Anion-Exchange Membranes. *ACS Appl. Energy Mater.* **2021**, *4*, 9701–9711. [[CrossRef](#)]
33. Gupta, G.; Scott, K.; Mamlouk, M. Performance of polyethylene based radiation grafted anion exchange membrane with polystyrene-b-poly(ethylene/butylene)-b-polystyrene based ionomer using NiCo<sub>2</sub>O<sub>4</sub> catalyst for water electrolysis. *J. Power Sources* **2018**, *375*, 387–396. [[CrossRef](#)]
34. Du, N.; Roy, C.; Peach, R.; Turnbull, M.; Thiele, S.; Bock, C. Anion-Exchange Membrane Water Electrolyzers. *Chem. Rev.* **2022**, *122*, 11830–11895. [[CrossRef](#)]
35. Stiber, S.; Balzer, H.; Wierhake, A.; Wirkert, F.J.; Roth, J.; Rost, U.; Brodmann, M.; Lee, J.K.; Bazylak, A.; Waiblinger, W.; et al. Porous Transport Layers for Proton Exchange Membrane Electrolysis Under Extreme Conditions of Current Density, Temperature, and Pressure. *Adv. Energy Mater.* **2021**, *11*, 2100630. [[CrossRef](#)]
36. Dai, P.; Mo, Z.-H.; Xu, R.-W.; Zhang, S.; Wu, Y.-X. Cross-Linked Quaternized Poly(styrene-b-(ethylene-co-butylene)-b-styrene) for Anion Exchange Membrane: Synthesis, Characterization and Properties. *ACS Appl. Mater. Interfaces* **2016**, *8*, 20329–20341. [[CrossRef](#)]
37. Hao, J.; Gao, X.; Jiang, Y.; Zhang, H.; Luo, J.; Shao, Z.; Yi, B. Crosslinked high-performance anion exchange membranes based on poly(styrene-b-(ethylene-co-butylene)-b-styrene). *J. Membr. Sci.* **2018**, *551*, 66–75. [[CrossRef](#)]
38. Yu, N.; Dong, J.; Li, H.; Wang, T.; Yang, J. Improving the performance of quaternized SEBS based anion exchange membranes by adjusting the functional group and side chain structure. *Eur. Polym. J.* **2021**, *154*, 110528. [[CrossRef](#)]
39. Wang, F.; Li, C.; Sang, J.; Cui, Y.; Zhu, H. Synthesis and characterization of a long side-chain double-cation crosslinked anion-exchange membrane based on poly(styrene-b-(ethylene-co-butylene)-b-styrene). *Int. J. Hydrogen Energy* **2021**, *46*, 36301–36313. [[CrossRef](#)]
40. Al Munsur, A.Z.; Hossain, I.; Nam, S.Y.; Chae, J.E.; Kim, T.-H. Hydrophobic-hydrophilic comb-type quaternary ammonium-functionalized SEBS copolymers for high performance anion exchange membranes. *J. Membr. Sci.* **2020**, *599*, 117829. [[CrossRef](#)]

41. Li, Z.; Li, C.; Long, C.; Sang, J.; Tian, L.; Wang, F.; Wang, Z.; Zhu, H. Elastic and durable multi-cation-crosslinked anion exchange membrane based on poly(styrene-*b*-(ethylene-co-butylene)-*b*-styrene). *J. Polym. Sci.* **2020**, *58*, 2181–2196. [[CrossRef](#)]
42. Sung, S.; Chae, J.E.; Min, K.; Kim, H.-J.; Nam, S.Y.; Kim, T.-H. Preparation of crosslinker-free anion exchange membranes with excellent physicochemical and electrochemical properties based on crosslinked PPO-SEBS. *J. Mater. Chem. A* **2021**, *9*, 1062–1079. [[CrossRef](#)]
43. Xu, Z.; Wilke, V.; Chmielarz, J.J.; Tobias, M.; Atanasov, V.; Gago, A.S.; Friedrich, K.A. Novel piperidinium-functionalized crosslinked anion exchange membrane with flexible spacers for water electrolysis. *J. Membr. Sci.* **2022**, *670*, 121302. [[CrossRef](#)]
44. Pandey, T.P.; Sarode, H.N.; Yang, Y.; Yang, Y.; Vezzù, K.; Noto, V.D.; Seifert, S.; Knauss, D.M.; Liberatore, M.W.; Herring, A.M. A Highly Hydroxide Conductive, Chemically Stable Anion Exchange Membrane, Poly(2,6 dimethyl 1,4 phenylene oxide)-*b*-Poly(vinyl benzyl trimethyl ammonium), for Electrochemical Applications. *J. Electrochem. Soc.* **2016**, *163*, H513–H520. [[CrossRef](#)]
45. Zhang, M.; Shan, C.; Liu, L.; Liao, J.; Chen, Q.; Zhu, M.; Wang, Y.; An, L.; Li, N. Facilitating Anion Transport in Polyolefin-Based Anion Exchange Membranes via Bulky Side Chains. *ACS Appl. Mater. Interfaces* **2016**, *8*, 23321–23330. [[CrossRef](#)]
46. Shin, D.W.; Lee, S.Y.; Lee, C.H.; Lee, K.-S.; Park, C.H.; McGrath, J.E.; Zhang, M.; Moore, R.B.; Lingwood, M.D.; Madsen, L.A.; et al. Sulfonated Poly(arylene sulfide sulfone nitrile) Multiblock Copolymers with Ordered Morphology for Proton Exchange Membranes. *Macromolecules* **2013**, *46*, 7797–7804. [[CrossRef](#)]
47. Su, X.; Gao, L.; Hu, L.; Qaisrani, N.A.; Yan, X.; Zhang, W.; Jiang, X.; Ruan, X.; He, G. Novel piperidinium functionalized anionic membrane for alkaline polymer electrolysis with excellent electrochemical properties. *J. Membr. Sci.* **2019**, *581*, 283–292. [[CrossRef](#)]
48. Omasta, T.J.; Park, A.M.; LaManna, J.M.; Zhang, Y.; Peng, X.; Wang, L.; Jacobson, D.L.; Varcoe, J.R.; Hussey, D.S.; Pivovar, B.S.; et al. Beyond catalysis and membranes: Visualizing and solving the challenge of electrode water accumulation and flooding in AEMFCs. *Energy Environ. Sci.* **2018**, *11*, 551–558. [[CrossRef](#)]
49. Fan, J.; Willdorf-Cohen, S.; Schibli, E.M.; Paula, Z.; Li, W.; Skalski, T.J.G.; Sergeenko, A.T.; Hohenadel, A.; Frisken, B.J.; Magliocca, E.; et al. Poly(bis-arylimidazoliums) possessing high hydroxide ion exchange capacity and high alkaline stability. *Nat. Commun.* **2019**, *10*, 2306. [[CrossRef](#)]
50. Movil, O.; Frank, L.; Staser, J.A. Graphene Oxide–Polymer Nanocomposite Anion-Exchange Membranes. *J. Electrochem. Soc.* **2015**, *162*, F419. [[CrossRef](#)]

**Disclaimer/Publisher's Note:** The statements, opinions and data contained in all publications are solely those of the individual author(s) and contributor(s) and not of MDPI and/or the editor(s). MDPI and/or the editor(s) disclaim responsibility for any injury to people or property resulting from any ideas, methods, instructions or products referred to in the content.

## Article III

# Highly Efficient, Low-Cost and Durable Anion Exchange Membrane Water Electrolyser Operating in Pure Water: Key Components and Fabrication Strategies

S. Delgado<sup>1,2,3a)</sup>, Z. Xu<sup>3a)</sup>, V. Wilke<sup>3</sup>, A. Gago<sup>3</sup>, A. Mendes<sup>1,2\*\*</sup>, K. A. Friedrich<sup>3</sup>

<sup>1</sup> LEPABE - Laboratory for Process Engineering, Environment, Biotechnology and Energy, Faculty of Engineering, University of Porto, Rua Dr. Roberto Frias, 4200-465 Porto, Portugal

<sup>2</sup> ALiCE - Associate Laboratory in Chemical Engineering, Faculty of Engineering, University of Porto, Rua Dr. Roberto Frias, 4200-465 Porto, Portugal

<sup>3</sup> Institute of Engineering Thermodynamics/Electrochemical Energy Technology, German Aerospace Center (DLR), Pfaffenwaldring 38-40, 70569 Stuttgart, Germany

## Abstract

Anion exchange membrane water electrolyzers (AEMWE) are expected to be important devices for achieving sustainable green hydrogen generation. Nonetheless, they still require a corrosive alkaline electrolyte and thus effective, and economical components with excellent chemical stability must be developed for operation in pure water. In this work, we present a AEMWE cell that has stainless steel components, no precious metal catalysts and that runs continuously in pure water while exhibiting one of the lowest degradation rates reported up to now. The used AEM is composed of pyrrolidinium functionalized styrene – b – ethylene – b-butylene-b-styrene copolymer. The cell can achieve 2 V at 0.7 A cm<sup>-2</sup> and 60 °C and shows a degradation rate of 3 mV h<sup>-1</sup> at constant operation of 0.2 A cm<sup>-2</sup>. It outperforms the state-of-the-art AEMWE composed of Sustainion membrane (Dioxide Materials) and precious metal catalysts. The activation conditions of the novel Pyrrolidinium multi-cation comb-shaped polymer structure-based

membrane and the concentration of the same formulation-based ionomer (20 wt.% ionomer/catalyst) are key factors for increasing performance and durability. Our results show that low cost AEMWE operating with pure water is possible, becoming a promising alternative to replace the expensive proton exchange membrane electrolyzers (PEMWE).

a) Both authors contributed equally to this work

\*\* corresponding author

## **Introduction**

Low-temperature water electrolysis stands out as the leading technology for assisting in the intermittent and fluctuating nature of renewables, acting as backup storage of power in the form of chemical energy, specifically extremely pure hydrogen<sup>1</sup>.

Alkaline electrolysis (AE) is the most widely used commercial technology at the MW scale. The high alkalinity provided by the highly concentrated circulating KOH solution (30 – 40 wt.%) allows the use of earth-abundant, non-precious metals with low CAPEX, such as nickel, iron, and cobalt-based oxides. However, various technical challenges develop as a result of the strong reactivity of hydroxyl ions with CO<sub>2</sub> from ambient air, which causes the creation of K<sub>2</sub>CO<sub>3</sub> salts, which completely undermines the stability of the electrolyzer<sup>2,3</sup>. Alkaline electrolyzers normally do not exceed 400 mA·cm<sup>-2</sup> at *ca.* 80 °C in the potential windows ranging from 1.8 V to 2.4 V. One of the reasons concerning this performance refers to the fact salt precipitates build up in the pores of the transport layers, obstructing the flow of reactants and products while impeding anion OH<sup>-</sup> transfer to active sites<sup>4</sup>. Furthermore, the diaphragm that separates both electrodes does not prevent excessive gas mixing, triggered by hydrogen and oxygen cross-over from one half-cell to the other, which, in addition to raising major security concerns, decreases the device's effectiveness<sup>5</sup>. This is a concern especially at part load conditions.

On the other hand, proton exchange membrane water electrolyzers (PEMWEs) have an interconnected membrane-electrode interface taking advantage of the non-porous and polymeric proton exchange membranes (PEM) which allow obtaining high current densities that surpass 4 A cm<sup>-2</sup> with cell efficiencies of *ca.* 74 %<sub>HHV</sub><sup>6-8</sup>. In addition, PEMWEs

allow differential pressure operation, which prevent a second step mechanical hydrogen compression for eventual storage. Despite its numerous advantages, the anodic chamber's highly oxidative environment limits the choice of electrocatalysts and peripheral components to Precious Group Metals (PGM) and other scarce or expensive materials, adding to the technology's high capital cost. According to the European FCH-JU and US department of energy (DOE)<sup>9</sup>, for PEMWEs to be competitive at the MW scale, investment costs must be reduced by at least half; currently, 1000-2000 € k<sup>-1</sup> W<sup>-1</sup> needs to be reduced to 300-600 € k<sup>-1</sup> W<sup>-1</sup>.

The alkaline exchange membrane water electrolyzers (AEMWEs), a third emerging type of low-temperature electrolyzer, reveal numerous eye-catching benefits because the goal is to combine the kernel advantages of PEMWEs, the use of solid polymeric membranes, with the benefits of AWEs, by relying on cheap and abundant PGM-free materials<sup>10</sup>. A striking difference from the counterpart PEMWE concerns the use of a supporting electrolyte (*i.e.*, KOH or K<sub>2</sub>CO<sub>3</sub> solutions) that has been associated to both increase the hydroxide ion transport in the membrane and the catalyst layers, which is required for boosting the kinetics of the reaction, due to the increment of local pH at the catalyst-electrolyte interface<sup>11</sup>. Naturally, interest in the generation of green hydrogen using AEMWEs has grown over the last decade, and numerous advances have been made, primarily in membrane technology and the creation of PGM-free catalysts for the oxygen evolution reaction (OER). It is generally known that AEMs based on quaternary ammonium (QA) are susceptible to degradation, especially when exposed to alkaline conditions and high temperatures. The unintentional loss of ionic groups and breakage of the polymer backbones are both possible outcomes of this degradation event. The processes such as Hofmann elimination<sup>12</sup>, direct nucleophilic substitution<sup>13</sup>, and different rearrangement events are predominantly included in the acknowledged mechanisms responsible for the degradation of QA cations. To effectively address this challenge, researchers have pursued an alternative strategy involving the integration of stable organic cations into polymeric AEMs. Consequently, this exploration has given rise to a diverse spectrum of novel cationic groups within the realm of AEM development. These alternative cationic moieties encompass imidazolium<sup>14</sup>, phosphonium, guanidinium<sup>15</sup>,



and triazolium<sup>16</sup>, among others. Importantly to mention, these alternative cationic entities offer enlarged stabilities and have demonstrated considerable potential in bolstering the chemical robustness and durability of AEMs.

Quaternized imidazolium polystyrene-based membranes and ionomers, such as Sustainion 37-50, have allowed reaching unprecedented current densities of *ca.* 3.3 A cm<sup>-2</sup> at 1.8 V @ 60 °C using 1 M KOH and PGM-based catalysts (IrO<sub>2</sub>|Pt)<sup>17,18</sup> and 0.47 A cm<sup>-2</sup> with PGM-free catalysts (NiFe|NiFeCo) at the same operating conditions<sup>17</sup>. Still, operating under demineralized water is the primary objective for making AEMWEs a competitive technology.

The typical material for AEM electrolysis includes nickel-based catalysts and components; however, during positive polarization, its chemical stability declines at pH 9, preventing its usage in ultra-pure water conditions. Another pressing and critical technical issue is the poor stability of water-fed AEMs due to CO<sub>2</sub> contamination, which causes the formation of dissolved carbonate and bicarbonate ions, known to decrease the ionic conductivity of the binders and membranes - a drop of 200 mA cm<sup>-2</sup> has been observed in just 30 min at a fixed potential (1.8 V) in ultra-pure water<sup>19</sup>. Besides some promising performances reported for pure water-fed membrane based alkaline electrolyzers that reach 1.5 A cm<sup>-2</sup> at 2.0 V and 85 °C or 800 mA cm<sup>-2</sup> at 2.0 V at 70 °C<sup>20,21</sup> using PGM-free anodes, the stability of the cell at fixed and moderate current densities is rather poor and short-termed (< 50 h). Researchers have used a highly quaternized polystyrene membrane, a NiFe anode, and a PtRu/C cathode in pure water at 200 mA cm<sup>-2</sup> (60 °C) and achieved a quick deterioration rate of 15 mV h<sup>-1</sup> after just 40 hours of operation - equal to a 600 mV overpotential<sup>21</sup>. The particles washout due to chemical imbalances at the catalyst-electrolyte interface at neutral pH operation, had been assigned as possible degradation mechanism; therefore, while the immediate observed steep loss of performance remains an ambiguous subject, it is critical to fundament the understanding on the actual best preparation approaches and critical components for obtaining practical and high-performing AEMWE systems using pure water.

Furthermore, it is significant to note that critical raw materials (CRM) avoidance is now more essential than planning for the creation of sustainable systems that solely include

catalysts devoid of PGMs. These CRMs include raw materials like nickel, cobalt, copper, and lithium in addition to the noble metals that are commercially and strategically significant for the European economy but have a high supply risk.

This paper describes a full CRM-free, high-performance AEM electrolyzer with exceptional endurance in ultra-pure water operation ( $> 85$  h @  $60$  °C at  $200$  mA cm<sup>-2</sup>). The breakthrough preparation strategies that led to record stabilities, in both KOH concentrated electrolytes and ultrapure water, of membrane electrode assemblies (MEAs) consisting of pyrrolidinium functionalized styrene-ethylene butylene- styrene-based (SEBS-Py2O6) membrane and PGM-free based electrodes are detailed. The activation of the polymers in alkaline media, both membrane and solid electrolyte, and specific configuration of peripheral components, was discovered to be critical in maintaining high performances in ultra-pure water and moderate current densities while also preserving the stability of metal transition catalysts (Ni) and other low-cost components, such as stainless-steel bipolar plates and current collectors. These outcomes are one step closer to unknot high-performing and durable AEMWEs into pilot commercialization operating in ultrapure water, enabling for the replacement of high-cost PEMWEs that already run with pure water (UPW).

## Results and Discussion

### Physical-chemical properties of SEBS-Py2O6

Fig.1 a) illustrates the synthetic pathway to produce a pyrrolidinium-functionalized multi-cation comb-shaped polymer structure of styrene-ethylene-butylene-styrene (SEBS-Py2O6). AEM water electrolyzers require mechanically stable AEMs to operate at high differential pressures, and therefore, membrane thickness is a critical factor. The final thickness of the produced pyrrolidinium membranes (SEBS-Py2O6) was approximately  $70 \pm 3.3$   $\mu\text{m}$ , and no visible surface defects were detected.

High-performing anion exchange membranes (AEMs) typically exhibit an ion exchange capacity (IEC) for OH<sup>-</sup> ions of around  $1.50$  mequiv g<sup>-1</sup>, similar to that of commercial Sustainion X37-50<sup>22</sup>, as shown in Table 1. However, exceeding a certain threshold of IEC to OH<sup>-</sup> ion ratio, such as IEC  $>2$  mequiv g<sup>-1</sup>, can result in swelling and potential dissolution

of AEMs in water or aqueous alkaline electrolyte solutions due to an increase in the number of charged hydrophilic functional groups on the polymer backbone<sup>23,24</sup>. This leads to potential degradation in performance and mechanical stability. Despite a lower conductivity in OH<sup>-</sup> form of  $28.5 \pm 2.3 \text{ M cm}^{-1}$  for SEBS-Py2O6, compared to that of commercial Sustainion, the synthesized pyrrolidinium-functionalized multi-cation comb-shaped polymer (SEBS-Py2O6) exhibited a reasonable water uptake ratio of  $38.3 \pm 4.8 \text{ wt.}\%$ , consistent with its larger thickness. While for example, poly(aryl piperidinium) AEMs with lower water uptake ratios (15 wt. % - 25 wt. %)<sup>25</sup> may be generally preferred for high performance and long-term stability due to their reduced susceptibility to swelling and degradation over time, a balance must be found between this property and high ionic conductivity, as these properties are often inversely related.

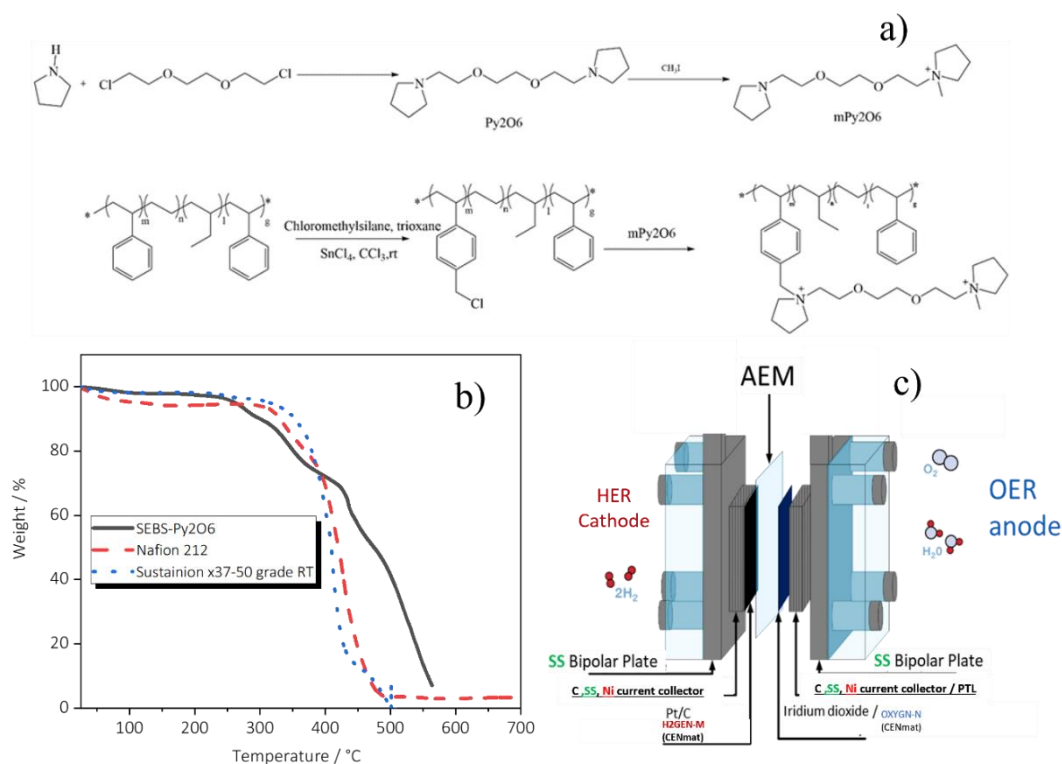


**Fig. 1. (a)** Synthesis route of pyrrolidinium functionalized SEBS anion exchange membrane (on top – synthesis route of functional group Py2O6; below – synthesis of backbone and SEBS and functionalization step); **(b)** thermogravimetric curves for

prepared SEBS-Py206 membrane, commercial Nafion 212 and Sustainion X37-50 grade RT under oxygen flow; **(c)** Schematic illustration of the single cell electrolyzer configuration used to conduct the experiments with several current collectors (Stainless Steel felt (SS), hydrophilic carbon paper (C) and Nickel felt (Ni)) and MEA configurations (catalyst coated membranes – CCM – or catalyst coated substrates – CCS) using commercial noble metal catalysts (40 wt. % Pt/C and Ir black, Alfa Aesar) or CRM-free (OXYGN-N and H2GEN-M, purchased from CENmat).

**Table 1.** Summary of prepared SEBS-Py206 AEM and commercial AEM/PEM properties.

	<b>Conductivity OH<sup>-</sup> form  (mS cm<sup>-1</sup>)</b>	<b>Ion Exchange Capacity/IEC  (mmol g<sup>-1</sup>)</b>	<b>Water Uptake (Cl<sup>-</sup>)  (%)</b>	<b>Swelling ratio  (%)</b>	<b>Thickness  (μm)</b>
<b>SEBS-Py206</b>	28.5 ± 2.3	1.40 ± 0.13	38.3 ± 4.8	11.3 ± 2.3	70 ± 3.3
<b>Commercial Nafion 212*</b>	130 ± 6.4 (H <sup>+</sup> form)	1.20 ± 0.23	24 ± 3.0	25 ± 2.5	50 ± 1.2
<b>Commercial Sustainion X37-50 grade RT**</b>	77 ± 10	0.99 ± 0.04	30 ± 2.0	1.43 ± 1.0	125 ± 3.3

\*/\*\* retrieved from technical data sheet,  
from experiments conducted at 25 °C, DuPont  
and Dioxide materials (18,22)

The produced AEM was subjected to a thermogravimetric examination and compared with the well-known Nafion 212 membrane, which is renowned for its unparalleled stability, particularly for PEM water electrolysis. As evidenced by the significantly less weight loss observed for up to 250 °C at the high volatility first weight loss region where plasticizers are released from the polymer matrix<sup>26</sup>, the TGA results showed that the prepared SEBS-Py206 AEM displays a significantly higher thermal stability than Nafion 212 and similar to that of Sustainion X37-50, as shown in Fig.1b. The prepared AEM maintained its mechanical integrity fully up to 300 °C, whereas Nafion 212 lost about 6 wt.%

of its weight under the same conditions. Additives such as plasticizers are commonly added in polymer processing to improve flexibility, processability and to boost the films' ion transport properties<sup>27,28</sup>; these compounds are usually inert organic compounds and possess a low molecular weight with low vapor pressures, such as phthalates (esters of polycarboxylic acids<sup>27</sup>), glycerol, ethylene glycol, ionic liquids<sup>29</sup>, among others. While lower plasticizer content may lessen the likelihood of thermal degradation, which is suggested to be the case for the prepared AEM, high plasticizer ratios are associated with decreasing the dimensional stability of AEMs by potentially triggering changes in shape, thickness, and overall integrity, which is a significant issue during operation. Furthermore, the steep weight loss region associated with thermal decomposition at about 400 °C, which involves the breaking of chemical bonds primarily linked to the backbone chains and polymer ionic groups<sup>30</sup>, is delayed in the SEBS-Py2O6 sample by roughly 70 °C to 100 °C when compared to the reinforced Sustainion membrane. Because of this, SEBS-Py2O6 has the potential to operate and endure at temperatures higher than those at which commercially successful membranes are known, while retaining its chemical and mechanical stability.

#### **AEM Water Electrolysis Efficiency in Low Alkalinity and Pure Water Conditions: Impact of Current Collector Composition**

The effects of using different anode current collectors on the performance of alkaline anion exchange membrane water electrolyzers (AEMWEs) under low alkalinity and pure water operation were explored. The choice of current collector is crucial for ensuring the efficient transport of reactant water to the catalyst layer while allowing for effective removal of product gas; the latter act as a microporous extension of the porous transport layer (PTL). In fact, the electrical resistance at the interface between the MEA, the current collector, and the PTL, which performs as a multifunctional liquid/gas-diffusion layer<sup>31</sup>, affects ohmic resistances as well. Both PTLs and current collectors are essential for preventing ohmic losses and concentration overpotentials, which are the main causes of the overall cell voltage<sup>32,33</sup>. We compared the performance of stainless steel felt, hydrophilic carbon paper, and nickel felt current collectors, and found that the stainless

steel felt provided the optimal balance between structural properties such as porosity and tortuosity, electrical conductivity, and overall performance in both low alkaline environment and when circulating pure water through the electrolyser, Fig 2a) and Fig 2b).

The overall performance, regardless of the employed current collector, exhibits significantly higher current densities in alkaline environments when compared to pure water operation; this is not surprising because in pure water, several factors, such as the lower ion conductivity ( $\text{OH}^-$ ) of the electrolyte, inevitably trigger overall ohmic resistances and activation overpotentials, since achieving the necessary reaction rates at the electrode surfaces can be challenging, leading to reduced performance. In fact, the PGM-free catalyst reconstruction, mainly those composed of Ni or Fe alloys, is being assigned as the main factor for drop in performance in water fed electrolysers<sup>34</sup>. However, more active regions can be added to the catalyst-electrolyte interface by increasing the electrolyte's alkaline content<sup>35</sup>.

Stainless steel<sup>36</sup> typically passivates at anodic potentials, ensuring long-term stability but reducing the electrical conductivity, whereas Ni materials<sup>37,38</sup> are thought of as the standard substrate materials, (felts and foams), for alkaline electrolysis ( $\text{pH} > 13$ ). However, we observed the SS felt current collectors from Bekaert, provide a three-fold increase in performance compared to Ni-based collectors and a two-fold increase compared to carbon paper collectors when the potential difference is set at 2 V while running with pure water, at neutral pH, as seen in Fig. 2b). The Ni-based current collectors exhibited notable performance loss in ultra-pure water conditions. This degradation could be assigned to the dissolution of nickel ions in water. However, when operating at  $\text{pH} = 13$  with 0.1 M KOH, the Ni felt effectively extends the catalyst layer under OER conditions, achieving a current density of  $1.1 \text{ A cm}^{-2}$  at 2 V and  $60 \text{ }^\circ\text{C}$ , (see Fig. 2a)). In the pH range between 9.1 to 12.2, nickel remains stable and generates a protective layer in equilibrium with solid phases such as nickel hydroxide ( $\text{Ni}(\text{OH})_2$ ),  $\text{Ni}_3\text{O}_4$ , and nickel dioxide ( $\text{NiO}_2$ ). However, extreme potentials, exceeding the thermodynamic stability *i.e.*,  $> 1.6 \text{ V vs RHE}$  may be sufficient to drive electrochemical reactions / transformations on the surface of nickel/ nickel oxide. Specially, at pH-neutral environment and at potential

differences over 1.2 V, Nickel may dissolve in water in the form of  $\text{Ni}^{2+}$  ions<sup>39</sup>, that may trigger degradation mechanism such as some fiber/nanoparticles from the catalyst detachment and/or dissolution into the electrolyte, as seen in the Pourbaix diagram for Nickel-water at 25°C<sup>40</sup>, Fig S1. When the pH of the system experiences a slight decrease (pH below 7), the dissolution effect becomes significantly more pronounced. Moreover, operating the system at high temperatures exacerbates this situation<sup>41</sup>, (see Fig. S3).

Similarly, hydrophilic carbon paper showed fair performance in low alkalinity conditions but proved to be unsuitable for Ph-neutral media, Fig. 2b), most likely due to its tendency to oxidize to carbon dioxide at potentials  $> 0.8$  V vs. RHE, which limits its use in pH-neutral media despite their potential for increased electrical contact<sup>42</sup>. From a thermodynamic perspective, carbon's stability under alkaline conditions is markedly lower, up to 18 times, compared to its stability in an acidic environment. This discrepancy arises from the pronounced nucleophilic nature of hydroxide ions ( $\text{OH}^-$ ) present in alkaline solutions, which significantly accelerates the degradation of carbon<sup>43</sup>.

In addition, we observed that the use of catalyst coated membranes (CCMs) resulted in lower current density outputs compared to catalyst coated substrates (CCSs), which we attribute to the detrimental effect on the stability of polymeric chains during the catalyst spraying process<sup>44</sup>, which is noticeable attending to the sharper slope at the ohmic region in both high alkaline and pure water. Overall, our results provide insights into the optimal selection of current collectors and support materials to being based of stainless steel for AEMWEs, which allows paving the way for more efficient, stable, and sustainable water electrolysis systems, in both economic and environmental angles.

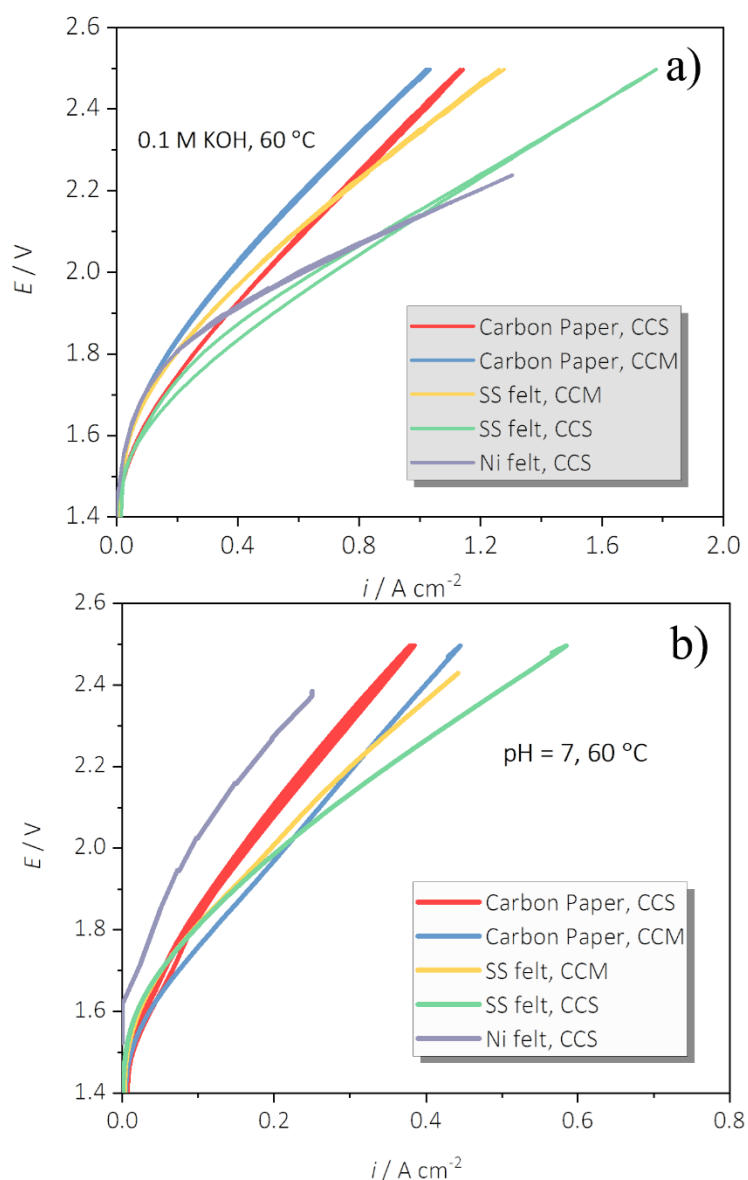


**Fig. 2.** Polarisation curves for AEM water electrolyzers using several anode/cathode current collectors (Ni felt, SS felt and carbon paper) with CRM-free catalysts (OXYGN-N and H2GEN-M) and the SEBS-Py2O6 based AEM and anion exchange ionomer (AEI) (30 wt. % I/C). Both CCSs and CCMs MEA configurations were tested in **(a)** 0.1 M KOH and **(b)** ultra-pure water in pH-neutral conditions (UPW, pH=7) at 60 °C.

#### **Ionomeric binder properties and concentration as AEMWEs performance-limiting parameters**

Both the properties and concentration of ionomeric binders within the catalyst layer had recently been identified as performance-limiting parameters for both hydrogen (HER)



and oxygen (OER) reactions in AEMWEs<sup>45,46</sup>. For AEM electrolyzers, compromise strategies had been lately reported to address the trade-off between using high-ion exchange capacity (IEC) binders and solid polymer electrolytes (AEM) with moderate water uptakes. The approaches aim to replace the common practice of using high-concentration circulating caustic electrolytes, which although enhancing the AEMWE's initial (BoL) performance, may lead to long-term operational instability<sup>47</sup>. Unlike AEM fuel cell systems, where intermediate IEC binders are preferred to prevent excessive co-adsorption of cation-hydroxide and water molecules<sup>47,48</sup> that impairs reactant gas transport, AEM electrolyzers benefit from higher water content. Therefore, it is suggested the use of binders with higher IEC in the catalyst layer (CL) to facilitate the water management and kinetics and thus improve overall performance<sup>45</sup>. In a direct performance comparison, when utilizing the commercial Sustainion X37-RT binder and the prepared SEBS-Py206 binder, both with an ion-to-catalyst ratio of 0.3 on both the anode and cathode sides while employing CRM-free catalysts (as depicted in Fig. 1c)), and operated with a circulating electrolyte based on 0.1 M KOH, a noticeable positive effect arises from the Sustainion binder. This effect is due to the approximately threefold larger OH<sup>-</sup> conductivity exhibited by the Sustainion binder ( $77 \pm 10 \text{ mS cm}^{-1}$ , Supplementary Fig. S4a); the effect of improved ability of the binder to conduct the electric current by allowing the ions to migrate inside it, is mostly observed in the reduced activation overpotential hence earlier onset (almost less 200 mV in 0.1 M KOH at 60 °C). However, when both binders were tested in a Ph neutral media with only pure water as reactant, the reverse scenario was seen (Supplementary Fig. S4b)). Regarding the SEBS-Py206 binder properties (shown in Table 1), it is likely that the higher IEC is critical to ensuring an increased ability to exchange and absorb ions (OH<sup>-</sup>) with the surrounding solution during operation and even during the initial pre-conditioning activation step where both Sustainion and SEBS-Py206 CCSs were immersed in a 1 M KOH bath; at Ph neutral media in 60 °C, the SEBS-Py206 based MEAs ensure substantially higher limiting current densities and lower activation overpotentials, *i.e.*,  $600 \text{ mA cm}^{-2}$  at 2.4 V for SEBS-Py206 binder vs.  $240 \text{ mA cm}^{-2}$  at the same potential for Sustainion, Fig. 3b) and Fig. 3a).

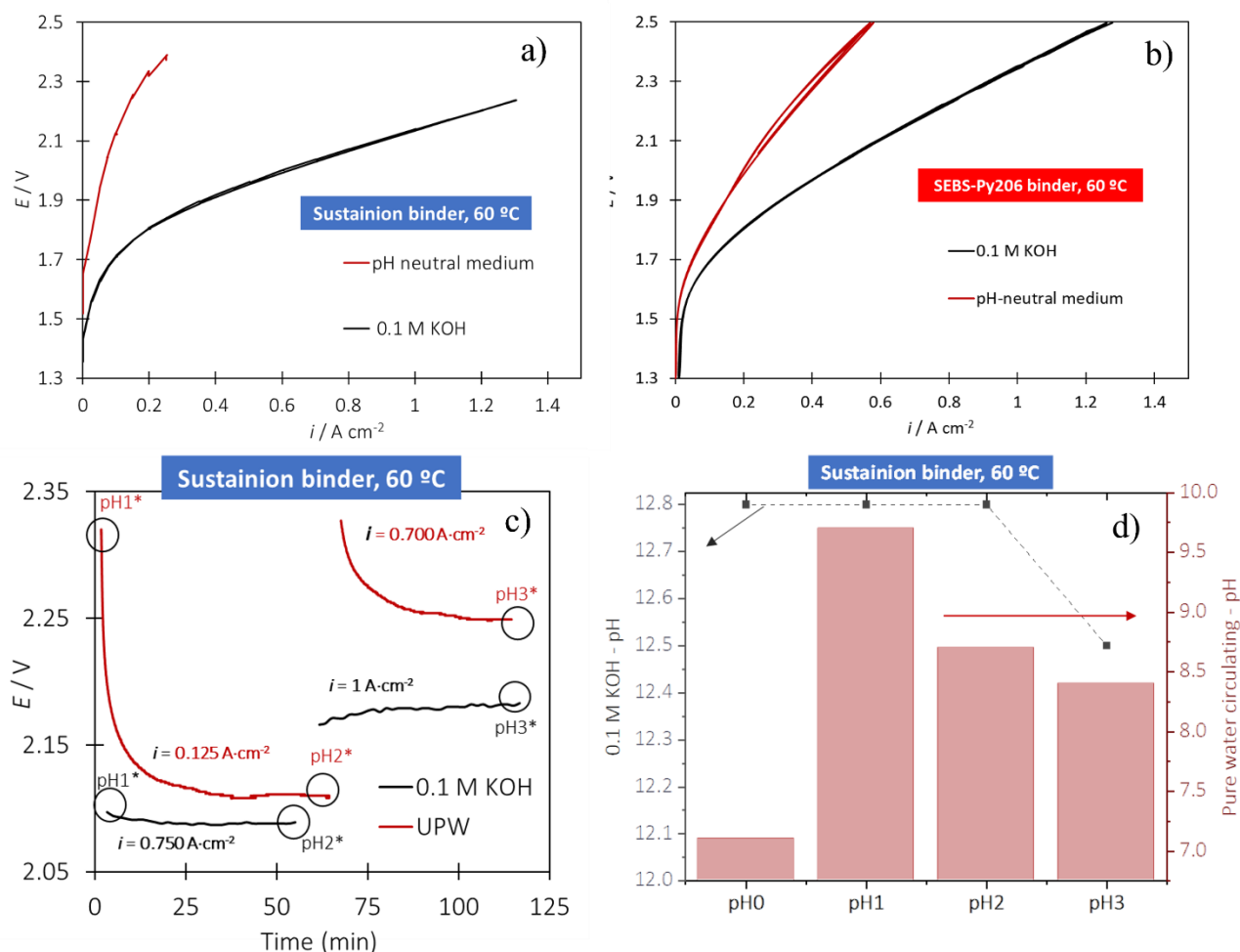


Fig.3 Polarisation curves for AEM water electrolyzers that screen the effect of using **(a)** commercial anion exchange ionomeric (AEI) binder Sustainion and the **(b)** prepared SEBS-Py206 binder using an equal I/C ratio of 30 wt. % and CRM-free catalysts (OXYGN-N and H2GEN-M = 4 mg cm<sup>-2</sup>) in 0.1 M KOH and ultra-pure water, Ph neutral media electrolyte at 60 °C; **(c)** chronopotentiometries of AEMWE composed of Sustainion binder in 0.1 M KOH and ultra-pure water at varying currents; **(d)** variation of electrolyte pH at the AEMWE exhaustion at specific moments when using Sustainion as binder in I/C = 0.3 (pH0 = pH of electrolyte prior to running the cell, pH1= after circulation of electrolyte for 10 mins, pH2 = after 1 h of operation at fixed current, pH3 = after two hours of operation at higher current densities) at 60 °C; inert Ti Felts were used as PTLs to screen binder

effect in CCM configuration using PGM-free catalysts.

Chronopotentiometries were performed in both low alkalinity solution, 0.1 M KOH, and pH neutral media to further investigate the causes for the commercial Sustainion ionomeric binder's poor efficiency in pH neutral media; the pH of the electrolyte was measured at the exhaust of the cell at specific currents and moments of operation, as shown in Fig. 3c). At current densities of 750 mA cm<sup>-2</sup>, 0.1 M KOH at 60 °C the overpotential remained constant for about one hour of operation; however, when the current density was increased to 1 A cm<sup>-2</sup>, an overpotential of approximately 4 mV began to build up after one hour of operation, and the pH (pH<sub>3</sub>) of the electrolyte dropped 0.4 units, from 12.8 (pH<sub>0</sub>) to 12.5, as seen in Fig. 3d). When the identical cell setup was operated in Ph neutral media, under a water-fed operation, a similar pattern was observed. In fact, a drop in overpotential was observed immediately after starting the AEMWE operation, but the pH of the electrolyte at cell exhaustion had increased significantly, indicating that both electrodes' binder was desorbing some of the hydroxyl ions (OH<sup>-</sup>) reticulated in Sustainion's matrix; with increasing current densities to 0.7 A cm<sup>-2</sup> most of OH<sup>-</sup> that could be at the membrane-ionomer-catalyst interface was presumably consumed, and pH began to precipitously drop to 8.2, pH at which the electrolyte samples at the exhaustion of the cell were filled of nanoparticles. The fact that particles detached from the electrode, particularly from the anode side compartment, may indicate a reduction in local Ph, caused as well by the formation of phenol at the ionomeric binder's surface (Sustainion), which is acidic ( $pK_a=9.6$ )<sup>45,49</sup>. **The presence of phenol at the catalyst-ionomer interface may cause the neutralization of Sustainion's quaternized hydroxide functional groups triggering poor activity and degradation mechanism on the Ni based catalysts. In fact, the Sustainion binder poses a wide propensity to adsorb phenyl groups and undergo electrochemical oxidation to phenol, attending to its specific chemical composition and specially at high-operating temperatures, (60 °C in this case), and alkaline environment. Sustainion compositions are known to utilize positively charged quaternary ammonium (QA) functional groups<sup>50</sup>, particularly imidazolium, as the primary ion-conductive**

**moieties. These functional groups exhibit an affinity for organic compounds, including phenyl groups which have the potential to** interact with and adsorb phenyl groups due to their electrostatic attraction<sup>51</sup>. In addition to QA groups, some AEMs/AEIs incorporate functional groups comprised of aromatic or pyridinium structures with high electron density. Such electron-rich functionalities have an increased tendency to create pi-pi interactions or alternative attractive forces with phenyl rings. Therefore, such AEMs/AEIs are particularly susceptible to phenyl oxidation<sup>52</sup>. The electrochemical oxidation of adsorbed phenyl groups on the surface may as well be influenced by the choice of electrocatalyst used for OER; it is worth mentioning that state-of-the-art catalysts such as IrO<sub>2</sub> have been observed to exhibit a propensity to adsorbing and subsequently oxidizing phenyl groups<sup>49</sup>. This phenomenon contributes to the observed challenges in maintaining the durability of the AEM electrolyzers. On the other hand, the prepared SEBS-Py2O6 membrane and ionomeric binder has reduced phenyl groups in its backbone structure and uses pyrrolidinium as positively charged functionalities rather than QA or pyridinium, and thus has a high potential to provide long-term operation to electrocatalysts of AEMWEs in low alkalinity and Ph neutral environments, Fig. 3b).

Consequently, the ionomer to catalyst ratio (I/C) was further evaluated using the promising prepared ionomer (SEBS-Py2O6) and AEM and cell configuration (CCs and bipolar plates composed of SS materials), as it is critical for ensuring efficient transfer of ionic charges from the membrane to the active sites within the 3D microstructure of the catalyst layer and minimize ohmic losses in the electrochemical system. An optimal I/C throughout the catalyst layer is important to avoid the insulating polymeric binder from obstructing the porous microstructure of the catalyst layer, which can compromise both the mass transfer of reactants and products and the passage of electrical charges. Based on the findings from the polarisation curves in both alkaline media and Ph-neutral media (UPW), Fig. 4a) and Fig. 4b), a desirable I/C ratio of 20 wt. % has been identified as particularly advantageous for enhancing the performance of the AEMWE when using CRM-free catalysts with 4 mg cm<sup>-2</sup> of metal loading. This is attributed to the increase in the number of triple-phase boundaries, which provides an enhanced interface for efficient

kinetics of both OER and HER, thereby contributing to the high performance observed in these conditions; in detail, a remarkable performance of  $1.4 \text{ A cm}^{-2}$  is accomplished at 2.5 V and  $60^\circ\text{C}$  for a AEMWE running with water using 20 wt. % of PSFA-free ionomer in both the anode and cathode catalytic layer. However, a 10 wt. % ionomer-to-catalyst ratio proves inadequate in achieving a proper equilibrium between the coverage and extension of ionic pathways to active sites and preventing the catalyst detachment from the fibers of porous transport layers. This effect is mostly felt due to the large activation overpotential observed in both media – *i.e.*, for I/C=10 wt. % 750 mV in 0.1 M KOH and *ca.* 950 mV in pH=7, UPW, Fig. 4a) and Fig. 4b).

Fig. 4 depicts the impedance complex spectra of the CRM-free based MEAs with various I/C ratios, recorded at  $200 \text{ mA cm}^{-2}$  to capture primarily the charge transfer resistance region, in 0.1 M KOH (Fig. 4c)) and Ph-neutral media Fig. 4d)). The cell's ohmic resistance is mostly generated by the hindrance to ion (hydroxide ions) mobility within the AEM and is directly proportional to electrolyte concentration. It was calculated using high-frequency resistance interception with the real impedance axis ( $Z'$ ). When the AEMWE was moved from alkaline to Ph-neutral electrolyte, the ohmic resistances increased by nearly 2.5, from the *ca.*  $350\text{-}450 \text{ m}\Omega \text{ cm}^2$  to  $750\text{-}1500 \text{ m}\Omega \text{ cm}^2$ , which is not surprising given that the hydroxyl ion's concentration in the circulating electrolyte decreases and, as a result, so does the ion conductivity throughout the membrane. In addition, it is noteworthy that different I/C ratios demonstrated a consistent impact on ohmic resistances in both environments. When employing concentrations of 30 wt. % we observed a notable increase in ohmic resistance which can be attributed to several factors. Initially, the high concentration appears to impede ion transport which may contribute to the formation of resistive pathways that hinder the efficient flow of  $\text{OH}^-$ ; secondly the excessive concentration is suggested to introduce challenges in ionic interactions at critical interfaces which include the ionomer, water and the membrane itself<sup>46,53</sup>. On the contrary, lower I/C ratios (10 wt. % and 20 wt. % configurations) yielded decreased ohmic resistance ( $R_{\text{ohm}}$ ). This decline can be attributed to the presence of a reduced amount of material available to contribute to the internal resistance within both

catalyst layers, consequently diminishing their resistive characteristics.

The selected equivalent circuit (EC) for fitting the EIS data is represented as inset of Fig. 4d), is characterized by an ohmic resistance ( $R_{\text{ohm}}$ ) in series with two simple and parallel Randle's circuits. The first circuit consists of a charge transfer resistance representing the system's anode and cathode reactions, OER and HER, respectively ( $R_{\text{ct,a/c}}$ ) and a constant phase element ( $\text{CPE}_{\text{a,c}}$ ) which characterizes the double-layer capacitance representative of the roughness of the electrode; the secondary circuit combination describes the mass transport challenges ( $R_{\text{N}}$  and  $\text{CPE}_{\text{N}}$ ) associated with the release of product gas at the catalyst- solid electrolyte interface<sup>31,35,54,55</sup>. The corresponding EC fitted parameters are detailed in Table S1. At a current density of  $200 \text{ mA cm}^{-2}$ , the EIS spectra reveal that MEA configurations utilizing 10 wt. % of ionomer exhibit a large impedance semicircle, indicating that most of the reactive sites are inactive, possibly due to suboptimal contact. This can be attributed to the ionomer's inability to extend the ionic paths to and from the membrane throughout the entire catalyst layer which compromises an efficient ion transport, further increasing  $R_{\text{ct}}$  due to a lower level of reaction activation and charge transfer. The catalyst layer is both dense, due to the type of used Ni based and Mo based catalysts, and thick due to the high loading of material deposited,  $4 \text{ mg cm}^{-2}$ . An overall  $R_{\text{ct}}$  of  $248.5 \pm 2.3 \text{ m}\Omega \text{ cm}^2$  was obtained for the configuration employing an I/C of 10 wt. % in comparison with almost half the resistance for the AEMWE with 20 wt. % I/C –  $134.9 \pm 3.4 \text{ m}\Omega \text{ cm}^2$  in alkaline media (0.1 M KOH, Fig 4c)). This same pattern was constant in pH neutral environment where the MEA configuration of 10 wt. % contributes to  $450.5 \pm 5.1 \text{ m}\Omega \text{ cm}^2$  whereas the counterpart 20 wt. % electrode's charge transfer resistance contribution is almost half, *i.e.*,  $230 \pm 4.2 \text{ m}\Omega \text{ cm}^2$ . When there is a deficit of ionomer concentration (10 wt. %) at the catalyst layer level in both environments, the overall capacitance (herein represented by  $\text{CPE}_{\text{a/c}}$  and  $\text{CPE}_{\text{N}}$ ) is much wider, which entails for the possibility of increased surface area and exposure of active sites/surface roughness for the formation of the double layer; that is the charge separation process that occurs at the interface between the electrode and electrolyte which by being larger can be associated with the observed larger activation overpotentials and slower response time; the latter

can be observed from the hysteresis generated between the forward and backward potential scan of the polarization curve in water (10 wt. %, see Fig. 4b)). On the other hand, increasing the ionomer content to 30 wt. % creates a binder effect between all the particles, improving the mechanical stability of the catalyst layer with noticeable benefits in comparison to using 10 wt. %. However, this increased ionomer content also appears to be causing a mass transport penalty, which leads to a sharp drop in performance after reaching 2 V and a large mass transport resistance semicircle, in both alkaline and pH-neutral environments, Fig. 4c) and Fig. 4d). The overall cell resistance and response time to power variations is lowered when 20 wt. % of I/C concentration is employed.

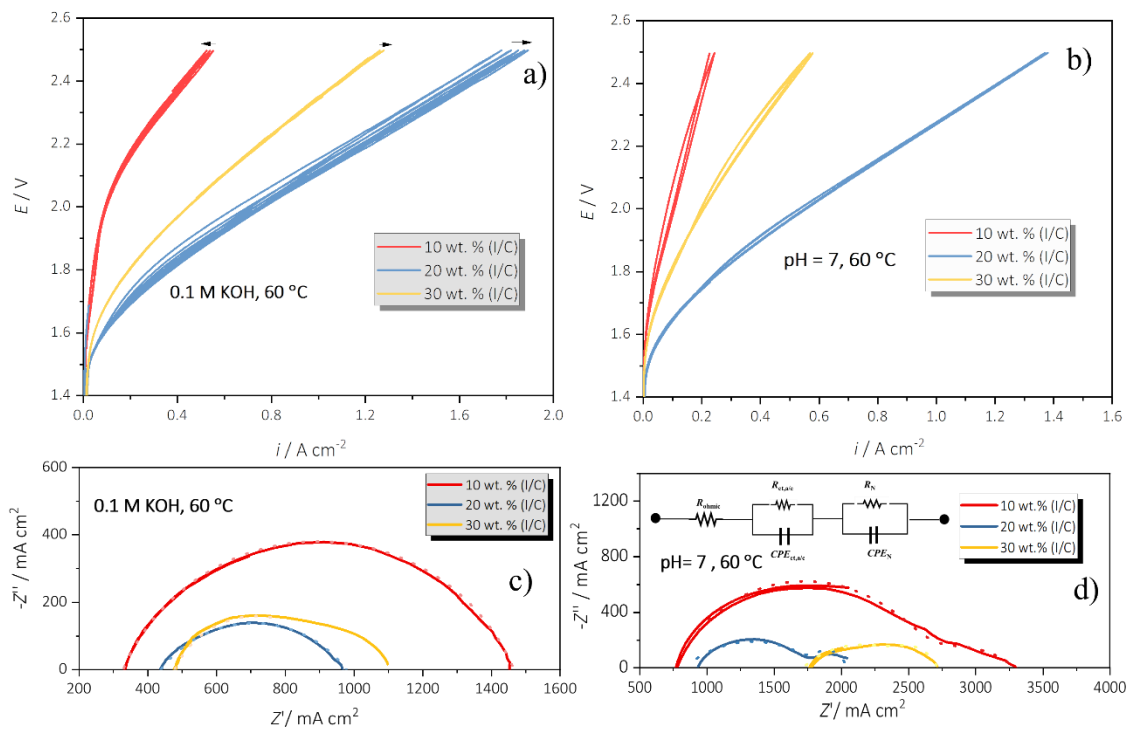


Fig. 4 Polarisation curves (a,b) and impedance complex plane plot (EIS) (c,d) of AEM water electrolyzers that screen the effect of using several SEBS-Py206 AEI concentration (10 wt. %, 20 wt.% or 30 wt. % of I/C) for operation with a) 0.1 M KOH and b) ultra-pure water (UPW) at 60 °C and the SEBS-Py206 AEM. Loading of CRM-free catalysts = 4 mg cm<sup>-2</sup> for anode and cathode and SS bipolar plates and PTLs, 4 cm<sup>2</sup> active area; EIS spectra recorded at 200 mA cm<sup>-2</sup>, 10 mV amplitude.

Several alkaline ionomers had been attempted on AEMWEs running with alkaline electrolytes, and their concentration had been studied, particularly polytetrafluoroethylene (PTFE) dispersion, Fumion<sup>55</sup>, trimethyl ammonium functionalized polystyrene based ionomers (TMA)<sup>21</sup>, Nafion and even Sustainion. Recently, Elena A. Baranova *et al.* studied Fumatech fumion ionomer content in AEMWE anodes using nickel-iron nanoparticles as well, though synthesized by chemical reduction and achieved the most active catalytic layer using 15 wt.% ionomer for high concentrations of circulating electrolyte, 1 M of KOH and elevated anodic loadings – 30 mg cm<sup>-2</sup>; *ca.* 0.8 A cm<sup>-2</sup> were obtained for 1.7 V<sup>46</sup>. TMA formulations with varying molar percentages of quaternized benzyl ammonium that influence final IEC (ranging from 2.2 – 3.3 mequiv g<sup>-1</sup>) ensure remarkable performances in low alkaline environments, *i.e.*, 0.1 M NaOH (2 A cm<sup>-2</sup> at 2 V, 60 °C using Pt/C and IrO<sub>2</sub>) and water (1.2 A cm<sup>-2</sup> at 2 V, 60 °C using 4.5 wt.% of I/C with noble metals)<sup>21</sup>. The higher efficacy in NaOH was attributed to the fact that the alkaline solution neutralized any acidic phenols produced by phenyl group oxidation.

In every situation, it is worth highlighting that a shift in the electrolyte feed conditions is sufficient to modify the ideal ionomer content. This suggests that for every distinct combination of operational parameters and cell components, a specific optimization process for I/C is required.

### **The impact of the AEM type and electrocatalyst, operating conditions, and activation procedures on AEMWE's activity and stability**

The incorporation of ethylene oxide spacers based on cross-linked piperidinium into SEBS-Py206 membranes is expected to result in improved performance and durability in AEM water electrolysis. This is due to the balanced trade-off between the WUR (water uptake ratio) and IEC (ion exchange capacity) properties ensured by the insertion the spacers as noticed from our measurements and previous works on this subject<sup>56,57</sup>. For our the AEM water electrolysis experiments, we evaluated the performance of both precious metal-free catalysts and noble metals. Specifically, we used critical raw material



free catalysts from CENmat, namely H2GEN-M at the cathode and OXYGN-N at the anode; for the noble metal category, we employed IrO<sub>2</sub> at the anode and Pt/C at the cathode. These catalysts were then tested in conjunction with two different types of membranes: commercial Sustainion membranes with ionomer and SEBS-Py206 membranes in both low alkaline media (0.1 M KOH, Fig. 5a)) and under Ph neutral circulating electrolyte (Fig. 5b)). The results provide insights into the performance variations under these different catalyst and membrane combinations, highlighting their effectiveness in AEM water electrolysis. Although there are currently no commercially available AEMWE systems that offer competitive stability at temperatures higher than 60°C<sup>58</sup>, we conducted experiments at 85°C given the positive thermal stability outlook demonstrated by TGA analyses. From direct comparison, the system that integrates the SEBS-Py206 based AEM and AEI outperforms all the CRM-free and noble metal-based cell counterparts, at 85 °C. In comparison to systems that use state-of-the-art noble metals, the CENmat catalysts exhibit a significantly lower onset in the activation region when using the prepared solid polymers, specifically, a 150 mV lower overpotential in the potential window range of 1.45 V to 1.65 V, Fig. 5a). Regarding the benchmark Sustainion X37-50 membrane, the AEMWE equipped with CRM-free MEA and Sustainion demonstrates poor current density outputs due to high ohmic resistance, particularly in pure water operation Fig. 5b). The overall *Rohm* in pH neutral for this system is almost the double in comparison to the most conductive system composed of SEBS-Py206 AEM/AEI and noble metals, *i.e.* - 0.95 Ω cm<sup>2</sup> vs 0.47 Ω cm<sup>2</sup>, respectively Fig. 5c). Additionally, this result is even more obvious when examining the charge transfer resistances at 200 mA cm<sup>-2</sup> in pure water (Fig. S6b)); combining Sustainion binder and CRM-free catalysts results in an overall 3.75 Ω cm<sup>2</sup> vs. Ω just 0.3 Ω cm<sup>2</sup> when using the manufactured polymers. The latter shows that, unlike SEBS-Py206 arrangements, Sustainion fails to maintain most of its ion conductivity in pH neutral conditions. Besides, the maximum current density achieved for such an AEMWE is 350 mA cm<sup>-2</sup> at 2.5 V and 60 °C, indicating that the local pH at the catalyst layer may be unfavourable, triggering deactivation mechanisms at the catalyst level, such as delamination of the catalyst layer from the membrane<sup>36</sup>. According to the latter, even if Sustainion AEMs and ionomeric binders work perfectly in alkaline medium (Fig. 5), they

shouldn't be considered for applications that are supplied by pure water that don't use CRM-free catalysts.

On the other hand, and as evidenced by the current densities of approximately  $1.2 \text{ A cm}^{-2}$  in  $0.1 \text{ M KOH}$  and *ca.*  $0.8 \text{ A cm}^{-2}$  @  $2 \text{ V}$ ,  $60 \text{ }^\circ\text{C}$  in pure water, the SEBS-Py206 membrane, demonstrates favourable features that are suggested to enable extending the pathways for  $\text{OH}^-$  transport from the cathode towards the anode, resulting in remarkable performances in both alkaline environments and pure water. This may be attributed to the relatively high IEC and low phenyl concentration, which allows for maintaining a local high pH<sup>51</sup> and allow rapid reaction rates. When the ionomeric binder is dispersed with the CRM-free catalysts and at higher temperatures, its advantageous effects are noticed even more strongly. The *Rohm* of a CRM-free SEBS-Py206 AEM/AEI combination at neutral pH and  $85 \text{ }^\circ\text{C}$  is below  $0.5 \text{ } \Omega \text{ cm}^2$ , and the total charge resistance of both electrodes is as low as  $0.3 \text{ } \Omega \text{ cm}^2$ , see Fig. 5c) and d). Additionally, we multiplied the real and imaginary impedance from the Nyquist plot *per* the steady-state current density at which the spectra were obtained,  $200 \text{ mA cm}^{-2}$ , to convert the impedance data (Fig.S6b) to Tafel impedance. The Tafel impedance is then calculated as the total diameter of the impedance arc for a kinetically constrained process<sup>55</sup>, Fig. S7. The lowest Tafel impedance in pure water operation, is obtained for the combination of CRM-free catalysts with SEBS-Py206 polymers, at  $85 \text{ }^\circ\text{C}$  with  $70 \text{ mV}$ , followed by the same configuration at lower temperatures,  $60 \text{ }^\circ\text{C}$ ,  $100 \text{ mV}$ . Moreover, all the experiments for analysing the performance and stability were performed while bubbling  $200 \text{ mL min}^{-1}$  of  $\text{N}_2$  gas as we have noticed in a parallel experiment that if  $\text{CO}_2$  is present in the circulating electrolyte, it can negatively impact the performance and stability of the AEMWE by competing with hydroxide ions for transport through the AEM, Fig. S8a). An increased overpotential of  $100 \text{ mV}$  is noticed at the ohmic-mass transport region when  $\text{CO}_2$  from ambient air is present in the electrolyte; in long-term experiments, the stability of the cell fed with electrolyte exposed to ambient air was much worse, indicating that  $\text{CO}_2$  may have exacerbated AEM degradation mechanisms as these are sensitive to acidic conditions arising from the generation of carbonic acid from  $\text{CO}_2$  dissolution, consult Fig. S8b.

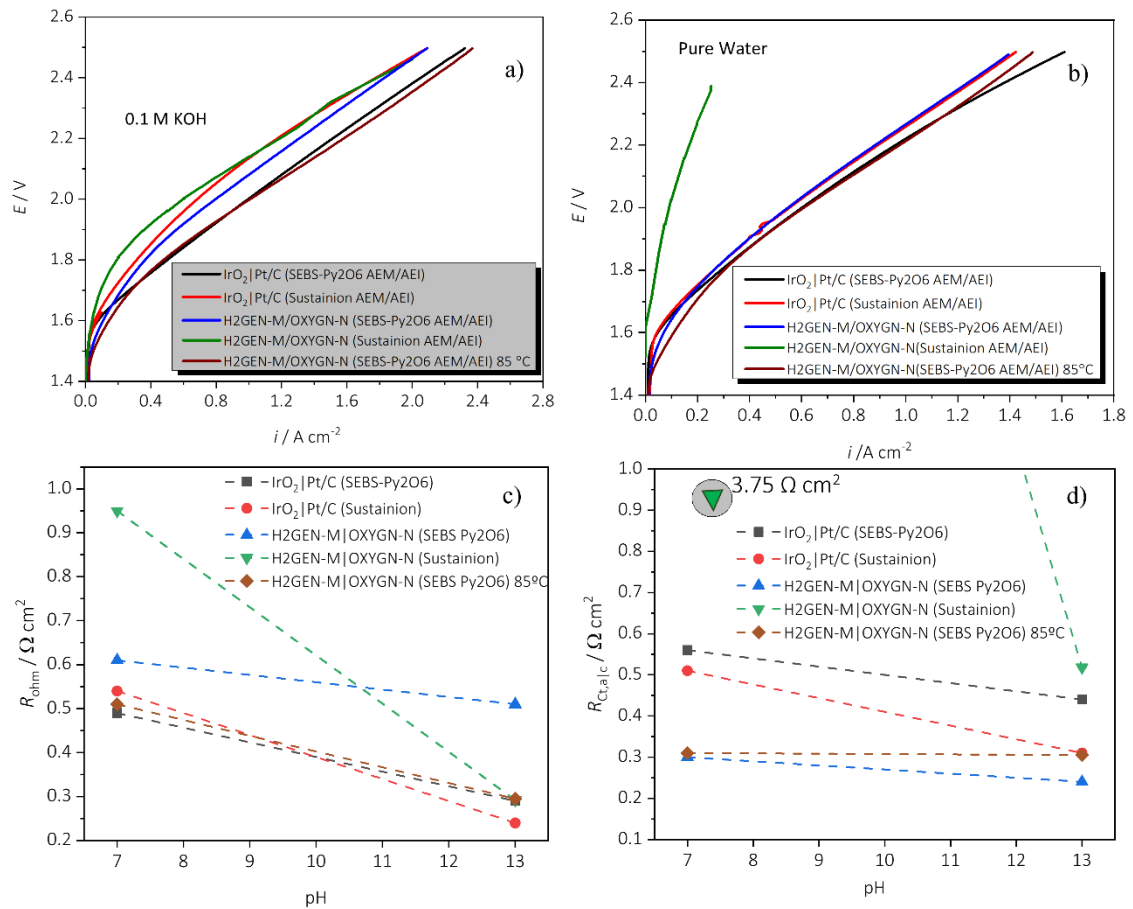


Fig. 5 Polarisation curves **(a,b)** and  $R_{ohm}/R_{ct,alc}$  fitting results from impedance complex plane of data shown in Fig. S 6 **(c,d)** of several AEM water electrolyzers with varying electrolyte feeding – 0.1 M KOH or pure water. AEM water electrolyzers include CRM-free catalysts from CENmat or noble metals (IrO<sub>2</sub>|Pt/C) using several SEBS-Py2O6 AEM/AEI or commercial Sustainion AEM/AEI with 20 wt.% I/C at 60 °C and 85 °; Loading of catalysts = 4 mg cm<sup>-2</sup> for CRM-free or 1 mg cm<sup>-2</sup> for noble metals; SS bipolar plates, PTLs and current collectors, 4 cm<sup>2</sup> active area; the experiments ran under a 100 % N<sub>2</sub> saturated electrolyte.

Subsequent galvanostatic degradation experiments were conducted to evaluate the performance of the best performing assemblies, by fixing the current at 200 mA cm<sup>-2</sup> under pure water operation, as illustrated in Fig. 6. The performance of the assembly comprising the SEBS-Py2O6 membrane tested at 85 °C showed a rapid deterioration after the initial characterization, as indicated by an overpotential of nearly 600 mV. However, the cell quickly stabilized to a lower overpotential which suggests a reversible mechanism had had happened, and thus exhibited little to no degradation rate for over 15 hours, as

shown in Fig. 6a).

By direct comparison with Sustainion AEM/AEI, it is possible that on the other hand, SEBS-Py206 polymers do not have a detrimental impact on performance due to the presence of phenyl groups in the ionomer backbone that may cause oxidization to phenolic acid, which in the case of Sustainion, highly limits the stability of CRM-free electrocatalysts. The AEMWE made of commercial Sustainion and PGMs exhibits a sharp performance loss, almost half, following potential cycling in the OER window, Fig. 6c), and a high deterioration rate in neutral pH operation (ca.  $10 \text{ mV h}^{-1}$  after 12 hours of operation at fixed current, Fig. 6a). On the contrary, the results suggest that the proton in the phenol group did not deprotonate to neutralize the hydroxide of the pyrrolidinium functional group in SEBS-Py206 polymers, attending to the large performance and stability obtained, as seen in Fig. 6b).

Furthermore, the prior activation step of the CCSs and AEMs with SEBS prior to operation, were found to be pivotal in ensuring the large current density outputs and stability. Longer crosslinking periods, *i.e.*, 24 h in amine bath, and soaking in alkaline (1M KOH) solutions ( $\geq 48$  h) are suggested to be beneficial for SEBS-Py206, leading to a high ion conductivity in ultra-pure water (UPW) and  $\text{OH}^-$  retention, as seen in Fig. S9. On the other hand, gas bubble-induced ionomer detachment and delamination of the catalyst layer from the membrane were found to occur more easily with Sustainion ionomer than with SEBS-Py206. This suggests that Sustainion ionomer, with its lower gas permeability and excessive swelling in contact with water, not only generates additional resistance but also may own a much lower adhesion. On the other hand, the strategic incorporation of robust pyrrolidinium as cationic functional groups represents a compelling avenue for strengthening the chemical durability of ionic groups within the SEBS; these are likely to allow introducing a pronounced steric hindrance effect, which holds promise in alleviating the chemical degradation of essential ionic constituents within the AEM/AEI during prolonged operation. Moreover, the presence of these groups is suggested to own a pivotal role in fostering the creation of interconnected ionic domains within the

structural framework of the membrane and ionomer which ensures the attainment of the requisite ionic conductivity levels imperative for the seamless and efficient functioning of AEMFC applications.

With such advancements, the highest stability at pH-neutral media for a CRM-free AEMWE (SEBS-Py206) was achieved for over 88 hours at 60 °C, Fig. 6b) with a recorded degradation rate of solely 3 mV dec<sup>-1</sup>, which to the best of the authors' knowledge is the most stable CRM-free AEMWE cell reported in the literature using solely earth- abundant and low-cost materials (SS felts and bipolar plates, check info Table S2).

Overall, these factors collectively underscore the intricate interplay between membrane and ionomer's composition, mainly surface functional groups, and the choice of electrocatalyst, which can significantly impact the stability and performance of the AEM-based electrolysis system in low alkalinity and pure water feeding conditions.

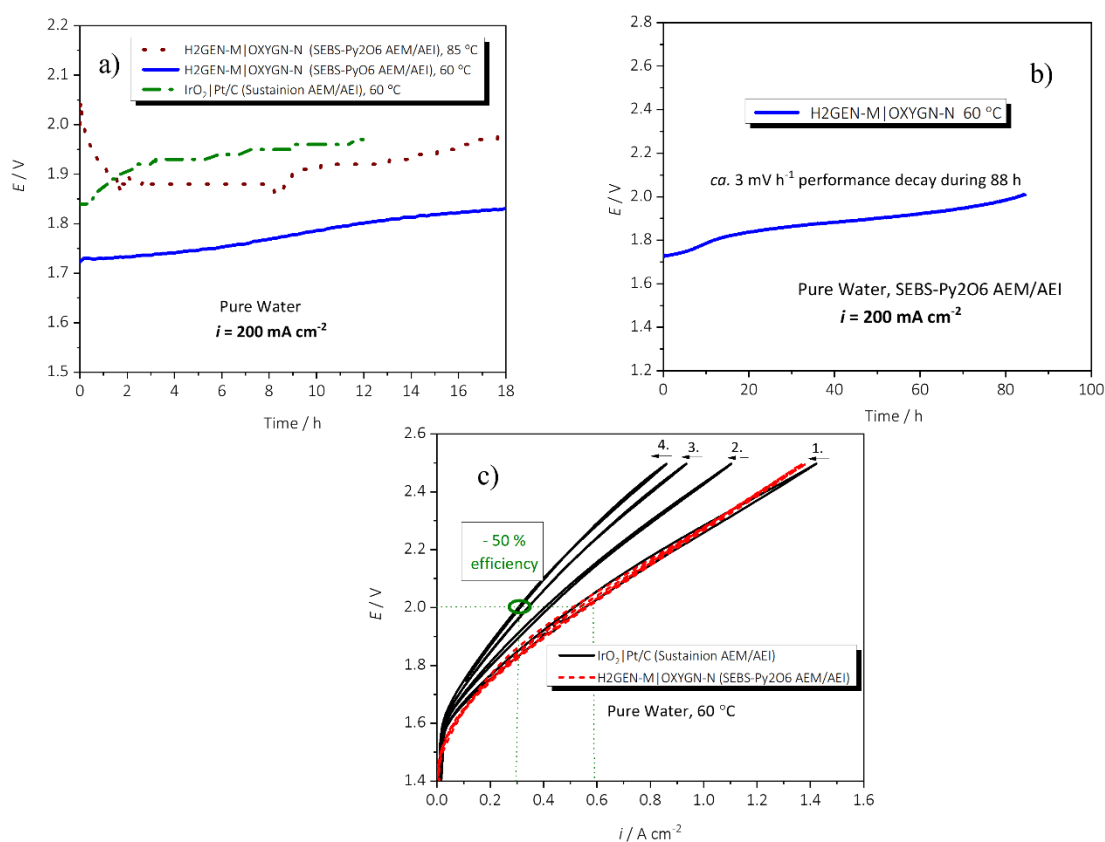


Fig. 6 Stability tests in pure water involving a chronopotentiometry at 200 mA cm<sup>-2</sup> for

**(a)** 12h/18h, 18h or **(b)** 80 h using the most promising AEMWE configurations while circulating pure water at 60 °C and 85 °C; **(c)** Potential cycling in the OER potential range in AEMWEs comprising either noble metals and commercial Sustainion AEM/AEI or CRM-free catalysts and SEBS-Py2O6 AEM/AEI in pure water at 60°C; Loading of catalyst = 4 mg cm<sup>-2</sup> for the anode and cathode and SS bipolar plates and PTLs, 4 cm<sup>2</sup> active area;

## Conclusions

The novel MEA fabrication strategy introduced in this study allows for effective OH<sup>-</sup> transport pathways during AEMWE cell operation by extending the electrical contact with the aqueous electrolyte and possibly enhancing the ion capacity retention. The findings of this study reveal some crucial observations, including:

i) CRM-free catalysts have the potential to serve as benchmark anode and cathode catalysts, respectively, in AEMWE. The catalysts not only thrive the necessary electrochemical reactions in highly alkaline conditions as well as in pure water– which offer a cost-effective alternative to noble catalysts such as IrO<sub>2</sub> and Pt/C.

ii) CCSs using stainless steel felts outperform CCM configurations, improving mechanical integrity of the electrodes compared to the CCM preparation that requires a conventional gun spraying in pre-heated plate at 50 °C.

iii) Ionomer/Catalyst ratios of 20 wt.% are pivotal for extending the number of triple-phase boundaries and AEMWE performance.

iv) Cell operations at 85 °C deliver higher performances but less stability than operations at 60°C throughout long-term tests.

v) The highest performance in ultra-pure water (UPW) occurred when using IrO<sub>2</sub>|Pt/C catalysts with SEBS-Py2O6 AEM & AEI- 1 A cm<sup>-2</sup> @ 2 V at 60 °C, surpassing commercial Sustainion-based MEAs.

vi) An entirely CRM-free cell achieved unprecedented current densities of approximately 0.8 A cm<sup>-2</sup> @ 2 V @ 60 °C in UPW with the novel membrane configuration.

vii) The most stable AEMWE cell in UPW reported in this study uses stainless steel components, CRM-free catalysts and the novel SEBS-Py2O6 membrane & ionomer,

achieving the one of lowest degradation rate to the best of the author's knowledge (3 mV h<sup>-1</sup>) for equivalent systems, and for approximately 90 hours in pH-neutral operation.

These findings highlight the potential to optimize this system and improve hydrogen production efficiency through sustainable cost-effective routes.

### Acknowledgements

This work was financially supported by LA/P/0045/2020 (ALiCE), UIDB/00511/2020 and UIDP/00511/2020 (LEPABE), funded by national funds through FCT/MCTES (PIDDAC) and mostly by EU Horizon 2020 FCH JU project NEWELY. The authors acknowledge the financial support of the project Baterias 2030, with the reference POCI-01-0247-FEDER-046109, co-funded by the Operational Programme for Competitiveness and Internationalisation (COMPETE 2020), under the Portugal 2020 Partnership Agreement, through the European Regional Development Fund (ERDF). Sofia Delgado acknowledges FCT for the doctoral grant with reference SFRH/BD/144338/201 and Ziqi Xu the Chinese Scholarship Council (201706060199).

### References

- 1 M. F. Orhan, I. Dincer, M. A. Rosen and M. Kanoglu, *Renew. Sustain. Energy Rev.*, 2012, **16**, 6059–6082.
- 2 E. Gülzow and M. Schulze, *J. Power Sources*, 2004, **127**, 243–251.
- 3 M. Schulze and E. Gülzow, *J. Power Sources*, 2004, **127**, 252–263.
- 4 M. S. Naughton, F. R. Brushett and P. J. A. Kenis, *undefined*, 2011, **196**, 1762–1768.
- 5 H. A. Miller, K. Bouzek, J. Hnat, S. Loos, C. I. Bernäcker, T. Weißgärber, L. Röntzsch and J. Meier-Haack, *Sustain. Energy Fuels*, 2020, **4**, 2114–2133.
- 6 K. E. Ayers, E. B. Anderson, C. Capuano, B. Carter, L. Dalton, G. Hanlon, J. Manco and M. Niedzwiecki, *ECS Trans.*, 2010, **33**, 3–15.
- 7 D. Li, A. R. Motz, C. Bae, C. Fujimoto, G. Yang, F. Y. Zhang, K. E. Ayers and Y. S. Kim, *Energy Environ. Sci.*, 2021, **14**, 3393–3419.
- 8 S. Stiber, H. Balzer, A. Wierhake, F. J. Wirkert, J. Roth, U. Rost, M. Brodmann, J. K. Lee, A. Bazylak, W. Waiblinger, A. S. Gago and K. A. Friedrich, *Adv. Energy Mater.*, 2021, **11**, 2100630.
- 9 Q. Feng, X. Z. Yuan, G. Liu, B. Wei, Z. Zhang, H. Li and H. Wang, *J. Power Sources*, 2017, **366**, 33–55.
- 10 L. Xiao, S. Zhang, J. Pan, C. Yang, M. He, L. Zhuang and J. Lu, *Energy Environ. Sci.*, 2012, **5**, 7869–7871.

- 11 J. Liu, M. R. Gerhardt, D. Li, M. Pak, Z. Kang, S. M. Alia, G. Bender, Y. S. Kim and A. Z. Weber, *ECS Meet. Abstr.*, 2020, **MA2020-02**, 2443.
- 12 G. Sudre, S. Inceoglu, P. Cotanda and N. P. Balsara, *Macromolecules*, 2013, **46**, 1519–1527.
- 13 A. D. Mohanty and C. Bae, *J. Mater. Chem. A*, 2014, **2**, 17314–17320.
- 14 A. N. Lai, L. S. Wang, C. X. Lin, Y. Z. Zhuo, Q. G. Zhang, A. M. Zhu and Q. L. Liu, *ACS Appl. Mater. Interfaces*, 2015, **7**, 8284–8292.
- 15 D. S. Kim, A. Labouriau, M. D. Guiver and Y. S. Kim, *Chem. Mater.*, 2011, **23**, 3795–3797.
- 16 L. Liu, S. He, S. Zhang, M. Zhang, M. D. Guiver and N. Li, *ACS Appl. Mater. Interfaces*, 2016, **8**, 4651–4660.
- 17 J. J. Kaczur, H. Yang, Z. Liu, S. D. Sajjad and R. I. Masel, *Front. Chem.*, 2018, **6**, 263.
- 18 Z. Liu, S. D. Sajjad, Y. Gao, H. Yang, J. J. Kaczur and R. I. Masel, *Int. J. Hydrogen Energy*, 2017, **42**, 29661–29665.
- 19 J. Parrondo, C. G. Arges, M. Niedzwiecki, E. B. Anderson, K. E. Ayers and V. Ramani, *RSC Adv.*, 2014, **4**, 9875–9879.
- 20 P. Thangavel, M. Ha, S. Kumaraguru, A. Meena, A. N. Singh, A. M. Harzandi and K. S. Kim, *Energy Environ. Sci.*, 2020, **13**, 3447–3458.
- 21 D. Li, E. J. Park, W. Zhu, Q. Shi, Y. Zhou, H. Tian, Y. Lin, A. Serov, B. Zulevi, E. D. Baca, C. Fujimoto, H. T. Chung and Y. S. Kim, *Nat. Energy* 2020 55, 2020, **5**, 378–385.
- 22 D. Henkensmeier, M. Najibah, C. Harms, J. Žitka, J. Hnát and K. Bouzek, *J. Electrochem. Energy Convers. Storage*, , DOI:10.1115/1.4047963/1085903.
- 23 J. R. Varcoe, P. Atanassov, D. R. Dekel, A. M. Herring, M. A. Hickner, P. A. Kohl, A. R. Kucernak, W. E. Mustain, K. Nijmeijer, K. Scott, T. Xu and L. Zhuang, *Energy Environ. Sci.*, 2014, **7**, 3135–3191.
- 24 M. A. Hickner, H. Ghassemi, Y. S. Kim, B. R. Einsla and J. E. McGrath, *Chem. Rev.*, 2004, **104**, 4587–4611.
- 25 C. Long, Z. Wang and H. Zhu, *Int. J. Hydrogen Energy*, 2021, **46**, 18524–18533.
- 26 X. Luo, D. I. Kushner and A. Kusoglu, *J. Memb. Sci.*, 2023, **685**, 121945.
- 27 M. M. Zareh and M. M. Zareh, *Recent Adv. Plast.*, , DOI:10.5772/36620.
- 28 C. Y. Wong, W. Y. Wong, K. S. Loh and A. B. Mohamad, *Renew. Sustain. Energy Rev.*, 2017, **79**, 794–805.
- 29 K. Täuber, A. Zimathies and J. Yuan, *Macromol. Rapid Commun.*, 2015, **36**, 2176–2180.
- 30 A. D. Mohanty, C. Y. Ryu, Y. S. Kim and C. Bae, *Macromolecules*, 2015, **48**, 7085–7095.
- 31 F. Razmjooei, T. Morawietz, E. Taghizadeh, A. Saul Gago, S. Asif Ansar, K. Andreas Friedrich, E. Hadjixenophontos, L. Mues, M. Gerle, B. D. Wood and C. Harms, *Joule*, 2021, **5**, 1776–1799.
- 32 M. Stähler, A. Stähler, F. Scheepers, M. Carmo, W. Lehnert and D. Stolten, *Int. J. Hydrogen Energy*, 2020, **45**, 4008–4014.
- 33 P. Lettenmeier, S. Kolb, N. Sata, A. Fallisch, L. Zielke, S. Thiele, A. S. Gago and K. A. Friedrich, *Energy Environ. Sci.*, 2017, **10**, 2521–2533.



- 34 C. Lei, K. Yang, G. Wang, G. Wang, J. Lu, L. Xiao and L. Zhuang, *ACS Sustain. Chem. Eng.*, 2022, **10**, 16725–16733.
- 35 L. Zhang, Q. Xu, Y. Hu, L. Chen and H. Jiang, *ACS Sustain. Chem. Eng.*, , DOI:10.1021/ACSSUSCHEMENG.3C01619/SUPPL\_FILE/SC3C01619\_SI\_001.PDF.
- 36 X. Chu, Y. Shi, L. Liu, Y. Huang and N. Li, *J. Mater. Chem. A*, 2019, **7**, 7717–7727.
- 37 C. C. Pavel, F. Cecconi, C. Emiliani, S. Santuccioli, A. Scaffidi, S. Catanorchi and M. Comotti, *Angew. Chemie Int. Ed.*, 2014, **53**, 1378–1381.
- 38 I. Vincent, A. Kruger and D. Bessarabov, *Int. J. Electrochem. Sci.*, 2018, **13**, 11347–11358.
- 39 P. Li, R. Zhao, H. Chen, H. Wang, P. Wei, H. Huang, Q. Liu, T. Li, X. Shi, Y. Zhang, M. Liu and X. Sun, *Small*, 2019, **15**, 1805103.
- 40 E. Cattaneo and B. Riegel, *Encycl. Electrochem. Power Sources*, 2009, 796–809.
- 41 B. Beverskog and I. Puigdomenech, *Corros. Sci.*, 1997, **39**, 969–980.
- 42 J. Melder, S. Mebs, P. A. Heizmann, R. Lang, H. Dau and P. Kurz, *J. Mater. Chem. A*, 2019, **7**, 25333–25346.
- 43 X. Wu, K. Scott, F. Xie and N. Alford, *J. Power Sources*, 2014, **246**, 225–231.
- 44 R. R. Raja Sulaiman, W. Y. Wong and K. S. Loh, *Int. J. Energy Res.*, 2022, **46**, 2241–2276.
- 45 D. Li, E. J. Park, W. Zhu, Q. Shi, Y. Zhou, H. Tian, Y. Lin, A. Serov, B. Zulevi, E. D. Baca, C. Fujimoto, H. T. Chung and Y. S. Kim, *Nat. Energy* 2020 55, 2020, **5**, 378–385.
- 46 E. Cossar, A. O. Barnett, F. Seland, R. Safari, G. A. Botton and E. A. Baranova, *J. Power Sources*, 2021, **514**, 230563.
- 47 Y. S. Kim, *ACS Appl. Polym. Mater.*, 2021, **3**, 1250–1270.
- 48 H. T. Chung, U. Martinez, I. Matanovic and Y. S. Kim, *J. Phys. Chem. Lett.*, 2016, **7**, 4464–4469.
- 49 D. Li, I. Matanovic, A. S. Lee, E. J. Park, C. Fujimoto, H. T. Chung and Y. S. Kim, *ACS Appl. Mater. Interfaces*, 2019, **11**, 9696–9701.
- 50 R. B. Kutz, Q. Chen, H. Yang, S. D. Sajjad, Z. Liu and I. R. Masel, *Energy Technol.*, 2017, **5**, 929–936.
- 51 P. Shirvanian, A. Loh, S. Sluijter and X. Li, *Electrochem. commun.*, 2021, **132**, 107140.
- 52 A. Vöge, V. Deimede and J. K. Kallitsis, *RSC Adv.*, 2014, **4**, 45040–45049.
- 53 B. Chen, P. Mardle and S. Holdcroft, *J. Power Sources*, 2022, **550**, 232134.
- 54 I. Dedigama, P. Angeli, K. Ayers, J. B. Robinson, P. R. Shearing, D. Tsaoulidis and D. J. L. Brett, *Int. J. Hydrogen Energy*, 2014, **39**, 4468–4482.
- 55 A. Y. Faid, A. O. Barnett, F. Seland and S. Sunde, *Electrochim. Acta*, 2021, **371**, 137837.
- 56 Z. Xu, S. Delgado, V. Atanasov, T. Morawietz, A. S. Gago and K. A. Friedrich, *Membranes (Basel)*, 2023, **13**, 328.
- 57 Z. Xu, V. Wilke, J. J. Chmielarz, M. Tobias, V. Atanasov, A. S. Gago and K. A. Friedrich, *J. Memb. Sci.*, 2023, **670**, 121302.
- 58 G. Gupta, K. Scott and M. Mamlouk, *J. Power Sources*, 2018, **375**, 387–396.
- 59 W. Li, Z. Cao, X. Zhu and W. Yang, *J. Memb. Sci.*, 2019, **573**, 370–376.

- 60 Y. Leng, G. Chen, A. J. Mendoza, T. B. Tighe, M. A. Hickner and C. Y. Wang, *J. Am. Chem. Soc.*, 2012, **134**, 9054–9057.
- 61 X. Wu and K. Scott, *J. Power Sources*, 2012, **206**, 14–19.
- 62 J. Parrondo, C. G. Arges, M. Niedzwiecki, E. B. Anderson, K. E. Ayers and V. Ramani, *RSC Adv.*, 2014, **4**, 9875–9879.
- 63 E. J. Park, C. B. Capuano, K. E. Ayers and C. Bae, *J. Power Sources*, 2018, **375**, 367–372.
- 64 G. Gupta, K. Scott and M. Mamlouk, *J. Power Sources*, 2018, **375**, 387–396.
- 65 L. Xiao, S. Zhang, J. Pan, C. Yang, M. He, L. Zhuang and J. Lu, *Energy Environ. Sci.*, 2012, **5**, 7869–7871.
- 66 Y. C. Cao, X. Wu and K. Scott, *Int. J. Hydrog. Energy*, 2012, **37**, 9524–9528.
- 67 X. Wu and K. Scott, *J. Power Sources*, 2012, **214**, 124–129.
- 68 X. Wu and K. Scott, *Int. J. Hydrogen Energy*, 2013, **38**, 3123–3129.
- 69 L. Wan, Z. Xu, Q. Xu, P. Wang and B. Wang, *Energy Environ. Sci.*, 2022, **15**, 1882–1892.

Supplementary information

## Highly Efficient and Durable Anion Exchange Membrane Water Electrolyzers with Non-Precious Metal Catalysts in Pure Water: key components and fabrication strategies

S. Delgado<sup>1,2,3a)</sup>, Z. Xu<sup>3a)</sup>, V. Wilke<sup>3</sup>, A. Gago<sup>3</sup>, A. Mendes<sup>1,2</sup>, K. A. Friedrich<sup>3</sup>

<sup>1</sup> LEPABE - Laboratory for Process Engineering, Environment, Biotechnology and Energy, Faculty of Engineering, University of Porto, Rua Dr. Roberto Frias, 4200-465 Porto, Portugal

<sup>2</sup> ALiCE - Associate Laboratory in Chemical Engineering, Faculty of Engineering, University of Porto, Rua Dr. Roberto Frias, 4200-465 Porto, Portugal

<sup>3</sup> Institute of Engineering Thermodynamics/Electrochemical Energy Technology, German Aerospace Center (DLR), Pfaffenwaldring 38-40, 70569 Stuttgart, Germany

## Experimental section

### Membrane and ionomer preparation (cmSEBS-Py206)

Initially, the backbone of the membrane made of chloromethylated SEBS (cmSEBS) was produced following the method previously thoroughly described elsewhere<sup>56,58</sup>, and using Styrene-ethylene – butylene- styrene polymer (30 wt. % of styrene, Taipol 6152) supplied by TSRC cooperation. Specifically, 250 mL of chloroform was placed inside an inert-purged three-neck round-bottom flask and stirred together with the SEBS polymer (25 mmol, 4 g) for about 4 h at room temperature. The temperature was dropped to 1 °C using a cold bath and trioxane (5.4 g, 60 mmol), chlorotrimethylsilane (22.8 mL, 37.5 mmol) and tin chloride salt precursor (3 mL, 3 mmol) were added to the flask and stirred for 30 minutes. In the end, the solution was added to 300 mL of ethanol/water (50/50 wt. %) to finalize the reaction and finally, the precipitate (mess) was collected by filtration. The functional groups composed of 1,2-Bis(2-pyrrolidinyloxy) Ethane (Py206) were synthesized by dissolving pyrrolidine (250 mmol) in acetonitrile in argon at room temperature using a magnetic stirrer, and by thoroughly following the steps as described in our previous work<sup>56</sup>.

For the preparation of SEBS-Py206 membrane, 0.7 g of cmSEBS was dissolved in 25 mL of chloroform at 50 °C for 2 hours to form a nearly 2 wt.% solution. Then, 1 mL of P206 (approximately 0.003 mol) was added to 25 mL of chloroform, and 0.2 mL of iodomethane was dropped in while stirring for 2 hours to obtain mP206. Subsequently, the two solutions were mixed, and the membrane was cast from the solution onto a PTFE square dish (15 cm × 15 cm). The membrane was first dried at 50 °C for 4 hours and then at 100 °C for 20 hours in a vacuum. Finally, the SEBS-P206 membrane was detached from the PTFE dish and boiled in water to remove the remaining solvent. For the preparation of the anion exchange ionomer (AEI), tetrahydrofuran was used as solvent of cmSEBS precursor to produce a 10 wt.% solution. After the fabrication of the MEA, both electrodes and membrane were immersed in a 500 mL mPy206 solution overnight to functionalize both

the cmSEBS into SEBS-mPy2O6 ionomer.

### **Membrane Characterization**

At 25 °C, the through plane membrane conductivity to OH<sup>-</sup> of the SEBS-Py2O6 was measured using a four-electrode technique; Au electrodes and a Zahner-elektrik IM6 were utilized. The ohmic resistance was measured while a 1 M KOH solution was circulated across the membrane, and 1 V of potential and 5 mV of amplitude were applied. Water uptake (WUR) and swelling ratio were also measured using the weight and geometric length difference in Cl<sup>-</sup> form before and after soaking the membrane (48 hours at 25 °C in distilled water and then dried in vacuum).

The ion exchange capacity (IEC) implies the measurement of the total number of ionic sites on a membrane that are available for exchanging ions with the surrounding solution, and was determined following a back titration technique. The method involved immersing the membrane in a 1 M sodium hydroxide (NaOH) solution, washing the membrane to remove excess NaOH, and then immersing the membrane in a sodium chloride (NaCl) solution to exchange the Na<sup>+</sup> ions on the membrane surface with Cl<sup>-</sup> ions in the solution. The membrane was then added with a 0.1 M hydrochloric acid (HCl) solution, and the remaining HCl was titrated with a standard sodium hydroxide (NaOH) solution to determine the amount of HCl consumed in the reaction with the membrane. The IEC was then calculated using a formula reported elsewhere<sup>59</sup>. Such mechanical properties were compared to benchmark Nafion 212 and Sustainion, widely employed for PEMWE and AEMWE applications.

Thermogravimetric analysis (TGA) was performed using a thermogravimetric analyzer (TG 209 F1 iris, NETZSCH) under 30 cm<sup>3</sup> min<sup>-1</sup> of oxygen flow, heating the samples from room temperature to 600 °C at a 20 C min<sup>-1</sup> rate. A 1 x 1 cm square of each membrane, namely SEBS-Py2O6, Nafion 212 (Ion Power) and Sustainion (Dioxide materials) were cut for analysis.

#### **1.1 Membrane electrode assembly (MEA) preparation**

SEBS-Py2O6 membranes in Cl<sup>-</sup> form were rinsed with ultrapure water and dried at 50 °C for 2 hours before preparing the membrane electrode assemblies. Catalyst coated

membranes (CCMs) and catalyst coated substrates (CCSs) were produced by manually air spraying catalysts onto the membranes or felt substrates, respectively. For the anode side, a catalyst ink containing OXYGN-N catalyst (CENmat), SEBS copolymer-based ionomer suspension (10 wt.%, 20 wt.%, or 30 wt.% I/C), and THF was dispersed onto the SEBS-based membrane or substrate felt of Ni, stainless steel (SS, Bekipor ST 40 BL3, Bekaert), or carbon paper (SpectraCarb2050, 0.2 mm Sigracarb). Similarly, for the cathode side, a similar suspension with H2GEN-M catalyst (CENmat) was dispersed on the other side of the membrane or on the substrates. The depositions were performed using a spray gun using a 0.5 mm nozzle and nitrogen as pressurized carrier gas (2 bar), on a preheated plate at 50 °C to produce 4 cm<sup>2</sup> active area electrodes with 4 mg cm<sup>-2</sup> catalyst loading for CRM-free catalysts and 1 mg cm<sup>-2</sup> with noble metals. The CCMs or CCSs were immersed in a solution of mPy2O6 and 20 wt.% KOH to functionalize the cmSEBS ionomer present in the catalyst layer. This step serves as a crosslinking mechanism that enables the conversion of the chloromethyl group to a functional membrane. Subsequently, the CCMs, CCSs and AEMs were placed in a flask containing 200 mL of 1 M KOH solution, boiled at 60°C for 30 minutes, and stored in the same solution for 48h or 72 hours in the dark to convert the Cl<sup>-</sup> ions to OH<sup>-</sup>, prior to the cell assembly.

To facilitate comparison with benchmark materials, commercially available Sustainion X37-50 grade RT (Dioxide materials) membranes were employed, and catalyst ink solutions comprising either Pt/C (40 wt. %, Alfa Aesar) or Ir black (Alfa Aesar) and Sustainion-based AEI were dispersed to prepare cathodes or anodes, respectively comprising 1 mg cm<sup>-2</sup> of noble metal each. The ex-situ activation of Sustainion membranes was performed following the supplier instructions (soaking the membrane in 1 M KOH for 15h).

### **AEMWE Cell assembly and electrochemical characterization**

The membrane electrode assembly components underwent thorough rinsing in ultra-pure water before being assembled in an anion exchange membrane water electrolysis (AEMWE) cell with 0.6 Nm torque to clamp the cell. Porous transport layers made of a stainless-steel mesh were integrated with the membrane electrode assembly, while

bipolar plates made of stainless steel and end plates made of Polyether ether ketone (PEEK) with a thickness of 0.8 cm were included as supplementary components to ensure mechanical stability of the cell. The AEMWE was subjected to tests at temperatures of 60 °C and 85 °C in both 0.1 M KOH liquid electrolyte and ultrapure water (UPW), using a Zahner Zennium X potentiostat coupled with a Zahner PP241 booster. The electrolyte was fed to the anode and cathode via natural flow. To minimize the generation of  $K_2CO_3$  precipitates due to the side reaction of KOH with atmospheric  $CO_2$ , the cell was continuously purged with  $N_2$ . Initially, the cell underwent activation in potentiostatic mode and then in galvanostatic mode with lead times of approximately 4 minutes at each current up to  $2 A cm^{-2}$  in KOH and up to  $1 A cm^{-2}$  in ultrapure water. Ten polarization curves were retrieved in potentiostatic mode up to 2.5 V with a scan rate of  $20 mV s^{-1}$  in both alkaline media and neutral pH. Electrochemical impedance spectroscopy (EIS) spectra were recorded at  $200 mA cm^{-2}$  using a 10mV amplitude and scanning the frequency from 1 kHz to 100 mHz. Long-term chronopotentiometries were carried out in water-fed anion exchange membrane electrolyzers, at  $200 mA cm^{-2}$ . Zview 2 software was used to fit the EIS spectra data.

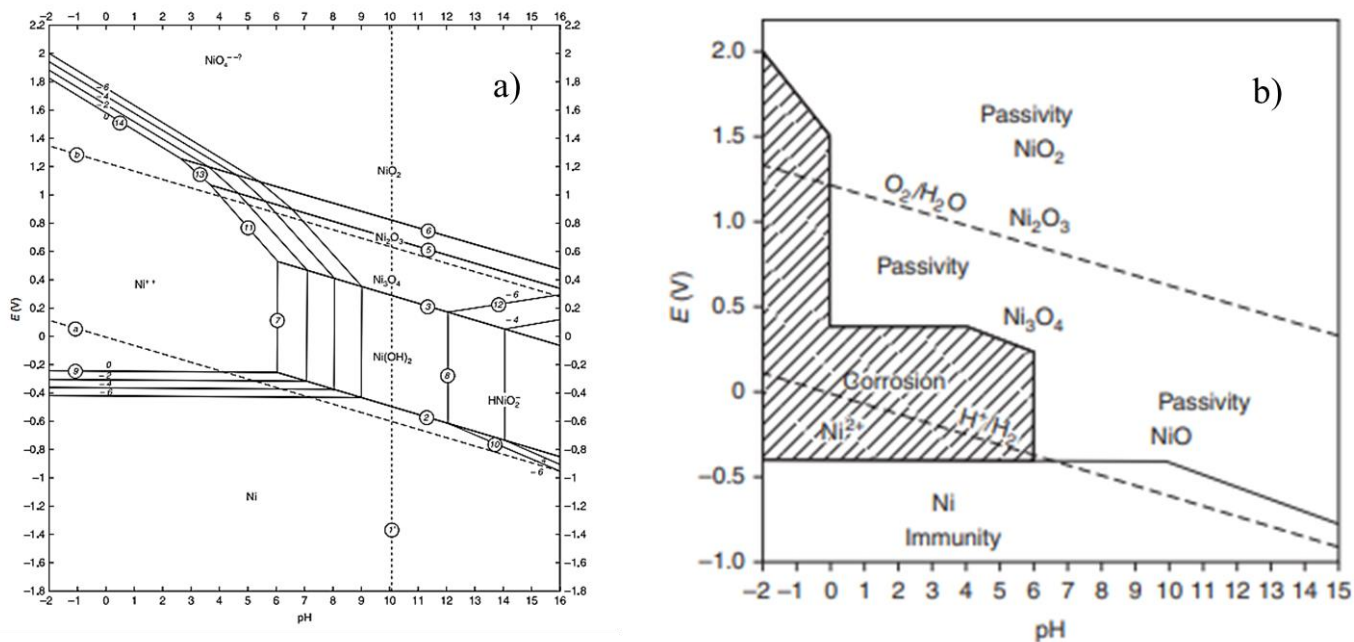


**Fig. S 1. (a)** Potential-pH diagram for nickel at 25 °C and corresponding **(b)** practical stability ranges . Both images reproduced from Cattaneo et. Al.

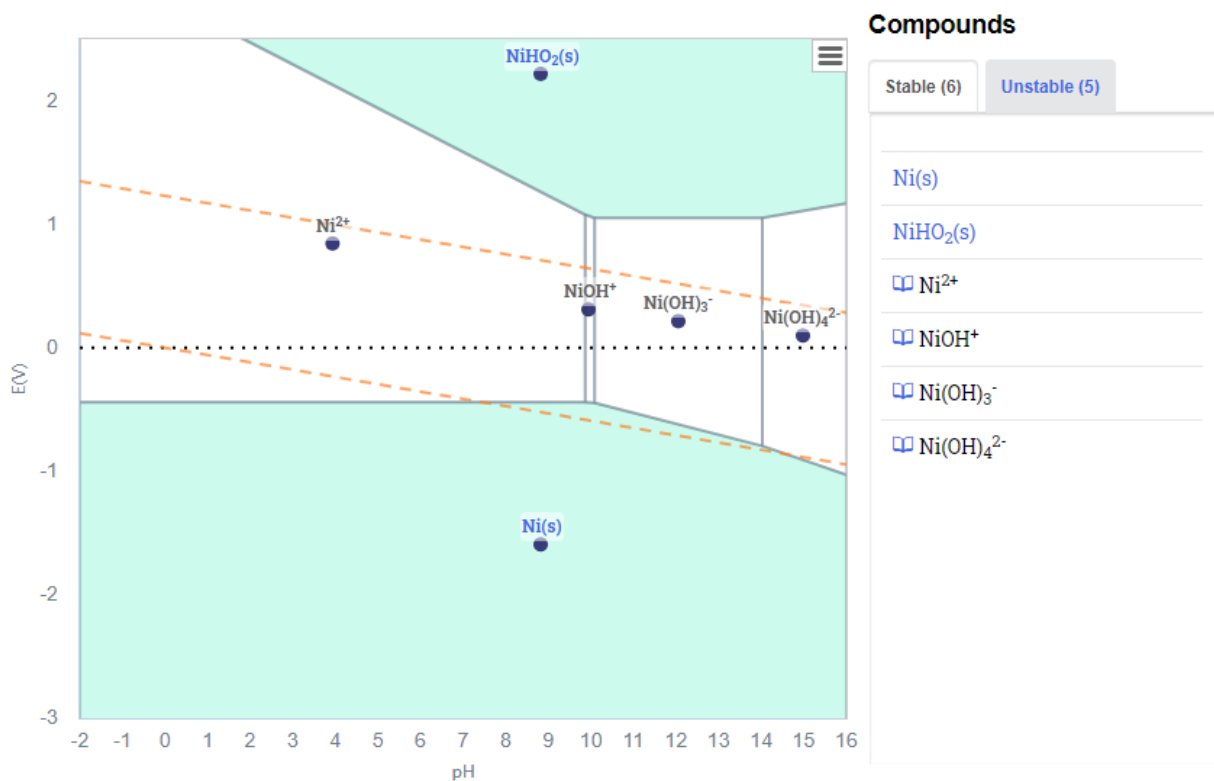


**Fig. S 2** Prediction of Ni species attending to specific composition of the anode and at 60 °C. Retrieved from open-source Materials project. <https://next-gen.materialsproject.org/about/cite>

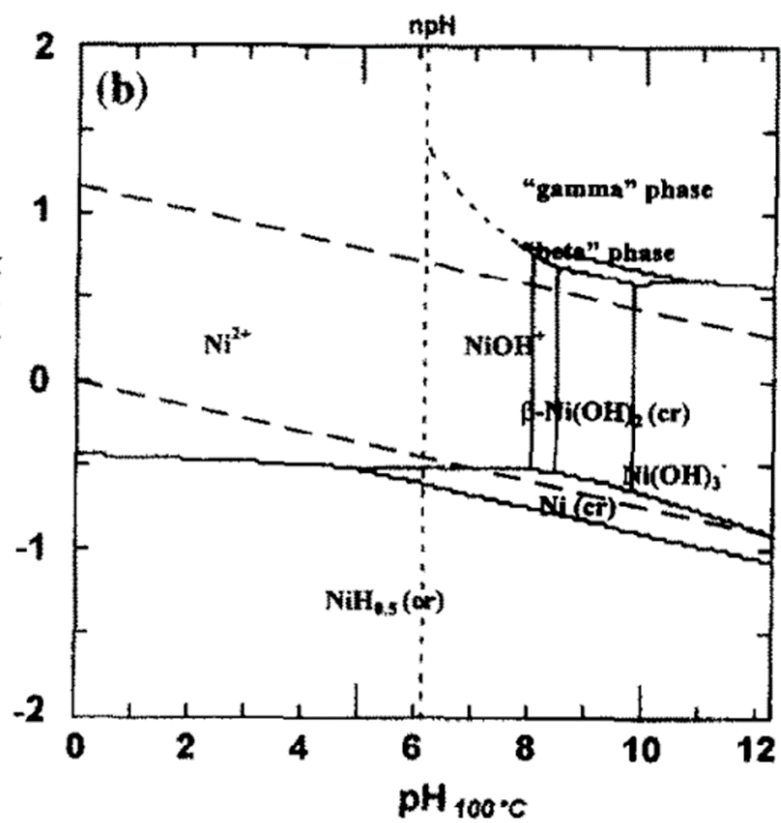
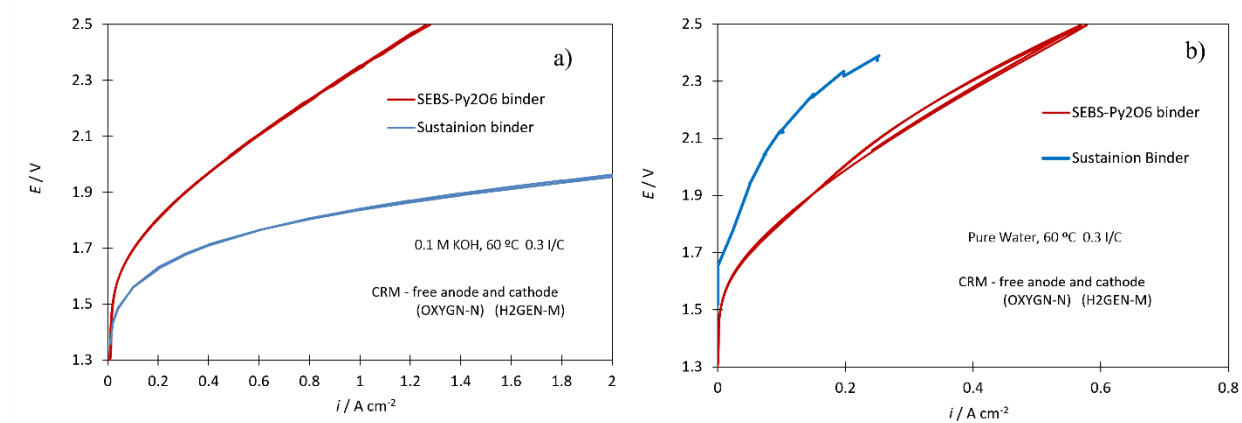
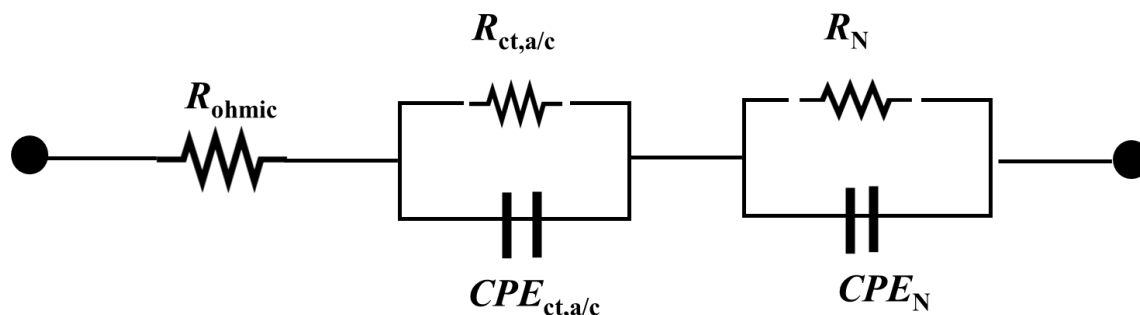


Fig. S 3 Potential-pH diagram for nickel at 100 °C. Retrieved from Beverskog and Puigdomenech, 1997.





**Fig. S 4** Polarisation curves of AEMWE employing Sustainion or SEBS-Py206 as binders in a ratio of 0.3 I/C **(a)** in 0.1 M KOH and **(b)** ultra-pure water in a pH-neutral media at 60 °C.



**Fig. S 5** Equivalent Circuit (EC) used to fit EIS data, in Zview software.

**Table S 1** Parameters extracted from impedance data fitting for electrolysis cells.

Cell configuration	$R_{ohmic}$ / $m\Omega$	$R_{ct,a/c}$ / $m\Omega$	$CPE_{a/c}$ / $mF$	$R_N$ / $m\Omega$	$C_N$ / $mF$
10 wt. % I/C - 0.1 M KOH/ SS CC	$82 \pm 1.4$	$248.5 \pm 2.3$	$0.57 \pm 0.01$	-	-
20 wt. % I/C - 0.1 M KOH/ SS CC	$109.6 \pm 3.4$	$134.9 \pm 3.4$	$9.55 \pm 0.05$	-	-
30 wt. % I/C - 0.1 M KOH/ SS CC	$119.6 \pm 2.2$	$119.5 \pm 2.4$	$1.35 \pm 0.03$	-	-
10 wt. % I/C Water / SS CC	$192.0 \pm 4.2$	$450.5 \pm 5.1$	$0.004 \pm$ $0.0005$	$180 \pm 4.2$	$4.6 \pm 0.8$
20 wt. % I/C Water / SS CC	$228.0 \pm 3.6$	$230.0 \pm 4.2$	$0.185 \pm 0.04$	$50.0 \pm 1.3$	$708.9 \pm 2.3$
30 wt. % I/C Water / SS CC	$438.8 \pm 6.8$	$175.5 \pm 6.3$	$0.387 \pm 0.05$	$61.0 \pm 3.1$	$28.3 \pm 2.6$

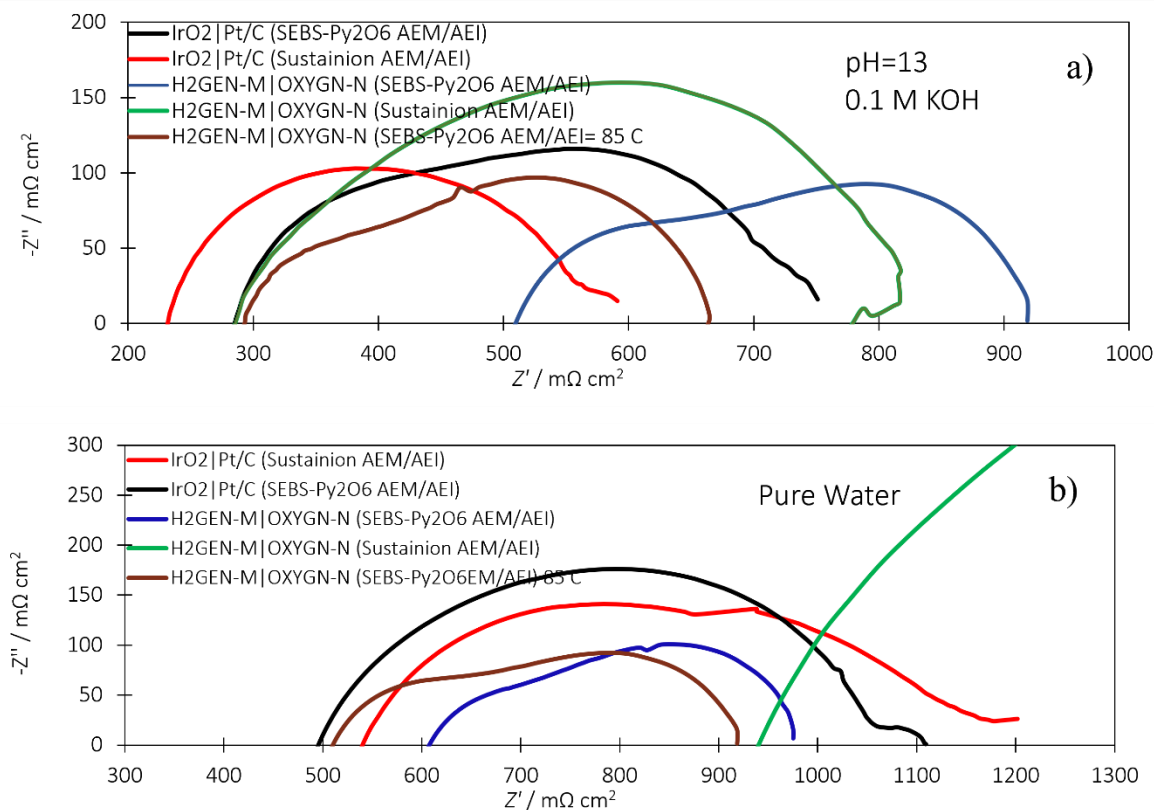


**Fig. S 6** Complex plane impedance spectra of CRM-free MEA or noble metals (IrO<sub>2</sub> and Pt/C) configurations using commercial Sustainion or prepared SEBS-Py2O6 AEM/AEI at 85 °C and 60 °C in (a) 0.1 M KOH (pH=13) and (b) pH neutral (pH=7) operation using 20 wt. % I/C AEs; EIS recorded at 200 mA cm<sup>-2</sup> with 10 mV amplitude.

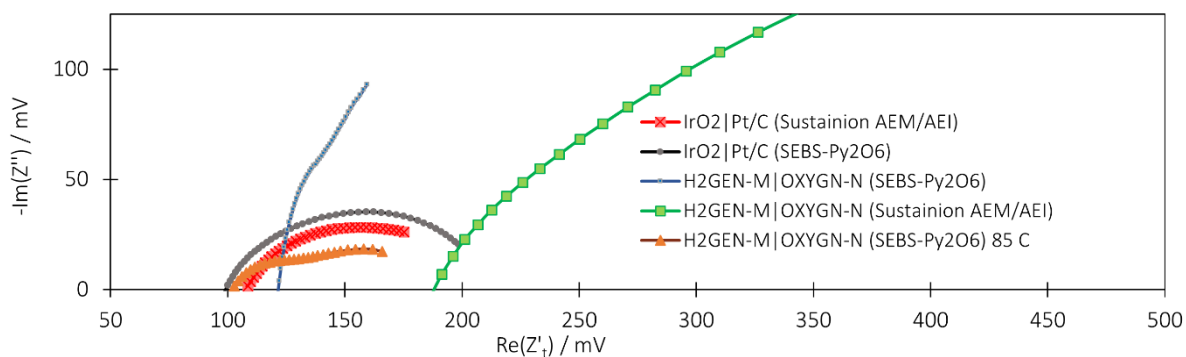


**Fig. S 7** Tafel impedance of CRM-free MEA or noble metals (IrO<sub>2</sub> and Pt/C) configurations using commercial Sustainion or prepared SEBS-Py2O6 AEM/AEI at 85 °C and 60 °C, using 20 wt. % I/C.

**Table S 2** AEMWE recent configurations (AEM/AEI, catalysts, current collector materials), performance and stability in low alkaline conditions and pure water at several temperatures.

Performance	Circulating Electrolyte	AEM	AEI	Anode		Cathode		Stability	Reference
				CC	Catalyst	PTL/current collector	catalyst		
0.8 A/cm <sup>2</sup> at 2 V	Water at 50 °C	Tokuyama A201	Tokuyama AS-4	Ti foam	IrO <sub>2</sub>	Toray CP (H-120)	Pt black		60
0.3 A/cm <sup>2</sup> at 2.2 V	Water at 40 °C	LDPE-g-VBC	-	Toray Carbon paper(H-090)	Cu Mn Co O <sub>4</sub>	Toray CP (H-090)	50 wt% Pt/C		61
0.65 A/cm <sup>2</sup> at 2.2 V	Water at 50 °C	PSF-TMA	PSF- TMA	Porous electrode	Pb <sub>2</sub> Ru <sub>2</sub> O <sub>6.5</sub>	Sigracet CP (10BC)	Pt black		62
0.5 A/cm <sup>2</sup> at 2 V	Water at 50 °C	Tokuyama A201	Tokuyama AS-4	GDE	PGM	GDE	PGM		63
1 A/cm <sup>2</sup> at 2V	0.1 M NaOH at 60 °C	LDPE-g-VBC-TMA	PSEBS-CM- TMA	Ti fibre felt	NiCo <sub>2</sub> O <sub>4</sub>	Carbon GDL+MPL	20 wt% Pt/C		64
0.6 A/cm <sup>2</sup> at 2.0 V	0.1 M KOH at 60 °C	Polyethylene based radiation grafted	Polystyrene-b-(poly ethylene) b-polystyrene	Carbon Paper	NiCo <sub>2</sub> O <sub>4</sub>	Carbon Paper	Pt		58
0.3 A/cm <sup>2</sup> at 1.80 V	Water at 50°C	LSCPi (Ling side chained Piperidinium)	PTFE	Carbon paper	IrO <sub>2</sub> (1 mg cm <sup>-2</sup> )	Platinized porous Ti plate	Pt/C (8 mg cm <sup>-2</sup> )	35 h @0.2 A cm <sup>-2</sup> (14 mV h <sup>-1</sup> )	36
0.7 A/cm <sup>2</sup> at 1.95 V	Water at 70°C	xQAPS	xQAPS	Ni infiltrated NF	Electroplated Ni/Fe	SS fiber felt	Ni/Mo		65
0.3 A/cm <sup>2</sup> at 2.3 V	Water at 50°C	mm-qPVBz/Cl-	qPVB/Cl-	SS mesh & CFP	Cu <sub>0.7</sub> Co <sub>2.3</sub> O <sub>4</sub>	SS mesh & CFP	Ni		66
0.6 A/cm <sup>2</sup> at 2.4 V	Water at 22°C	"Cranfield membrane"	QPDTB	SS mesh	Cu <sub>0.7</sub> Co <sub>2.3</sub> O <sub>4</sub>	SS mesh	Ni		67
0.3 A/cm <sup>2</sup> at 2.1 V	Water at 45°C	Cranfield membrane	QPDTB-OH-	SS mesh	Li <sub>0.21</sub> Co <sub>2.79</sub> O <sub>4</sub>	SS mesh	Ni		68
2 A/cm <sup>2</sup> at 1.8 V	10 mM KOH at 80 °C	QAPPT	QAPPT	Platinized anticorrosion sintered titanium particles	NiFeCo	Carbon paper	Pt/C 0.5 mg cm <sup>-2</sup>	100 h @ 0.2 A cm <sup>-2</sup> (2 mV h <sup>-1</sup> )	34

<b>2 A/cm<sup>2</sup> at 1.76 V</b>	Water at 80 °C	QAPPT	QAPPT	Platinized anticorrosion on sintered titanium particles	NiFeCo	Carbon paper	Pt/C 0.5 mg cm <sup>-2</sup>	100 h @ 0.2 A cm <sup>-2</sup> (4.5 mV h <sup>-1</sup> ) rapid decay after 60 h	34
<b>3.5 A/cm<sup>2</sup> at 2.0 V</b>	Water at 60 °C	HTMA-DAPP	TMA-70	Platinum coated titanium flow field / Platinized titanium GDL (Giner Labs)	NiFe Foam (3 mg cm <sup>-2</sup> )	Graphite plates (Fuel Cell Technologies)	Pt/Ru/C (2 mg cm <sup>-2</sup> )	64 h @ 0.2 A cm <sup>-2</sup> (43 mV h <sup>-1</sup> )	21
<b>1.5 A/cm<sup>2</sup> at 2.0 V</b>	Water at 85 °C	HTMA-DAPP	TMA-70	Platinum coated titanium flow field / Platinized titanium GDL (Giner Labs)	NiFe Foam (3 mg cm <sup>-2</sup> )	Graphite plates (Fuel Cell Technologies)	NiMo (2 mg cm <sup>-2</sup> )	N/A	21 <b>Sate of the art</b>
<b>N/A A/cm<sup>2</sup> at 2.0 V</b>	Water at 85 °C	HTMA-DAPP	TMA-70	Platinum coated titanium flow field / Platinized titanium GDL (Giner Labs)	NiFe Foam (3 mg cm <sup>-2</sup> )	Graphite plates (Fuel Cell Technologies)	Pt/Ru/C (2 mg cm <sup>-2</sup> )	8 h @ 0.2 A cm <sup>-2</sup> (75 mV h <sup>-1</sup> )	21
<b>2.5 A/cm<sup>2</sup> at 2.0 V</b>	Water at 60°C	PBI	PBI	Self supported VCoP/Ni foil	Ni	Self supported VCoP/Ni foil	N/A	600 h at 1 A cm <sup>-2</sup>	69
<b>1 A/cm<sup>2</sup> at 2.0 V</b>	<b>Water at 60°C</b>	<b>SEBS-Py206</b>	<b>SEBS-Py206</b>	<b>SS bipolar plate / SS felt (Bekaert)</b>	<b>IrO<sub>2</sub></b> (1 mg cm <sup>-2</sup> )	<b>SS bipolar plate / SS felt (Bekaert)</b>	<b>Pt/C</b> (1 mg cm <sup>-2</sup> )	N/A	<b>This work</b>
<b>0.8 A/cm<sup>2</sup> at 2.0 V</b>	<b>Water at 60°C</b>	<b>SEBS-Py206</b>	<b>SEBS-Py206</b>	<b>SS bipolar plate / SS felt (Bekaert)</b>	<b>OXYGN-N</b> (4 mg cm <sup>-2</sup> )	<b>SS bipolar plate / SS felt (Bekaert)</b>	<b>H2GEN-M</b> (4 mg cm <sup>-2</sup> )	<b>88 h @ 0.2 A cm<sup>-2</sup></b> <b>(3 mV h<sup>-1</sup>)</b>	<b>This work</b>

1.3 A/cm <sup>2</sup> at 2.0 V	Water at 85°C	SEBS-Py206	SEBS-Py206	SS bipolar plate / SS felt (Bekaert)	OXYGN-N (4 mg cm <sup>-2</sup> )	SS bipolar plate / SS felt (Bekaert)	H2GEN-M (4 mg cm <sup>-2</sup> )	18 h @ 0.2 A cm <sup>-2</sup> (5.5 mV h <sup>-1</sup> )	This work
-----------------------------------	------------------	------------	------------	---	-------------------------------------	--	-------------------------------------	---	--------------

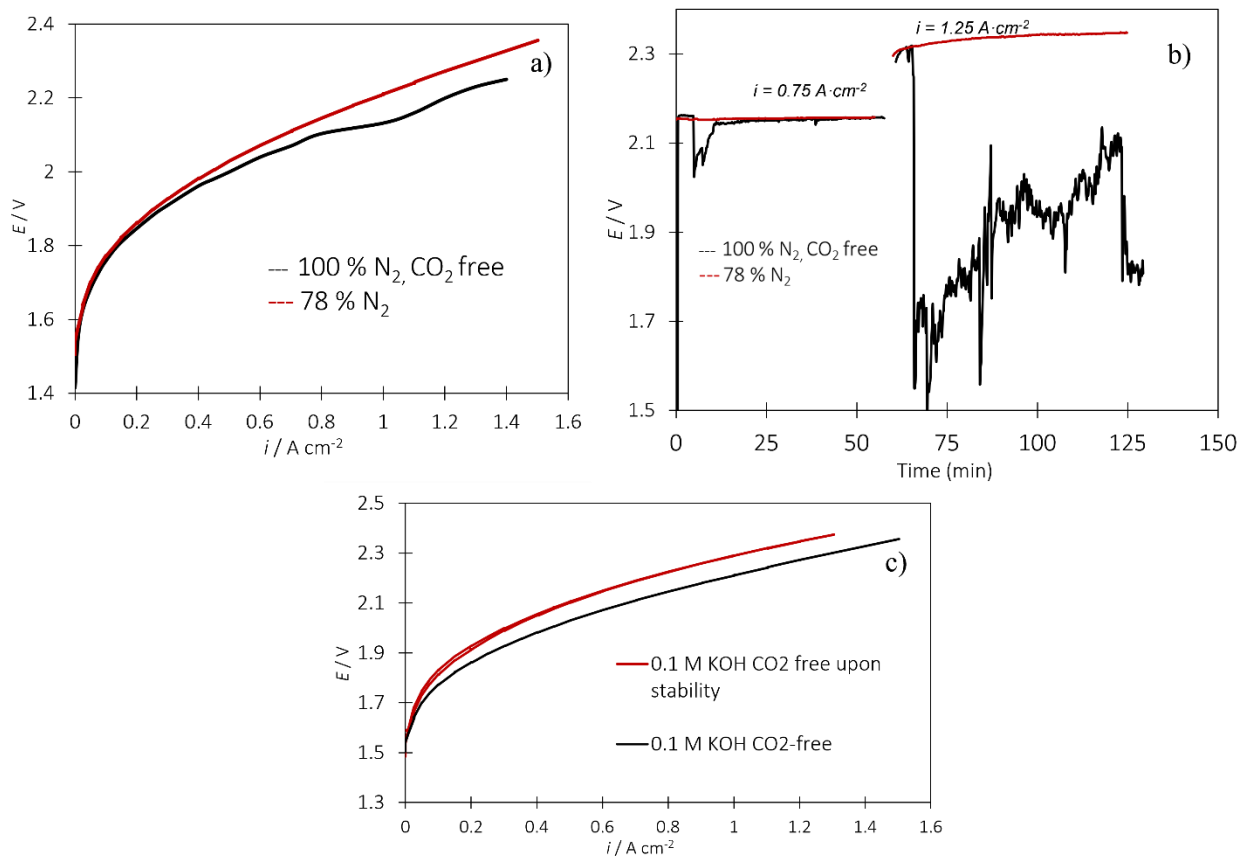


**Fig. S 8 (a)** Polarisation curves at beginning of life for AEMWE using Sustainion as AEM and AEI, with CRM-free catalysts in 0.1 M KOH under operation with saturation of the electrolyte with 200 mL min<sup>-1</sup> 100 % N<sub>2</sub> or air (not CO<sub>2</sub> free); **(b)** chronopotentiometries at 750 mA cm<sup>-2</sup> and 1250 mA cm<sup>-2</sup> of the AEMWE under saturation of both gas flow streams; **(c)** before and after stability test in CO<sub>2</sub> free environment polarisation curve.

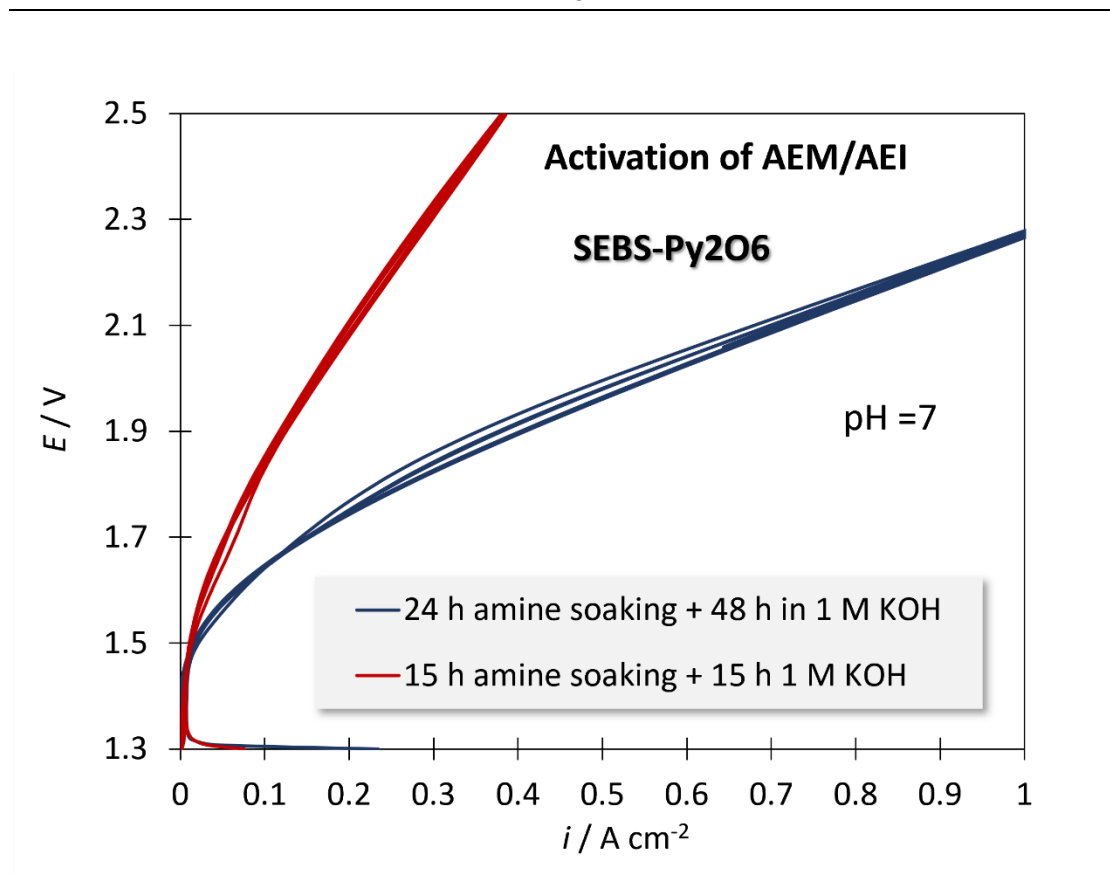


**Fig. S 9** Polarisation curve for AEMWE at 60 °C in pH neutral media where the SEBS-Py206 AEM and AEI based CCSs faced a crosslinking step in amine of 15h or 24 h followed by OH<sup>-</sup> substitution in 1 M KOH solution for 15 h or 48 h, respectively. The current collector used was carbon paper.